Alma Mater Studiorum – Università di Bologna

DOTTORATO DI RICERCA IN

Ingegneria Civile, Chimica, Ambientale e dei materiali

Ciclo XXXIII

**Settore Concorsuale:** 09/D2

**Settore Scientifico Disciplinare:** ING/IND 24

# NOVEL MEMBRANES FOR HEMODIALYSIS APPLICATIONS

Presentata da **Matilde De Pascale**

Supervisore

**Cristiana Boi**

Co-Supervisore

**Maria Grazia De Angelis**

Coordinatore Dottorato

**Luca Vittuari**

**Esame finale anno 2021**

# Abstract

The present work is focused on the synthesis and characterization of novel materials for hemodialysis applications. Cellulose acetate was chosen as base polymer for the preparation of porous Mixed Matrix Membrane adsorbers (MMMAs) and for the synthesis of hybrid ultrafiltration membranes. Hemodialysis is a renal replacement therapy used to eliminate, through diffusion and convection, the waste products and excess fluids accumulating in the blood of people affected by an end stage renal disease. The main environmental drawback associated to it is the large water consumption (156 billion liters worldwide every year). The MMMAs were prepared with the porpoise of eliminating waste metabolites (uremic toxins) from the spent dialysate solution, with the prospective of enabling the recycling of water, limiting the consumption related to the process. Batch tests of MMMAs showed that the removal of uric acid is almost complete while the one of urea and creatinine is limited to a 20/30 %. The thinking behind the concept of MMMAs was aimed to develop a small a lab scale chromatographic cartridge to continuously remove uremic toxins from an aqueous feed solution. The cartridge was packed with 22 MMMAs and tested with a mixture of urea, creatinine and uric acid. Experiments results shown a promising removal capability of the system even if the necessity of a higher surface area to achieve better efficiency is denoted.

The other important issue related to hemodialysis is the assessment of an overall mass transfer rates in hemodialyzers. The mass transfer correlations proposed in literature do not take into account the effect of permeation and are developed for turbulent flow regime. Therefore, hybrid cellulose acetate/Silica ultrafiltration membranes were prepared to characterize a surrogate system of an artificial kidney (AK) in terms of fluid mechanics and mass transfer. The effect of surface roughness and suction on the velocity profiles was determined and a new dimensionless mass transfer correlation accounting for permeation was developed for a range of Reynold number varying from $33<Re<114$ and for Schmidt number ranging from $384<Sc<7881$.

# Key words

Hemodialysis procedure

Water consumption

Uremic toxins

Zeolites

Activated carbons

Cellulose Acetate porous Mixed Matrix Membranes adsorbers

Cellulose acetate/Silica hybrid ultrafiltration membranes

Adsorption

Surrogate system of an artificial kidney (AK)

Fluid mechanics characterization

Mass transport coefficients and correlations

# Acknowledgments

To Professor Cristiana Boi of the department of Civil, Chemical, Environmental and Materials Engineering (DICAM) of the University of Bologna for supervising and advising me during the three years of PhD. To her constant support for my research activities, for letting me pursue my ideas guiding me in the pathways to follow and for transmitting me the knowledge necessary to complete this work.

To Professor Maria Grazia De Angelis of the department of Civil, Chemical, Environmental and Materials Engineering (DICAM) of the University of Bologna for her co-advising and for letting me participate to didactic activities that helped me develop communicative and organizational skills useful for myself and for my PhD research.

To professor Maria Norberta de Pinho of the Chemical Engineering Department of the Instituto Superior Técnico for fully orienting me during my period abroad, for her constant presence in the development of the research activities, her constructive attitude on the direction to take, shearing ideas and involving me in deciding the evolution of the project activities.

To professor Viriato Semião for his technical supporting in developing a part of this work and for patience in guiding me through the results elaboration and interpretation.

To my colleagues for them technical and psychological support during the three years helping me solving practical problems and guiding me mentally in the right direction.

To my family and friends that during the three years supported me, showing interest and giving me the strength to complete this work.

Dulcis in fundo I would like to thank Romeo for showing me love and support lying on his preferred spot on the sofa. His constant watching gave me the strength to finish the thesis writing.

# Contents

**1 INTRODUCTION AND MOTIVATIONS**.....1

1.1 Introduction.....1

1.2 Kidney functioning.....2

1.3 Kidney pathologies.....4

1.4 Chronical Kidney Disease (CKD).....5

1.4.1 Uremia and Uremic toxins classification.....7

1.4.1.1 Small water-soluble compounds.....8

1.4.1.2 Large (middle) molecules.....9

1.4.1.3 Protein-bound compounds.....10

1.5 Renal Replacement Therapy (RRT).....11

1.5.1 History and available modalities.....11

1.5.2 Hemodialysis and its general principles.....13

1.5.2.1 Artificial kidneys: Hemodialyzers.....15

1.5.2.2 Mass transfer in hemodialyzers.....16

1.6 Hemodialysis drawbacks and emerging alternative solutions.....19

1.6.1 WAK design principles.....21

1.6.1.1 Spent dialysate regeneration systems.....22

1.7 Pressure driven membrane processes.....25

1.7.1 Classification and principles.....26

1.7.2 Common membrane configurations.....29

1.8 Adsorption onto porous materials.....32

1.8.1 Adsorption isotherm models.....33

1.9 The concept of Mixed Matrix Membranes (MMMs) for water treatments.....35

1.9.1 MMMs for water treatment.....35

1.9.2 MMMs for adsorption and hemodialysis applications ..... 37

1.10 Aim of the project ..... 39

**2 MATERIALS AND METHODS** ..... 47

2.1 Introduction ..... 47

2.2 Hemodialysis molecules targeted and analysis protocol ..... 47

2.3 Solid adsorbents chosen and their characterization ..... 49

2.3.1 Particle size distribution and zeolite activation procedure ..... 54

2.3.2 Adsorption kinetics and equilibrium isotherm experiments ..... 55

2.4 Membrane synthesis ..... 55

2.4.1 Synthesis of Mixed Matrix Membrane Adsorbers (MMMAs) ..... 57

2.4.2 Synthesis of hybrid cellulose acetate/$SiO_2$ for AK applications (CA/$SiO_2$) 59

2.5 MMMAs morphology and surface characterization ..... 62

2.5.1 Scanning Electron Microscopy (SEM) and Energy Dispersive X-ray analysis (EDS) ..... 62

2.5.2 Contact angle measurements ..... 64

2.5.3 Solvent uptake and density ..... 66

2.6 MMMAs flow and adsorption properties ..... 67

2.6.1 Pure water fluxes and Hydraulic Permeability ..... 67

2.6.2 Single-toxin batch removal capacity ..... 68

2.6.3 Batch removal capacity for a mixture of toxins ..... 69

2.6.3.1 High Performance Liquid Chromatography (HPLC) procedure ..... 70

2.6.4 Continuous removal capacity for single-toxin solutions and for a toxin mixture ..... 71

2.6.4.1 Fast Protein Liquid Chromatography (FPLC) set-up and procedure ..... 72

2.7 CA/$SiO_2$ hybrid membranes characterization in a surrogate system of an Artificial Kidney (AK) ..... 73

2.7.1 Permeation towards reference solutes: Molecular Weight Cut-Off (MWCO) ..... 76

2.7.2 Hydraulic Permeability and Apparent rejections coefficient experiments .. 77

2.8 Fluid mechanics characterization of a surrogate system of an artificial kidney (AK) ..... 78

2.8.1 Analog of Hagen-Poiseuille equation for an impermeable slit (rectangular section) ..... 79

2.8.2 Evaluation of permeation effect on the velocity profile ..... 80

2.9 Mass transfer characterization of a surrogate system of an artificial kidney (AK) 83

2.9.1 Convective transport through a porous membrane layer ..... 83

2.9.2 Useful dimensionless number and parameters ..... 84

2.9.3 Mechanisms in the fluid phase adjacent to the membrane ..... 86

2.9.3.1 The film theory ..... 88

2.9.3.2 Revision on mass transfer coefficients ..... 89

2.9.3.3 Other parameters influencing the mass transport ..... 91

2.9.4 Mechanisms in the membrane ..... 93

2.9.4.1 Stereochemical permeation model ..... 93

2.9.5 New integrated model of mass transport and ultrafiltration ..... 94

2.9.5.1 Methods for the experimental determination of mass transfer coefficients . ..... 95

2.9.5.2 Determination of a new dimensionless mass transfer correlation ..... 97

**3 EXPERIMENTAL RESULTS AND DISCUSSION** ..... 106

3.1 Introduction ..... 106

3.2 Adsorbents particle size distribution and adsorption properties ..... 107

3.2.1 Adsorption kinetics ..... 108

3.2.2 Equilibrium isotherms ..... 110

3.3 MMMAs synthesis, morphology and surface characterization ..... 114

3.3.1 SEM and EDS ..... 115

3.3.2 Solvent uptake and densities ..... 120

3.3.3 Contac angles ..... 121

3.4 MMMAs flow and batch adsorption properties ..... 122

3.4.1 MMMAs water fluxes and hydraulic permeability ..... 122

3.4.2 MMMAs batch adsorption properties with single toxin solutions ..... 127

3.4.3 MMMAs batch adsorption properties with a mixture of toxins ..... 131

3.5 MMMAs continuous adsorption experiments ..... 132

3.5.1 Continuous adsorption experiments with a mixture of toxins using a MMMAs cartridge ..... 140

3.5.2 Sizing of a cartridge for purification of spent dialysate ..... 142

3.6 Hybrid CA/$SiO_2$ ultrafiltration membranes characterization ..... 144

3.7 Fluid mechanics characterization of a surrogate system of an artificial kidney (AK) ..... 146

3.8 Development of a new dimensionless mass transfer correlation ..... 150

**4 CONCLUSIONS** ..... 167

# List of Figures


**Figure 1.1** Kidney anatomy..... 2

**Figure 1.2** a) Nephron anatomy and b) steps in urine production..... 3

**Figure 1.3** Prognosis of chronic kidney disease by GFR and albuminuria. Glomerular filtration rate (GFR) is expressed per body surface area, 1.73 $m^2$..... 6

**Figure 1.4** Hemodialysis scheme..... 14

**Figure 1.5** WAK system for hemodialysis..... 22

**Figure 1.6** Plate and frame configuration..... 30

**Figure 1.7** Spiral wound configuration..... 31

**Figure 1.8** Tubular configuration..... 32

**Figure 2.1** Cellulose acetate structure..... 57

**Figure 2.2** Phase diagram of a three-component system..... 58

**Figure 2.3** The teardrop-shaped volume of the specimen (interaction volume) with the type of electrons emitted or deflected for each region..... 63

**Figure 2.4** Contact angle formed by the liquid spread over a surface. $\gamma_{LG}$ is the between the liquid and the gas (air), $\gamma_{SG}$ is the surface tension between the solid and the gas (air), $\gamma_{SL}$ is the surface tension between the solid and the liquid and $\theta_C$ is the contact angle..... 65

**Figure 2.5** Ultrafiltration apparatus for the test of hydraulic permeability of MMMAs..... 68

**Figure 2.6** FPLC components set-up..... 72

**Figure 2.7** FPLC injection valve positions..... 72

**Figure 2.8** Scheme of the apparatus used..... 74

**Figure 2.9** Prospective draw of the membrane cell: the surrogate system of an artificial kidney (AK)..... 75

**Figure 2.10** Rectangular channel with a cross-section height h and width w, used to derive the Poiseuille flow equation for a slit..... 79

**Figure 2.11** Feed circulation channel geometry and axis..... 81

**Figure 2.12** Concentration profile in the layer adjacent to the membrane..... 86

**Figure 2.13** Illustration of the resistance in series model in the boundary layer adjacent to the membrane..... 88

**Figure 2.14** Algorithm used to calculate the parameters for the experimental mass transfer correlation..... 99

**Figure 3.1** ZUF particle size distribution before and after the dealumination process in HCl..... 107

**Figure 3.2** ZSM-5 particle size distribution before and after the dealumination process in HCl..... 108

**Figure 3.3** AC particle average dimensions..... 108

**Figure 3.4** Urea adsorption kinetics..... 109

**Figure 3.5** Creatinine adsorption kinetics..... 109

**Figure 3.6** Uric acid adsorption kinetics……... 110

**Figure 3.7** Urea adsorption isotherm..... 111

**Figure 3.8** Creatinine adsorption isotherm..... 111

**Figure 3.9** Uric acid adsorption isotherm..... 112

**Figure 3.10** ZUF logarithmic adsorption isotherm..... 113

**Figure 3.11** ZSM-5 logarithmic adsorption isotherm..... 113

**Figure 3.12** AC logarithmic adsorption isotherm..... 114

**Figure 3.13** Pure cellulose acetate membrane aspect……. 115

**Figure 3.14** MMMA_ZUF-15, MMMA_ZSM5-15, MMMA_AC-15 aspects.. 115

**Figure 3.15** SEM images of MMMAs prepared: a) SEM of the pure cellulose acetate membrane; b) SEM of the pure Cellulose Acetate 117

membrane after being compacted; c) MMMA_ZUF-15; d) MMMA_ZUF-30; e) MMMA_ZSM5-5; f) MMMA_ZSM5-15; g) MMMA_ZSM5-20; h) MMMA_AC-5; i) MMMA_AC-15; j) MMMA_AC-20……..

**Figure 3.16** SEM image of MMMA_ZUF-20 on which EDS was performed (red and blue circles)..... 118

**Figure 3.17** EDS of ZUF..... 119

**Figure 3.18** EDS on MMMA_ZUF-20: a) red circle; b) blue circle..... 119

**Figure 3.19** MMMAs water uptake..... 120

**Figure 3.20** MMMAs densities..... 121

**Figure 3.21** ZUF-based MMMAs water fluxes..... 123

**Figure 3.22** ZSM5-based and AC-based MMMAs water fluxes..... 123

**Figure 3.23** ZUF-based MMMAs permeability in time..... 126

**Figure 3.24** ZSM5-based and AC-based permeability in time..... 126

**Figure 3.25** Urea percentage removed according to the fillers loading..... 128

**Figure 3.26** Creatinine percentage removed according to the fillers loading..... 128

**Figure 3.27** Uric acid percentage removed according to the fillers loading..... 129

**Figure 3.28** Urea, creatinine and uric acid mass adsorbed ($m_{ads}$) for each series of MMMAs: a) ZUF-based MMMAs; b) ZSM5-based MMMAs and c) AC-based MMMAs..... 130

**Figure 3.29** Percentage adsorbed of urea, creatinine and uric acid from a mixture of toxins in graph a), b) and c); percentage removed of urea, creatinine and uric acid from single toxin's solutions in graph a1), b1) and c1)..... 132

**Figure 3.30** Breakthrough curves of urea a), creatinine b) and uric acid c) for MMMA_ZUF-5..... 133

**Figure 3.31** Breakthrough curves of urea a), creatinine b) and uric acid c) for MMMA_ZUF-60..... 134

**Figure 3.32** Breakthrough curves of urea a), creatinine b) and uric acid c) for MMMA_ZSM5-5..... 136

**Figure 3.33** Breakthrough curves of urea a), creatinine b) and uric acid c) for MMMA_ZSM5-30..... 138

**Figure 3.34** Breakthrough curves of urea a), creatinine b) for MMMA_AC-5... 139

**Figure 3.35** Breakthrough curves of urea a), creatinine b) for MMMA_AC-20. 140

**Figure 3.36** Breakthrough curves of urea, creatinine and uric acid for the MMMAs cartridge in contact with a mixture of toxins at 0.5 mL/min..... 141

**Figure 3.37** Breakthrough curves of creatinine for the MMMAs cartridge in contact with a mixture of toxins at the three different feed flow rates..... 141

**Figure 3.38** Maximum adsorption capacities, $q_{max}$, as a function of the flow rates..... 144

**Figure 3.39** MWCO of CA_30 a) and CA_22 b)..... 145

**Figure 3.40** Permeation fluxes as a function of the transmembrane pressure for CA_30 and CA_22..... 145

**Figure 3.41** Theoretical pressure drop calculated with different slit heights and experimental pressure drop with impermeable walls conditions..... 147

**Figure 3.42** Theoretical velocity profile u (y,z) at the slit middle planes, vertical and horizontal respectively (y=0; z=h/2)..... 147

**Figure 3.43** Theoretical and experimental pressure drop (permeable and impermeable walls conditions)..... 149

**Figure 3.44** Experimental pressure drops (permeable and impermeable walls conditions) with different solutes at different concentrations..... 150

**Figure 3.45** Urea permeation fluxes at 4 mg/mL and at 0.5 mg/mL..... 151

**Figure 3.46** Creatinine permeation fluxes at 0.24 mg/mL and at 0.012 mg/mL.. 151

**Figure 3.47** Uric acid permeation fluxes at 0.03 mg/mL and at 0.003 mg/mL.... 152

**Figure 3.48** para-Cresyl Sulphate (p-CS) permeation fluxes at 0.23 mg/mL, 0.10 mg/mL and at 0.05 mg/mL..... 152

**Figure 3.49** Bovine Serum Albumin (BSA) permeation fluxes at 10 mg/mL, 5 mg/mL, 1 mg/mL and at 0.2 mg/mL..... 153

**Figure 3.50** Urea apparent rejection coefficients at 4 mg/mL and at 0.5 mg/mL 154

**Figure 3.51** Creatinine apparent rejection coefficients at 0.24 mg/mL and at 0.012 mg/mL..... 154

**Figure 3.52** Uric acid apparent rejection coefficients at 0.03 mg/mL and at 0.003 mg/mL..... 155

**Figure 3.53** para-Cresyl Sulfate (p-CS) apparent rejection coefficients at 0.10 mg/mL and at 0.05 mg/mL..... 155

**Figure 3.54** Bovine Sereum Albumin (BSA) apparent rejection coefficients at 0.2 mg/mL, 1 mg/mL, 5 mg/mL and at 10 mg/mL..... 156

**Figure 3.55** Urea data elaboration for rejections experiments at 0.5 mg/mL a) and 4 mg/mL b)..... 156

**Figure 3.56** Creatinine data elaboration for rejections experiments at 0.012 mg/mL a) and 0.24 mg/mL b)..... 157

**Figure 3.57** Uric acid data elaboration for rejections experiments at 0.03 mg/mL a) and 0.003 mg/mL b)..... 157

**Figure 3.58** Para-Cresyl Sulphate (p-CS) data elaboration for rejections experiments at 0.05 mg/mL a), 0.1 mg/mL b) and 0.23 c)..... 158

**Figure 3.59** Bovine Serum Albumin (BSA) data elaboration for rejections experiments at 0.2 mg/mL a) and 1 mg/mL b)..... 158

**Figure 3.60** Comparison graph between $Sh_{exp}$ and $Sh_{corr}$..... 161

# List of Tables


**Table 1.1** Classification of the most common types of uremic toxins..... 8

**Table 1.2** Current WAK prototypes..... 24

**Table 1.3** Overview of the pressure driven membrane processes and their characteristics..... 26

**Table 2.1** Urea, creatinine, uric acid, p-CS and BSA characteristics..... 48

**Table 2.2** Characteristics of the zeolites chosen..... 53

**Table 2.3** Membranes casting solutions composition..... 62

**Table 2.4** Topological surface polar area of the toxins considered..... 70

**Table 2.5** Reference solutes used for MWCO calculation..... 76

**Table 2.6** Uremic toxins and BSA concentrations used in apparent rejection experiments..... 78

**Table 2.7** Types of accidentality present in the system from the pressure sensors till the membrane cell and their k values..... 82

**Table 2.8** Local pressure drop correlation for conical (tapered) geometries.. 82

**Table 2.9** Mass transfer correlation for Newtonian fluid for turbulent flow regime in pipes or between parallel plates..... 90

**Table 3.1** MMMAs advancing and receding contact angles..... 122

**Table 3.2** MMMAs hydraulic permeabilities..... 124

**Table 3.3** Mass of urea, creatinine and uric acid adsorbed by ZUF-based MMMAs in dynamic adsorption conditions..... 135

**Table 3.4** Mass of urea, creatinine and uric acid adsorbed by ZSM5-based MMMAs in dynamic adsorption conditions..... 138

**Table 3.5** Mass of urea, creatinine and uric acid adsorbed by AC-based MMMAs in dynamic adsorption conditions..... 140

**Table 3.6** Mass of urea, creatinine and uric acid adsorbed by the MMMAs cartridge from a mixture of toxins..... 142

**Table 3.7** Cartridge volumes obtained for the different flow rates..... 143

**Table 3.8** Experimental and calculated Sherwood number for urea..... 159

**Table 3.9** Experimental and calculated Sherwood number for creatinine and uric acid..... 159

**Table 3.10** Experimental and calculated Sherwood number for p-CS..... 160

**Table 3.11** Experimental and calculated Sherwood number for BSA..... 160

# 1 INTRODUCTION AND MOTIVATIONS

## 1.1 Introduction

The kidneys are bilateral organs, reddish-brown in color and located in the posterior abdomen. Healthy kidneys filter about 140 L of blood per day and excrete waste products producing urine. The urine flows from the kidneys to the bladder through two thin tubes called ureters, one on each side of the bladder. In case of renal failure (RF), a condition for which kidney function undergoes a decrease, products of metabolism and excess fluid are accumulated in the blood and cells. Renal failure can be reversible, Acute Renal Failure (ARF), or, when it is caused by other health problems damaging permanently the kidneys, the decrease in functionality normally is progressive and can lead to a Chronic Kidney Disease (CKD). When the kidney filtration rate becomes too low, the sole adequate treatment is a kidney transplant. To help patients to eliminate waste products and fluids while they are waiting for a transplant, a Renal Replacement Therapy (RRT) is needed. The most common renal replacement therapy is an extracorporeal method called hemodialysis and almost 10.5 million people need it approximately 3 times a week[1]. Despite being a fundamental treatment for people who suffer from a chronic kidney disease in a progressed phase, hemodialysis has several drawbacks for patients and from an environmental point of view:

- Patients are unable to live a normal life since the dialytic session lasts 4 hours and needs to be repeated at least 3 times a week. This can be partially solved with home dialysis sessions[2].
- Patients have dietary and fluid restrictions as to avoid too much liquid accumulation or high levels of sodium, potassium and phosphorus in blood.
- Being a substitutive therapy, hemodialysis is no able to completely replace the renal function and this leads to an accumulation of waste products in the blood and a consequent onset of correlated pathologies.
- The number of patients being treated for an end stage renal disease globally were estimated to be 3 million at the end of 2012. The minimum water consumption associated to dialysis every year is around 118 million liters. The annual minimum global power usage for hemodialysis is 17 billion kWh, while the minimum global disposable waste produced is 903 million kg each year[3].To face hemodialysis drawbacks, since more than 40 years, scientists and engineers are trying to develop

technologies that will enable the creation of a Wearable Artificial Kidney (WAK). This device will allow patients to have more mobility and freedom to conduct a normal life and moreover will significantly decrease the amount of water consumed and the energy and material costs associated to the process. Nevertheless, WAK technologies are far from being commercialized and a lot of work needs to be done to achieve the native kidney functionality.

## 1.2 Kidney functioning

The kidneys are two bean-shaped organs located in retroperitoneal space in vertebrates. They receive blood from the renal arteries and blood exits purified from waste products from renal veins. Each kidney is attached to a tube called ureter that carries urine to the bladder.

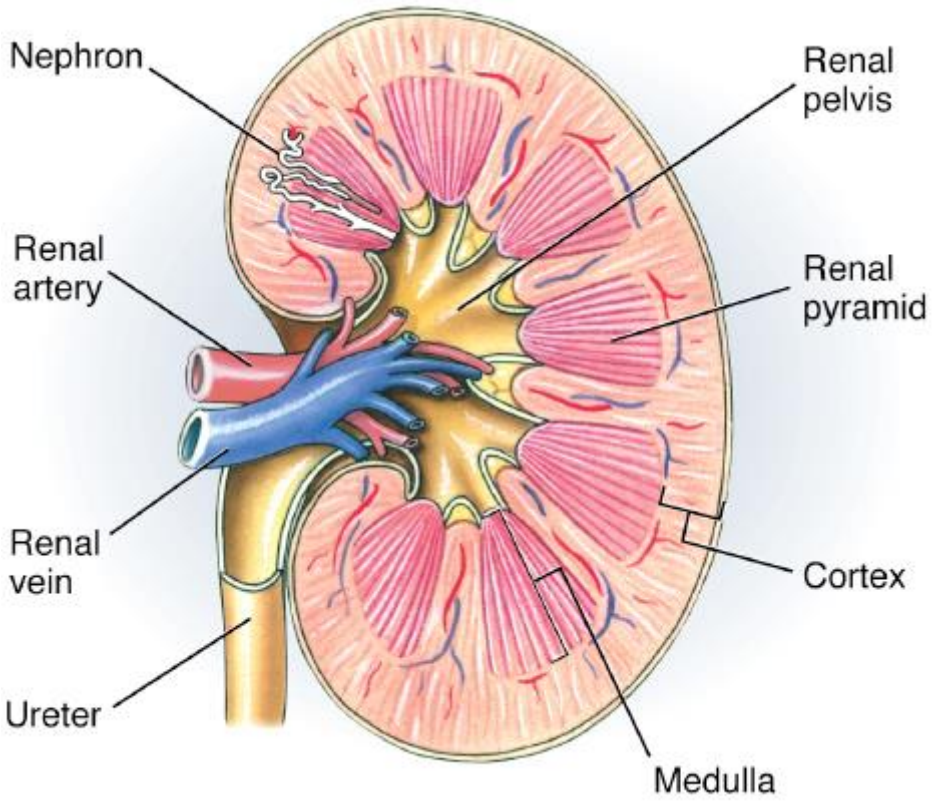


**Figure 1.1***: Kidney anatomy.*

The kidneys are involved in several organisms' activities and they excrete a variety of waste products produced by metabolism into urine. The structural and functional unit of the kidney is the nephron and each kidney of a human adult contains 1 million of them. The

nephron processes the blood supplied to it through filtration, reabsorption, secretion and excretion; the consequence of these processes is the production of urine.

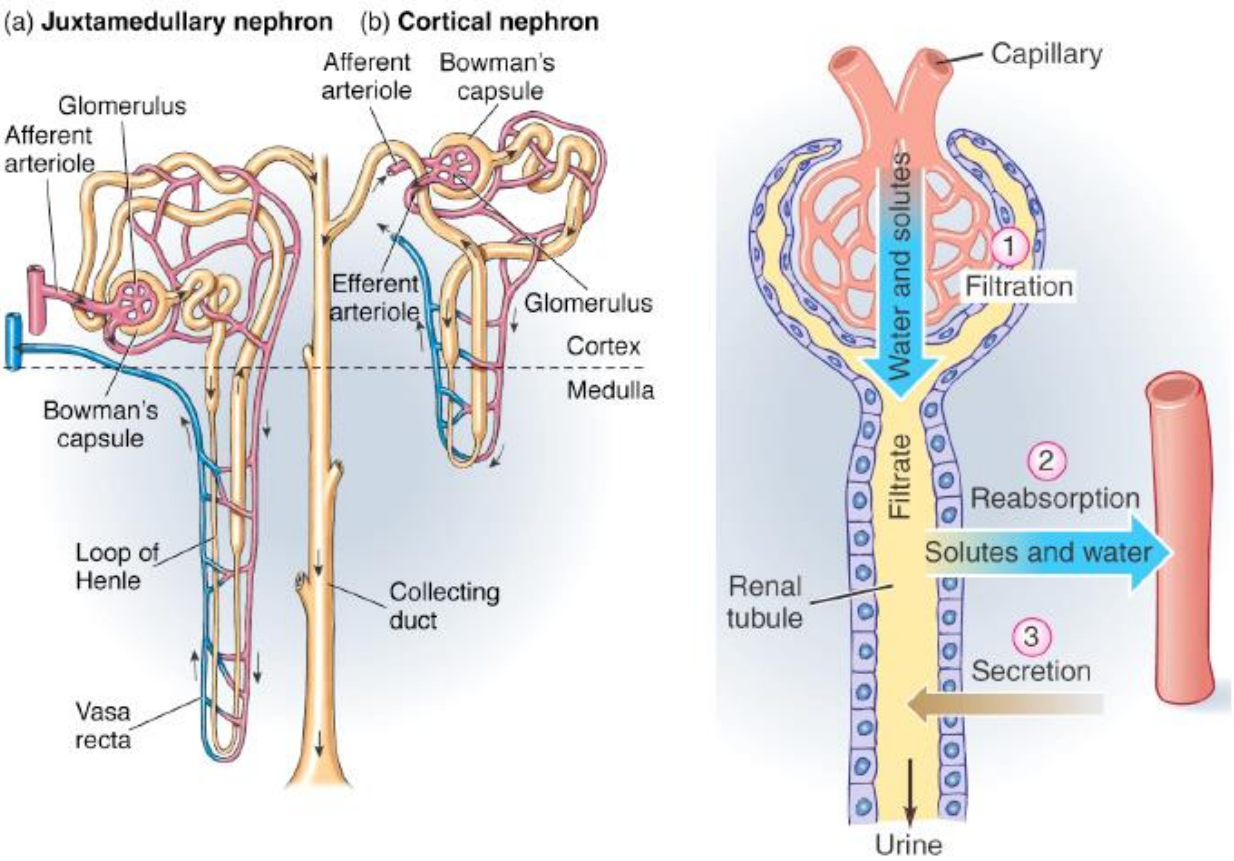


**Figure 1.2**: *a) Nephron anatomy and b) steps in urine production.*

The ability of mammals to concentrate wastes into a volume of urine much smaller than the volume of blood from which the wastes derived is the consequence of an elaborated countercurrent multiplication mechanism. This requires several independent nephrons abilities and characteristics: a tight hairpin configuration of tubules, water and ion permeability in the descending limb loop, water impermeability in the ascending loop, and active ion transport.

Urine production can be schematized by considering 4 main processes: filtration, reabsorption, secretion and excretion.

- **Filtration**: is the process through which cells and large proteins are retained, while substances of smaller molecular weights are ultrafiltered from the blood. The real protagonists of blood filtration in a kidney are the glomerulus. When blood flows in each nephron, it enters a cluster of tiny blood vessels, the glomerulus, and its thin

walls allow small molecules, waste and fluid to pass into the tubule. Larger molecules, such as proteins and blood cells, stay in the blood vessel.

- **Reabsorption**: The ultrafiltrate formed in the first process passes through a specific region of the nephron in which, through selective receptors, some vital components of blood are reabsorbed (water, glucose, amino acids and several ions). Reabsorption occurs in the tubule that returns the needed substances to the blood thanks to a blood vessel that runs alongside it. As the fluid flows inside the tubule, the blood vessel reabsorbs almost all of the water, minerals and nutrients.
- **Secretion**: Molecules are transferred into the ultrafiltrate; is the reverse of reabsorption.
- **Excretion**: The ultrafiltrate passes out of the nephron and travels through a collecting duct and then to ureters, where is renamed urine. It is the last step of urine formation.

The kidney participates in whole-body homeostasis, regulating acid-base balance, electrolyte concentrations, extracellular fluid volume, and blood pressure. The kidneys accomplish these functions both independently and jointly with other organs[4].

## 1.3 Kidney pathologies

Kidneys are fundamental organs for every of mammals specie, since they are involved in several vital function as explained in Chapter 1.2. Different pathologies can affect them[5]:

- **Kidney stones** are the most common kidney problem and they occur when minerals and other substances in the blood crystallize in the kidneys, forming solid masses (stones). They usually come out of the body during urination. The passage can be extremely painful, but kidney stones rarely cause significant problems.
- **Glomerulonephritis** is an inflammation of the glomeruli. This pathology can be caused by infections, drugs or congenital abnormalities. It often gets better on its own.
- **Polycystic kidney disease** is a genetic disorder that causes numerous cysts (small sacs of fluid) to grow in the kidney. The cysts can interfere with the kidney functions and cause kidney failure

- **Urinary tract infections** are bacterial infections of any part of the urinary system. Infections in the bladder and urethra are the most common. They are easily treatable and rarely lead to subsequent health problems. However, if left untreated, these infections can spread to the kidneys and cause kidney failure
- **Chronic Kidney Disease (CKD)** is the most common form of kidney disease. It is a long-term condition that does not improve over time and, commonly, it is caused by high blood pressure. High blood pressure is dangerous for the kidneys because it can increase the pressure on the glomeruli and damage their blood vessels. If the filtration rate of glomeruli is decreased, the kidney functions begin to decline. Another major cause of CKD is diabetes: the accumulation of sugar in the blood damages the kidney blood vessels over time leading to a reduction of filtration efficiency. Kidney function will eventually deteriorate to the point where the kidneys can no longer perform their job properly. In this case a person would need a Renal Replacement Therapy (RRT). One kind of renal replacement therapy is dialysis: it filters extra fluid and waste out of the blood through an extracorporeal circulation. This therapy can help treat kidney disease, but it cannot cure it.

## 1.4 Chronical Kidney Disease (CKD)

Chronic kidney disease (CKD) is a long-term condition caused damage to both kidneys which is usually irreversible and can lead to bad health. In some case dialysis or transplantation may become necessary. CKD affect 753 million people globally and in 2015 it caused 1.2 million of deaths. Diabetes mellitus, hypertension and glomerulonephritis are three most common causes of CKD and the sooner the diagnosis the better is the chance to survival, even if is a degenerative disease.

CKD can be related to a damage in the kidney (like albuminuria) or to a decrease in kidney filtration rate. The Kidney Disease Improving Global Outcomes (KDIGO) initiative classifies an individual as having CKD if abnormalities of kidney structure or function persist for more than 3 months. The severity of CKD can be described by the glomerular filtration rate (GFR, estimated or measured) and by the extent of albuminuria. They are used as indicators to classify CKD since GFR is a well-established marker of renal excretory function and albuminuria is an indicator of renal barrier disfunction[6].

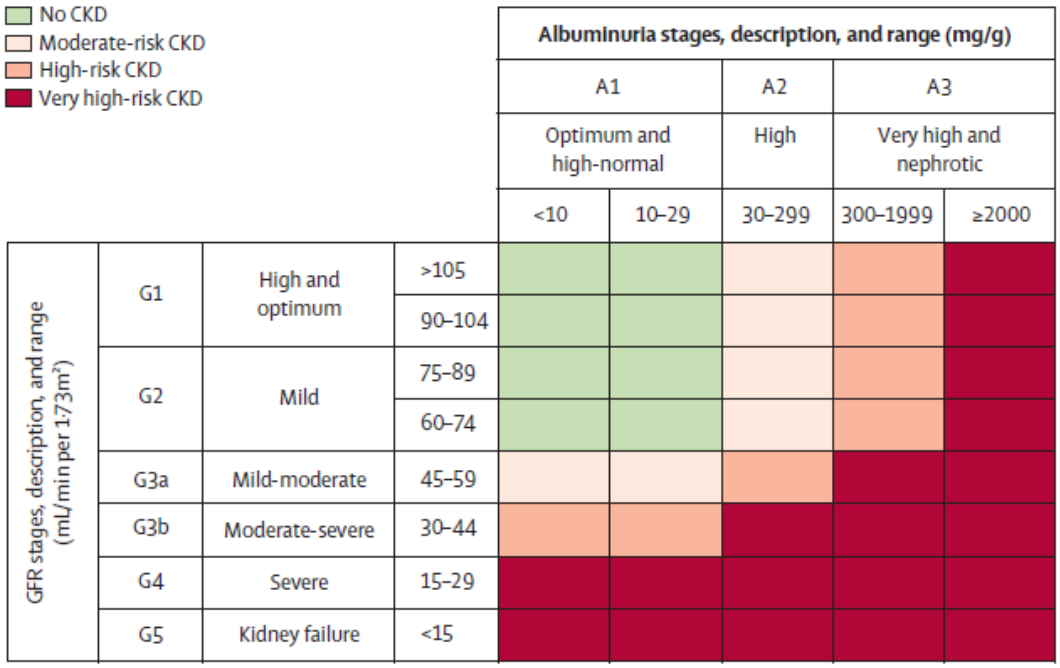


**Figure 1.3**: *Prognosis of chronic kidney disease by GFR and albuminuria. Glomerular filtration rate (GFR) is expressed per body surface area, 1.73 m$^2$.*

A normal GFR, expressed in mL/min per body surface area (1.73 m$^2$), according to the National Kidney Foundation range from 90 to 120 ml/min/1.73m$^2$ and it changes logically with age[7].

According to the gravity of the damage, CKD can be classified as follow

- **Stage 1**: GFR is around 90 ml/min/1.73m$^2$ with other associated sings of kidney malfunctioning like protein in the urine or physical damage of the organ.
- **Stage 2**: GFR is between 60 to 89 ml/min/1.73m$^2$ with other associated signs of kidney damage.
- **Stage 3**: GFR is between 30 to 59 ml/min/1.73m$^2$ and this parameter alone is sufficient to diagnose a reduction in kidney function
- **Stage 4**: GFR is between 15 to 30 ml/min/1.73m$^2$ and this means that the kidneys are moderate or severely damage and it is the last stage before kidney failure
- **Stage 5**: GFR is less than 15 ml/min/1.73m$^2$ and kidneys are getting really close to failure. Once failure come, the only solutions available for a patient are dialysis or transplant.

The prevalence of all stages of CKD varies between 7-12% worldwide. CKD stage G3-G5 are common in adults with values ranging between 1.7% in China to 6.7% in the USA. In Europe, the prevalence varies from 2.3% in Germany to 5.2% in England. The incidence of CKD is prevalently in people over 65 years of age, but the probability of progression to ESRD is higher in younger people. The most common treatments for CKD are hemodialysis and peritoneal dialysis; unfortunately, these renal replacement therapies can only slow down the progression of the disease, reducing the complications of the decrease of GFR and the risk of cardiovascular complications by trying to improve survival and quality of life of patients. The importance of the proper therapy chosen by doctors is crucial to increase the survival chances while waiting for a transplant.

The incidence of CKD is destined to increase year after year worldwide and together with the high costs and poor outcomes of the treatment it constitutes a threat to the public health system. Costs of dialysis and transplantation are increasing alongside with the costs of other chronic disease[8]. The ageing of population and obesity epidemic mean that this disease will probably be a menace to both developed and developing nations in a near future.

### 1.4.1 Uremia and Uremic toxins classification

The accumulation of toxic compounds in the body-serum compartments during the progressive development of a chronic kidney disease (CKD) is responsible for many of the clinical consequences of the condition called uremic syndrome or uremia. The solutes retained exhibit a vast range of physical-chemical characteristics, mechanism of generation and patho-biological action at a cellular or molecular level. They are called uremic toxins and they can be classified according the chemical fundamental and biological principles[9][10][11].

To properly understand uremic toxins, a precise definition of uremia needs to be given. Bergstrom and Frust defined uremia as a toxic syndrome caused by a severe glomerular deficiency associated with disturbance in endocrine functions of kidney. It is characterized by the retention of toxic metabolites associated with changes in volume and composition of the body fluids. The toxic metabolites can be classified on the base of several characteristics, but the most known categorization is the one according to their size and their distribution in the body fluid:

- **Small water-soluble compounds (molecular weight < 300 Da)**

- **Large (middle) molecules (molecular weight between 300 Da and 12000 Da)**
- **Protein-bound compounds (normally molecular weight < 300 Da)**

Table 1.1 summarizes the classification and lists the most common uremic toxins for each category

**Table 1.1**: *Classification of the most common types of uremic toxins.*

| Type | Water-soluble | Hydrophobic | Protein-bound |
|---|---|---|---|
| *Small molecules* | | | |
| *Guanidines* | √ | | |
| *Purines* | √ | | |
| *Oxalate* | √ | | |
| *Phosphorous* | √ | | |
| *Urea* | √ | | |
| *Middle molecules* | | | |
| *Cystatin C, Leptin* | | √ | |
| *Oxidation products* | | √ | |
| *Advanced glycosylation end products* | | √ | |
| *β-lipoproteins* | √ | | |
| *$\beta_2$-microglobulin* | √ | | |
| *Parathyroid hormone* | √ | | |
| *Protein-bound compounds* | | | |
| *Indoles* | | √ | √ |
| *Hippuric acid* | | √ | √ |
| *P-cresol* | | √ | √ |
| *Polyamines* | | √ | √ |

#### *1.4.1.1 Small water-soluble compounds*

Small water-soluble compounds are the one with the highest dialytic removal since they pass easily through the dialyzer membrane. Among this category the most abundant compounds are:

- **Guanidines** are structural metabolites of arginine, the substrate of nitric oxide (NO) production. Dialytic removal of the individual guanidino compounds is characterized by the substantial variability that cannot be explained by their physical-chemical characteristics. Protein binding or multi-compartmental distribution plays a role in this kinetic behavior.

- **Creatinine** is an end-product of muscle breakdown and it is a precursor of methylguanidine. It diffuses from red blood cells to plasma during transit of the blood through the dialyzer, so it is mainly extract during dialysis.
- **Purine**: the best-known purines retained in uremia are uric acid, xanthine, hypoxanthine and guanosine. The purines are involved in disturbances of calcitriol production and metabolism and they possibly could take part in calcitriol resistance that has been observed in renal failure. Dialytic removal of xanthine and hypoxanthine show no correlation with the removal of small water-soluble compounds while uric acid is removed from plasma efficiently. However, its removal from the intracellular compartment is less effective.
- **Oxalate**: oxalate clearance by peritoneal dialysis is only 8% of the normal renal clearance. Due to its water solubility and its size, it can be easily removed by efficient modern hemodialysis processes.
- **Phosphorous**: high level of organic phosphates are related to pruritus and hyperparathyroidism. The blood phosphorus concentration is the result of protein catabolism and intake of protein or phosphorus-rich dietary sources. Phosphate is easily removed by hemodialysis, but clearance from the intracellular component is considerably less substantial. Therefore, its dialytic removal is not always predictable.
- **Urea**: the presence of urea in blood is associated for the decrease affinity of oxygen for hemoglobin. Urea is the only solute that has been correlated with clinical outcome of hemodialysis and low reduction rates are related to increase of mortality. For these reasons, urea is considered as a marker of uremic toxins removal.

#### *1.4.1.2 Large (middle) molecules*

The accumulation in blood of large and middle molecules (molecular weight between 300 and 12000 Da) is responsible for several aspects of uremic syndrome like appetite inhibition and suppression of food intake. Dialysis membranes with a capacity to remove middle molecules have been related to lower morbidity and mortality of dialysis patients.

The middle/large toxins most representative of uremic syndrome are listed below:

- **Advanced glycosylation end products (AGE)** are involved in the modification of tissue structure and in functional alteration of enzymes. AGE are not efficiently removed by conventional dialysis, but elimination is significantly better with high-flux dialysis; however, despite the more efficient removal, levels in blood remain far from normal.
- **Peptides** are larger molecules that can be eliminated only with large pores dialyzers or they are not removed at all. Even if the removal is present level far away from normal are reached.
- **$\beta_2$-microglobulin**: dialysis-related amyloid, as found in amyloid bone disease and carpal tunnel syndrome after long-term dialysis, it is to a large extent composed of $\beta_2$-microglobulin. It has been suggested that the use of high permeability membranes lessens the possibility to develop dialysis amyloidosis.
- **Parathyroid hormone** is a middle molecule and is general recognized as a major uremic toxin, even if its increment during end stage renal disease is mainly attributed to enhanced glandular secretion.

#### *1.4.1.3 Protein-bound compounds*

This category of solutes is the most difficult to remove through hemodialysis since at least 90% of the total concentration of these toxins is bound to proteins, especially to albumin. Nevertheless, the protein-binding affinity varies from compound to compound. They normally enhance toxicity of protein-bound drugs competing for the binding to protein active site[12] [13].

- **Indoles** are found in various plants and they are produced by the intestinal flora. Some indoles concentration is not increased in uremia (like tryptophan and melatonin). Some of them are carcinogens whereas others are tumor growth inhibitors.
- **Hippuric acid**: Toluene is transformed to benzyl alcohol, then to benzoic acid and after glycination to hippuric acid. The free fraction of hippuric acid is easily removed during hemodialysis (up to 60% of removal), but since the majority is attached to proteins, its kinetic during the process is comparable with the one of large molecules.

- **P-cresol**: it is a phenolic, volatile compound and it is produced by intestinal bacteria as a result of tyrosine and phenylalanine degradation. Its removal during hemodialysis is markedly lower than the one of urea or creatinine because of the lipophilicity and its protein binding.

## 1.5 Renal Replacement Therapy (RRT)

Chronic Kidney Disease (CKD) induces the progressive loss of kidney functions. The gravity of the disease can be classified in 5 stages taking as reference the glomerular filtration rate. At stage 5 CKD, Renal Replacement Therapy (RRT) or kidney transplant is normally required. Nowadays, renal function support encompasses a broad range of methods and clinical scenarios, from the ambulatory patient to the critically ill. RRT can be applied continuously or periodically through extracorporeal (hemodialysis) or paracorporeal (peritoneal dialysis) techniques.

### 1.5.1 History and available modalities

Artificial support of the functions of failing organs has a history rooted at the beginning of the last century when Dr. John J. Abel and Dr. W. J. Kolff first dialyzer fed blood through cellophane tubing wrapped around a rotating drum placed in a dialysate batch. The rotation moved the blood through the dialysis bath and then, the return to the patients was controlled with a burette[14]. Nowadays, the modern hemodialysis treatment is inspired by the work of Dr. Nils Alwall. He compressed blood-filled cellophane tubing between an inner and outer cylinder. Dialysate passed in countercurrent to blood between the cylinder[15]. Apart from hemodialysis, peritoneal dialysis can be used as a support for kidney failure. The peritoneum was known as a “living dialyzer” since 1920 but, despite this early discover, clinical peritoneal dialysis was delayed until 1940 with the presentation of four cases by Dr. Jacob Fine. The continuous therapies of today have their origins in the 1960s, with an early description of pump assisted arterio-venous hemofiltration (CAVH) by Dr. Scribner[16].

RRT includes in its definition any modalities of blood purification therapies intended to substitute for impaired renal function. It employs only two types of physiologies for solute and fluid movement. Both techniques require blood passing through one side of a semi-

permeable membrane. In diffusive clearance (dialysis), thanks to a concentration gradient, the solutes move from blood towards a nonsterile aqueous electrolyte solution called dialysate. The solutes must have the right size and charge to pass through the membrane. This process must remove or add solutes to the plasma water according to the relative concentrations in plasma and dialysate. In addition to solutes diffusion, in RRT an important role is played by ultrafiltration; thanks to a pressure gradient, fluid movement from blood side to dialysis fluid side takes place. Moreover, this convective transport helps the removal of middle-size toxins improving the dialysis clearance.

This simple description hides much more complicated processes which involve a diffusion gradient dependent on the blood flow rate, on the dialysate flow rate, on the initial concentration gradients and on the concentration polarization at the membrane surface. Moreover, proteins affect the equilibrium of ions and the combination of diffusion and convection across the membrane alters the properties of individual methods in a complex manner.

RRT can be performed in different modalities and these can be classified according to the manner of access, to the duration, and to the dominant mechanism of solute clearance. The combination of these three parameters describes the permutations of RRT. This partition does not include peritoneal dialysis modalities, which can be ambulatorial or automated.

The subdivision according to the duration is the following:

- **Continuous Renal Replacement Therapy (CRRT)** replaces renal function at a relative low pace. The rate of solute and fluid removal is sufficiently slow that even hemodynamically unstable patients can tolerate the transcompartment water shift. The therapy is relatively efficient in replacing renal function, but since it runs continuously it is capable of doing enough kidney-like work to compensate the complications of renal failure.
- **Intermitted Hemodialysis (IHD)** is the much faster alternative; it does 72 hours of kidney work in 3/4 hours. As a result, the movement of solutes and fluid from the compartment is vigorous. The hemodynamic consequences of IHD often make it unsuitable for critically ill patients.

Apart from the faster flow rates, a key feature distinguishing IHD from CRRT is the origin of the dialysate fluid. Unlike CRRT which usually relies on pre-mixed bags of sterile dialysate and replacement fluid, IHD typically uses ultrapure water coming from

a reverse osmosis purification plant. As it is administered into the circuit, the water is mixed with solutes (sodium chloride, bicarbonate, potassium etc.) to more closely approximate plasma. This is probably the only feasible way to produce sufficient volumes of dialysate for IHD, because a massive number of people require intermittent dialysis and would be impractical to store sterile dialysate in bags.

According to the dominant mechanism of solutes clearance the methodologies can be classified as:

- **Hemodialysis** in which the diffusional clearance is the dominant mechanism.
- **Hemofiltration** in which convection and ultrafiltration are the principal mechanisms.
- **Hemodiafiltration** it combines both diffusional clearance and ultrafiltration.

### 1.5.2 Hemodialysis and its general principles

The history of dialysis dates back to the 1940s. The first artificial kidney was built in 1953 by William Kolff, a Dutch physician. He had the idea of developing a machine to clean the blood after watching a patient suffering from kidney failure. After several insolvency attempts, he went to the United States in the late 1940s and he tried to get kidney treatment to become a health service. In the early 1950s, more experimentation lead to the manufacturing of an improved design. However, Kolff's device was able to treat only kidney failure and not end stage renal disease (ESRD).

Dr. Scrinber, in 1962 opened the first official dialysis clinic for patients. He developed a portable dialysis machine that allows patients to receive treatment at home. By 1973, 40 % of patients were receiving home dialysis treatments. Nowadays, over 90 % of dialysis patients receive treatment at dialysis centers and several treatment options become available, among which hemodialysis is the most common.

In hemodialysis, waste is removed using an external filter called dialyzer, which contains a semipermeable membrane[17]. The separation of waste is done in counter-current flow gradient, where blood flows one way and the dialysis fluid in the opposite direction. The basic principle involved in the process is the movement or diffusion of solutes across the semipermeable membrane. The concentration of solutes normally found in urine (uremic toxins, potassium, phosphorous) are undesirably high in the blood, but low or absent in the

dialysis solution and the constant replacement of dialysate ensures that the concentration of undesired solutes is kept low on this side of the membrane. During their diffusion into the dialysis fluid (dialysate) the size of the molecules plays an important role defining the rate of diffusion across the dialyzer. The larger the molecule, the slower is the rate of diffusion across the membrane. The pore size of the semipermeable membrane is varied according to the size separation required. Solvents, ions and buffer can diffuse easily across the membrane, but large molecules are unable to pass through the pores. Apart from diffusion, ultrafiltration is another process occurring during dialysis, capable of removing excess fluid accumulating in patients with ESRD.

The dialyzer is composed of thousands of tiny synthetic hollow fibers through which the patient blood is pumped. In counter-current flows the dialysate wets the outer surface of the fibers. Solutes and excess fluid pass from blood to dialysate. The cleansed blood is returned to the circuit and back to the body as depicted in Figure 1.4:

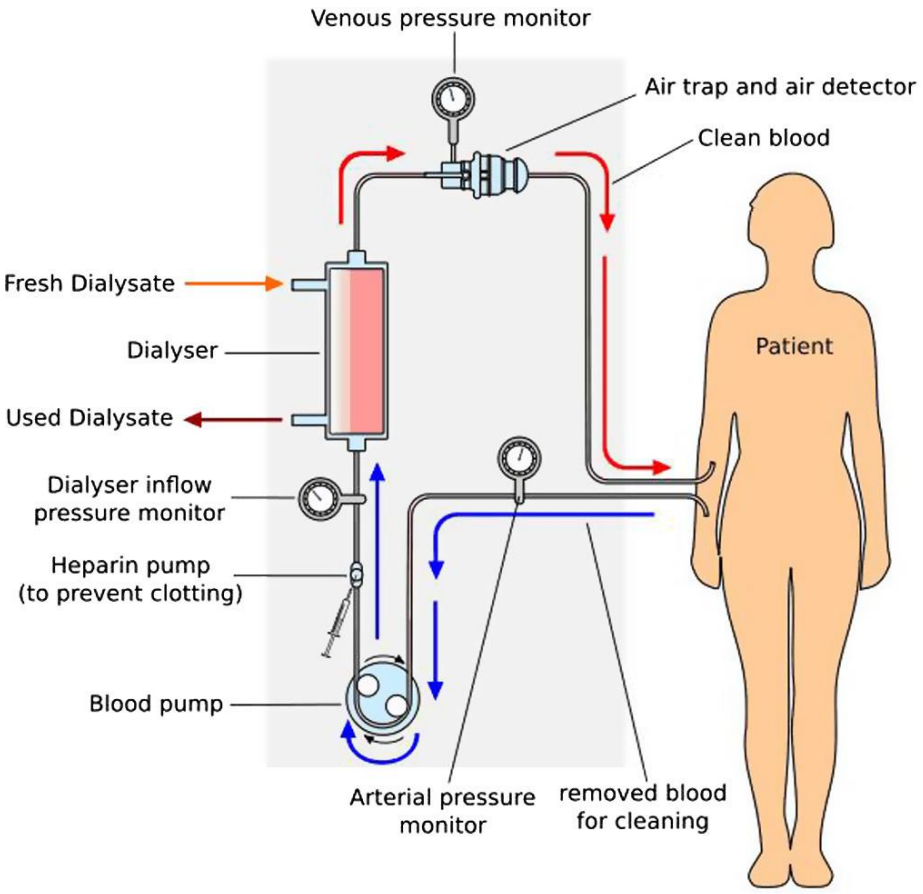


**Figure 1.4**: *Hemodialysis scheme*

The exhaust dialysis fluid, spent dialysate, is collected and disposed. Normally for each hemodialysis session, 120 L of fresh dialysate are used. Each patient, according the gravity

of the kidney malfunctioning, receives 3/4 treatment per week with a duration varying from 3.5 to 4.5 hours.

#### *1.5.2.1 Artificial kidneys: Hemodialyzers*

In this paragraph a more detailed description of the membrane performing the blood cleaning is given. In hemodialysis the blood of patient affected by kidney disease is cleaned through an extracorporeal circulation in a membrane module that removes excess fluids and toxic components substituting the kidneys function. Thus, the artificial kidney needs to filter, as efficiently as possible, the whole patient blood assuring a high removal of small and medium metabolites with an adequate filtration rate. Moreover, it must guarantee negligible losses of vital component such as proteins and amino acids together with a minimal activation of the immune system response pathways[18].

A dialyzer is composed of a selective membrane, a blood compartment, a dialysate compartment and a membrane support structure.

Dialyzers can be fabricated with different materials all tailored to minimize the negative interaction with blood that may cause immune system reactions.

- **Cellulose-based dialyzers** were the first one produced and used. They are obtained from regenerated cellulose, cuprammonium cellulose, cuprammonium rayon and saponified cellulose.
- **Substituted cellulose-based dialyzers** are based on cellulose polymers like cellulose acetate, diacetate and triacetate. Unfortunately, the presence of hydroxyl groups on the surface of the membrane makes them bio-incompatible due to the associated blood cell activation. They are not used anymore.
- **Cellulosynthetic-based dialyzers** are produced adding a synthetic component (a tertiary amino compound) to liquefy cellulose during the membrane formation resulting in a membrane surface modification to increase the biocompatibility.
- **Synthetic dialyzers** are made of synthetic polymers like polyacrylonitrile (PAN), polysulfone (PS), polycarbonate (PC), polyamide (PA), polyethersulfone (PES) and polymethyl-methacrylate (PMMA). Nowadays, they are the most used for their biocompatibility, high removal efficiency and ultrafiltration fluxes.

Configurations of hemodialyzers underwent several modifications during the years with the scope of increase their efficiency, both in terms of uremic toxins removal and in ultrafiltration capacities. The common dialyzers configurations are listed below:

- **Coil dialyzers** in which flattened tubes are wrapped as a coil through which blood patients flows. Unfortunately, the blood channel was so long and it was not possible to obtain the surface area needed and the resistance to the flow was too high. Moreover, the ultrafiltration rate was not predictable and blood leakages were frequent.
- **Parallel plate dialyzers** in which flat sheets of membranes are positioned between supporting plates which have ridges and grooves to support them and to let the dialysate flow. They have a low resistance to the blood current and the surface area can vary between 0.25 to 1.5 $m^2$.

  They present several advantages, such as relatively low blood volume (which increases with TMP), low heparin requirement, minimal blood compartment clotting and predictable and controllable ultrafiltration. On the other hand, the formation of thrombi is frequent close to the inlet and outlet ports and corners and the plates are not reusable due to bacterial growth and endotoxin formation.
- **Hollow fiber dialyzers**: nowadays they are the most used. They have the typical hollow fiber membrane module configuration where thousands of fibers, with a really small diameter (150-250 μm) are packed. Normally the blood flows inside the fiber and the dialysate wets the outside part. It has a low blood volume, low blood resistance, it can be easily reuse and ultrafiltration can be precisely controlled. On the other hand, the fibers need to be treated before the use to prevent air trap into them and use of heparin is intense[19].

#### *1.5.2.2 Mass transfer in hemodialyzers*

As mentioned in the previous paragraphs, the transport phenomena that occur in dialysis processes are diffusion and convection[20]. The diffusion mechanism follows Fick's law:

$$J = -D_s \cdot A \cdot \frac{dC}{dx} \qquad (1)$$

where $J$ is the net solute flux (mol/s), $D_s$ is the solute diffusivity ($m^2/s$) being a unique property of the solute/solvent system at a specific temperature, $A$ is the area of diffusion ($m^2$) and $dC/dx$ is the concentration gradient ($mol/m^3$) over the membrane thickness (m)

Ultrafiltration is the convective mechanism that allows, thanks to a pressure difference, the flow of fluids and solutes. It is governed by the Darcy's law:

$$Q = L_p \cdot A \cdot \Delta P \tag{2}$$

where $Q$ is the volumetric flow rate (L/h), $\Delta P$ is the transmembrane pressure (bar) and $L_p$ is the hydraulic permeability (L/(h $m^2$ bar) and A is the area involved in the permeation ($m^2$).

When Equation (1) is practically applied in hemodialysis, it requires the introduction of coefficients that can help the clinical practice and the dialyzer design. It is possible to define an overall mass transfer coefficient $K_0$ (m/s) transforming Equation (1) in:

$$J = -K_0 \cdot A \cdot \Delta C \tag{3}$$

The inverse of $K_0$ can be defined as the resistance to diffusive transport comprehensive of the blood side, the membrane and dialysate side resistances, respectively. Thus, the dialyzer performance can be improved reducing the largest resistance. The blood and dialysate resistances are mainly due to the diffusional distances from the bulk of the fluid to and from the membrane. The resistance associated to the membrane depends on its thickness as well as on its diffusivity that varies according to its chemical composition. The diffusive dialysance D (mL/min) is defined as the change in solute content in the blood entering the dialyzer per unit of concentration:

$$D = \frac{Q_{Bi} \cdot (C_{Bi} - C_{Bo})}{C_{Bi} - C_{Di}} = \frac{Q_{Di} \cdot (C_{Do} - C_{Di})}{C_{Bi} - C_{Di}} \tag{4}$$

where $Q_{Bi}$is the blood flow rate in (mL/min) and $C_{Bi}$, $C_{Bo}$, $C_{Di}$ and $C_{Do}$ are the concentration of the target components in the blood inlet, blood outlet, dialysate inlet and outlet respectively. Since in hemodialysis the inlet concentration of the dialysate of the components to be removed is zero, Equation (4) can be simplified, obtaining the definition of diffusive clearance K (mL/min) (definition that is the analog of the physiological kidney clearance):

$$K = \frac{Q_{Bi} \cdot (C_{Bi} - C_{Bo})}{C_{Bi}} = \frac{Q_{Di} \cdot (C_{Do} - C_{Di})}{C_{Bi}} \tag{5}$$

When ultrafiltration takes place, the diffusive clearance is enhanced by the net ultrafiltration contribution $Q_{UF}$ (mL/min):

$$K' = \frac{Q_{Bi} \cdot (C_{Bi} - C_{Bo})}{C_{Bi}} + Q_{UF} \cdot \frac{C_{Bo}}{C_{Bi}} = K + Q_{UF} \cdot \frac{C_{Bo}}{C_{Bi}} \quad (6)$$

In reality, to assess the adequacy of dialysis a clearance index, $K \cdot t/V_{urea}$, is used and it normally ranges from 1.2 to 1. This indicator is higher for better clearance K, longer dialysis time, t, and for small patient distribution volume, $V_{urea}$. An increase of the clearance index is associated with a decrease of death risk due to cardiac and infectious diseases. This index monitors only the removal of low molecular weight solutes, it is defined by multiplying the overall mass transfer coefficient $K_0$ for the membrane area, A. $K_0 \cdot A$ and $K \cdot t/V_{urea}$ are related through the Michaels Equation:

$$K_0 \cdot A = \frac{Q_B}{\frac{Q_B}{Q_D} - 1} ln\left(\frac{Q_B - D}{Q_B - D \cdot \frac{Q_B}{Q_D}}\right) \quad (7)$$

$K_0 \cdot A$ is a dialyzer specific parameter.

Together with the mass transfer to and from the patient, there is also a water movement towards and from the dialysate compartment to control the patient's fluid volume distribution. The ultrafiltration coefficient, $K_{UF}$ (mL/min/mmHg) can be written as:

$$K_{UF} = \frac{Q_{UF}}{\Delta P - \Delta\pi} = \frac{Q_{UF}}{TMP} \quad (8)$$

where $\Delta P$ is the hydraulic pressure difference between blood and dialysate and $\Delta\pi$ is the osmotic pressure difference associated to the presence of proteins in the blood side. The difference between the two terms is the effective transmembrane pressure, TMP, that allows the fluids filtration. High flux dialyzers, able to remove solutes also through ultrafiltration, have therapeutic advantages, since they can remove small solutes by diffusion through the pores and middle molecules by diffusion and convection. One disadvantage of high flux dialyzers is the occurrence of back filtration that can cause bacterial contamination by liquid bicarbonate and the consequent transport of endotoxins in the blood compartment. Moreover, after the membrane exposure to proteins, their adsorption on the membrane occurs and the hydraulic permeability and the diffusive transport decrease significantly. Furthermore, the linear increase of ultrafiltrate flux with TMP is lost at high pressures due to the concentration polarization of high molecular weight solutes which are not filtered through the membrane pores.

## 1.6 Hemodialysis drawbacks and emerging alternative solutions

Dialysis is a necessary procedure for most people with kidney failure. Although the past decade had witnessed a modest improvement in the survival of people undergoing dialysis, the mortality continues to be unacceptably high[21]. Numbers of prevalent CKD patients will continue to rise, denoting the growing of elderly population and the increasing number of patients with diabetes and hypertension. Progress of CKD is connected to several serious complications, including the increased incidence of cardiovascular diseases, hyperlipidemia, anemia and metabolic bone disease. CKD patients should be carefully treated according to the complications associated to the renal pathology to reduce the mortality and morbidity to a minimum. To achieve this goal a multidisciplinary approach is required.

Some of the common CKD complications are listed below:

- **Gout** is a type of arthritis that causes swelling and pain in joints. It is a chronic disease that causes sudden and severe attacks often in the big toe. CKD and gout are often associated and interconnected.
- **Anemia**; The kidneys help the body to produce red blood cells (RBCs) and CKD patients may present a shortage RBCs and they may experience anemia. People suffering from an ESRD undergoing dialysis often have anemia as complication of their kidney loss of function.
- **Metabolic acidosis**: is a buildup of acid in the body due to the impaired ability of kidneys in regulating the acid balance in the body.
- **Bone disease and high phosphorus (hyperphosphatemia)**: healthy kidneys help to keep the right amount of phosphorus in the body. When their functionality is damaged dangerous levels of phosphorus can accumulate in the patient blood (hyperphosphatemia). Phosphorous with calcium and vitamin D are responsible for the health of bones, so the three components need to be balanced. The body when it is in phosphorous shortage pulls calcium from the bones to try to maintain the balance. This causes bone diseases.
- **Heart disease** is the most common cause of death. When the kidneys are not working properly, they cannot support other organs as they should.
- **Fluid buildup**: the kidneys filter extra fluid from the body producing urine and when they are affected by a disease, they reduce this function and extra fluids start

to accumulate. High amount of fluid in the body is connected to lungs and heart pathologies. It can also cause high blood pressure, which is the second most common cause of kidney failure.

Among all, cardiovascular syndrome has become a major concern in clinical practice since it is responsible for approximately half of the death of patients with CKD. Protein-bound uremic toxins (PBTUs) have been lately recognized as possible missing connection in cardiovascular syndrome. This has been well demonstrated with two potent toxins: indoxyl sulfate (IS) and p-cresyl sulfate (p-CS). Their removal during dialysis is problematic since they are found preferentially attached to albumin, a vital protein that needs to be retained during renal replacement therapy. Both IS and p-CS are implicated in CKD progression and cardiovascular complications which are the most common cause of death for ESRD patients.

Moreover, another drawback of having a renal disease is associated to the complete change of life affecting CKD patients. Their life needs to be reorganized and arranged according to the gravity of the failure and the treatment method. The therapy also implies limitations on the diet as well as on physical activities. Therefore, the intensity of mental and somatic symptoms largely affect the level of quality of life as perceived by the patients[22].

In addition to the health and life consequences associated to the hemodialysis procedure, studies have shown a tremendous environmental impact connected to water, electricity, and disposable materials consumption of the process. Fresenius Medical Care reports three million of ESRD patient with 7% of annual growth worldwide in 2012; if this is matched with the information regarding the consumption of natural resources by dialysis services, the environmental impact of an apparently small individual medical treatment like dialysis becomes conspicuous. Even if water consumption for hemodialysis depends on the type of machine, pre-treatment system (RO, prime, rinse and sterilization) and session length and frequency, the mean water consumption for each session is 500 L. Of this 500 L, approximately 1/3 is used is used for dialysis after the purification and sterilization process, while 2/3 are sent to the drain. Although not all hemodialysis patients receive the treatment 3-4 times per week, using these values to calculate the annual water usage for hemodialysis worldwide brings to 164 billion L. Moreover, the weight of recyclable post-hemodialysis consumables is between 2.5-2.9 kg per treatment. Assuming an average value of 2.75 kg

of waste, which is almost all classified as infectious waste and sent to landfill or incineration, the overall waste produced per year is 900000 ton.

Therefore, there is an urgent need to find smart solutions to alleviate both the weight of this procedure for the public health care system and for patients whose life is completely put on hold.

For more than 40 years, researchers are trying to miniaturize dialysis machines to make them portable and wearable. The main reasons associated to these efforts are to increase the compatibility and cost-efficiency of the process and, more important to increase the life expectancy and improve the quality of patients' life. One way to achieve this is to operate a continuous blood filtration like kidneys do, for approximately 168 h per week, differently from quick traditional hemodialysis filtration (20 h per week) that badly affect the organism. Along with this, common treatment imposes to patient to be near the dialysis machine while with the wearable system ESRD patients could lead a normal life. Therefore, a wearable artificial kidney (WAK) has potentialities to overcome the negative sides of the common renal replacement therapies[23].

WAK potentially presents several advantages with respect to the common hemodialysis treatment:

- increasing patient's mobility reducing the size of the apparatus.
- adjusting blood purification to human physiology.
- reduction of water consumption (21 L of dialysate per procedure instead of 120-150 L for hemodialysis).
- cost reduction; ~45,000 € per patient per year using WAK instead of 59,600 € for ambulatory treatments.
- higher life quality due to the ability of using WAK in everyday life routine.

### 1.6.1 WAK design principles

To be used as a valid alternative to the common dialysis procedure a WAK system needs to respect several requirements:

- safety and biocompatibility; it must be equipped with temperature, volume, pH, ionic solution sensors and must have a bacterial contamination prevention system.
- ease to use: ergonomic and light.

- durability and reliability: must work properly for a long period.
- availability: must be affordable for everyone.
- continuous power supply needed; it must be equipped with a battery that guarantees at least 8 hours of functioning.
- portability and implantability.
- equipped with a dialysate regeneration system that needs to remove uremic toxins from the dialysis fluid with an adequate speed and with an acceptable efficiency.

In the last years, WAK technology was applied mainly to peritoneal dialysis (PD) while for the implementation in hemodialysis (HD) it is necessary an anticoagulant infusion to prevent blood clotting in the dialyzer. In addition, the system needs to be equipped with an air trapping tool and it must have fix blood catheters. Figure 1.5 represent a scheme of WAK system for hemodialysis, where DRU stands for dialysate regeneration unit.

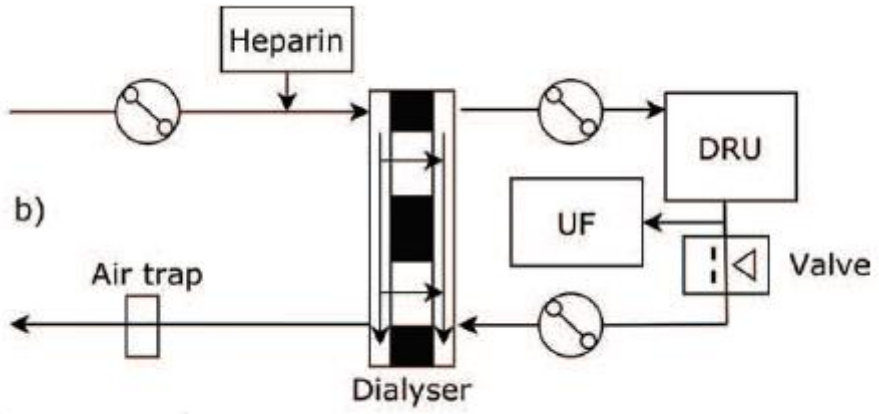


**Figure 1.5**: *WAK system for Hemodialysis.*

Another characteristic of WAK is the method of ultrafiltration that for hemodialysis implies the use of two peristaltic pumps to guarantee the pressure difference between the two compartments of the dialyzer.

#### *1.6.1.1 Spent dialysate regeneration systems*

Regeneration of spent dialysate in WAK occurs in the regeneration units; this can be achieved with different technologies. Ideally, WAK must eliminate all the contaminants (uremic toxins) from the dialysis solution, but it is difficult to implement and validate. To work properly, the dialysis fluid coming out from the regeneration unit must be chemically

equivalent to the fresh dialysate. At the current state of WAK development this is not achievable. Urea, creatinine, uric acid, phosphates, p-cresol and potassium must be eliminated from the dialysis fluid to guarantee the blood purification in the dialyzer again. Moreover, spent dialysate regeneration is crucial to maintain the ionic balance of the dialysis fluid ($Ca^{2+}$, $Mg^{+}$, $K^{+}$, $Cl^{-}$).

Adsorption is the most common method for removing a wide range of contaminants. Even if it is a powerful decontamination technique, the elimination of urea and other small metabolites is not efficient, and therefore, there is the need to couple it with a functional removal method for low molecular weight solutes. Among them, urea is the most problematic due to its size and high concentration in the spent dialysate.

The most widespread methods for the elimination of urea are:

1. Enzymatic decomposition
2. Electrolysis
3. Thermal decomposition

1. Enzymatic decomposition implies the use of animal or plant derived urease to hydrolytically decompose urea into ammonia and carbon dioxide. Its combination with sorption is currently used in WAK prototypes. The advantage of this solution is its simple use, since the tubing and the adsorption unit can be easily replaced by the patient. On the other hand, several system drawbacks are observed: the complexity of storing and preparing immobilized urease (up to one month at 4°C), together with its excessive cost and the presence of aluminum in the restored dialysate make it not suitable for the purpose.

2. Electrolysis involves the use of electrolytes and apposite electrodes to decompose urea and other metabolites. This implies the production of side-products which must be removed by activated carbon adsorption. The main issue for urea electrolysis is the choice of an effective and safe electro-catalyst. From a literature review[24], it emerged that urea can be electrochemically oxidized in neutral medium using noble metals catalyst such as Ru-$TiO_2$, Ti-Pt, Ti-(Pt-Ir). Nevertheless, their high cost is precluding their practical application. The research and development of electrode cheaper materials (like graphite or other carbon-based materials) is under investigation.

3. Thermolysis heats the spent dialysate until the urea decomposition temperature. This method is not indicated to be used in WAK due to its high energy consumption and by-products generation.

Considering what reported above, the combination of electrolysis, enzymatic decomposition and adsorption can be considered the most effective way to regenerate spent dialysate eliminating all the metabolites. Several research groups have already prototyped WAKs with different regeneration methods, system configuration and characteristics. Table 1.2 reports a summary of the WAK systems developed so far.

**Table 1.2***: Current WAK prototypes.*

| Name | Type | Regeneration method | Characteristics | Current Status |
|---|---|---|---|---|
| *ViWAK[25]* | PD | Sorption + urease | 0.2 kg, 17x8x3 cm, 10 h battery life | Prototype |
| *The WAK[26]* | HD | Sorption + urease | 5kg, on-waist wearable 8 h battery | Pre-clinical trials |
| *EO NAIP[27]* | PD | Sorption + electrolysis | 3.5 kg, backpack | Pre-clinical tests |
| *SORB[28]* | PD | Sorption + urease | 2 kg, on-waist wearable | Prototype |
| *AWAK[29]* | PD | Sorption + urease | 1 kg, shoulder bag, 16 h of battery life | Pre-clinical trials |
| *WAK-MAN[30]* | HD | Sorption | Vest, 24 h battery life | Prototype |
| *WAKD[31]* | HD and PD | Sorption + electrolysis | 3.2 kg, on-waist wearable | Pre-clinical trials |

In a near future, wearable dialyzers will be the common blood purification treatment overcoming the existing apparatuses and methods. To start this revolution, WAK systems need to be implemented with a valid dialysate regeneration system that effectively removes small water-soluble compounds. Moreover, a problem that must be solved especially for WAK application in PD, is the choice of the osmotic agent. It is needed to remove excess fluid from the body, and it needs to be biocompatible, cheap and with the right molecular weight as to avoid absorption in the blood stream. There still a lot of research and work to do, since the ultimate goal is to achieve the performance of a native kidney. However, if the proposed technology will be more economical then HD and PD treatment, it will

revolutionize ESRD patients life and it will be able to raise the number of people with CKD who receive a renal replacement therapy.

As already mentioned in the previous paragraphs, hemodialysis is based on a membrane process. The advancement in membrane technology achieved in the last decades allow the obtainment of the present hemodialysis solutions. Therefore, in the next paragraphs an overview of the principal membranes processes, with a particular focus on pressure driven membrane processes, is presented.

## 1.7 Pressure driven membrane processes

Membrane technology is widely utilized for different engineering approaches and it involves the transport of substances between two streams with the help of a semipermeable membrane. Generally, mechanical separation of gaseous or liquid fractions presuppose a membrane technology. It uses less energy than conventional thermal separations such as distillation, crystallization or sublimation. It is a physical separation process that produces two phases, permeate and retentate, which can be both used according to the product of interest. The mechanisms of transport through the membrane can be generally classified with two basic models: solution-diffusion and hydrodynamic. According to the driving force involved in the process, it possible to classify membrane operations into:

1. Pressure driven processes
    - Microfiltration
    - Ultrafiltration
    - Nanofiltration
    - Reverse Osmosis
2. Concentration driven processes
    - Dialysis
    - Pervaporation
    - Forward Osmosis
    - Artificial Lungs
    - Gas separation
3. Processes in an electric potential gradient
    - Electrodialysis

- Membrane electrolysis
- Electrodeionization
- Fuel cell

4. Processes in a temperature gradient
    - Membrane distillation

Hemodialysis is based on a membrane filtration process, in which the driving forces present are a difference in concentration and in pressure between the blood and the dialysate side.

### 1.7.1 Classification and principles

Membrane operations can be described as a feed stream, separated by a membrane into a retentate fraction (or concentrate) and a permeate. In the case of pressure driven operation, the driving force for the process is a pressure difference between the feed side and the permeate one and this allow the transport of liquid and or solid particles through the membrane[32]. According to their size, shape and charge, dissolved components in the feed solution can pass through the membrane or they can be retained (almost completely or partially). In Table 1.3 an overview of pressure driven membrane processes and their characteristics is reported.

**Table 1.3***: Overview of pressure driven membrane processes and their characteristics.*

| | **Microfiltration (MF)** | **Ultrafiltration (UF)** | **Nanofiltration (NF)** | **Reverse Osmosis (OR)** |
|---|---|---|---|---|
| *Permeability (L/(h m$^2$ bar)* | >1000 | 10-1000 | 1.5-30 | 0.05-1.5 |
| *Pressure (bar)* | 0.1-2 | 0.1-5 | 3-20 | 5-120 |
| *Pore size (nm)* | 100-10000 | 2-100 | 0.5-2 | <0.5 |
| *Rejection* | Particles | Multivalent ions<br>Macromolecules<br>Particles | Multivalent ions<br>Small organics compounds<br>Macromolecules<br>Particles | Monovalent ions<br>Multivalent ions<br>Small organics compounds<br>Macromolecules<br>Particles |
| *Separation mechanism* | Sieving | Sieving | Sieving<br>Charge effects | Solution-Diffusion |

| | | | | |
|---|---|---|---|---|
| *Applications* | Clarification<br>Pretreatment<br>Bacteria removal | Macromolecules, bacteria and viruses removal | Multivalent ions and small organic removal | Ultrapure water<br>Desalination |

From Table 1.3 is possible to understand that pressure driven processes can be classified according to several characteristics. In the following list, the main features and fabrication materials of each category are presented[33]:

- **Microfiltration (MF) membranes**: only large particles, with diameters in excess of about 0.1 μm are separated by the membrane that is a symmetric or asymmetric porous one. The diffusion of particles and the osmotic pressure difference between the feed and the filtrate solution are negligible and the mass flux through the membrane is regulated by the hydraulic permeability, the pressure difference and the membrane thickness. The type of transport involved in MF membranes is based on viscous flow, where the filtration is caused by a hydrostatic pressure difference between the two phases (feed and permeate) and the mass transport takes place through the pores. The solid membrane matrix is completely impermeable. Therefore, the hydraulic permeability can be expressed in terms of viscosity, pore size and porosity according to the Hagen-Poiseuille law. An important parameter to take into account is the membrane tortuosity that is defined as the ratio between the actual pore length and thickness of the membrane. The efficiency of the separation is described by the rejection coefficient, R, of a particle of a certain size. This is a parameter that defines the separation achievement of all the pressure driven membrane processes, and it is always less than one and a function of the particle size and the pore size distribution. Both ceramic and polymeric materials can be used to fabricate these types of membranes; ceramics has the advantage of high chemical, thermal and mechanical stability together with the ease of cleaning and long durability. However, the production processes in large scale are expensive and difficult due to the brittleness of the materials. Polymeric membranes, due to their easy use, flexibility, adaptability and low cost, dominate the international market. Common commercial polymers for MF and UF are poly (ether sulfone) (PES), poly (vinylidene fluoride) (PVDF), polyethylene (PE), polypropylene (PP) and

polytetrafluorethylene (PTFE). Apart from PES, are all hydrophobic materials and PE, PP and PTFE are not soluble at room temperature in organic solvent, making the manufacturing process difficult.

- **Ultrafiltration (UF) membranes**: in ultrafiltration the driving force is a pressure gradient and the mass transport is dominated by the convective flux through pores. UF membranes, differently from MF, have an asymmetric pore structure, with the smallest pore on the surface (active layer) facing the stream to be treated. The solutes retained by UF have a molecular weight ranging from 5000 Da to several million Dalton. Since UF can also reject relatively low molecular weight components, osmotic pressure plays and important role in affecting the separation and diffusive fluxes cannot be neglected for this category. Therefore, the components fluxes can be represented as a function of the hydrostatic pressure and a difference in chemical potential of the different components between the feed and the permeate streams. Thus, the volumetric flux will be the sum of fluxes of the individual components. In real applications, the osmotic water transport, if the hydrostatic pressure difference is significantly higher than the osmotic pressure difference between the feed and the permeate solution, can be neglected. The materials used to fabricate these membranes are the same as the ones used for MF.
- **Nanofiltration (NF) membranes**. Differently from membranes with larger pore size, solute transport in nanofiltration is more complex. Because of the pore size, three mode of transport are possible through these membranes: 1) diffusion (due to concentration gradients), 2) convection (flow through the pores, like in MF) and 3) electromigration (attraction o repulsion from charges within and near the membrane). Most filtrations operate only by size exclusion, but in NF the effects of surface charge on the small charged solutes and the impacts of hydration, where solutes have a solvation shell of water molecules must also be considered. An important parameter that affects UF processes is the pH, that strongly impact surface charge, providing a better control of the performances. The transport and exclusion mechanisms are heavily influenced by the membrane pore size, solvent viscosity, membrane thickness, solute diffusivity, solution temperature and pH. Generally, charged solutes are much more effectively retained in NF than uncharged solutes, and multivalent solutes rejection is elevated. Typical polymers used for this

category are PES, PVDF and polyacrylonitrile (PAN). They are normally used as substrates on which is deposited a thin selective layer performing the separation.

- **Reverse Osmosis (RO) membranes**: in reverse osmosis the driving force is still the hydrostatic pressure difference. A solution containing low molecular weight solutes is separated by a membrane from the solvent resulting in a flux of solvent from the solution into a pure solvent stream. The membrane is asymmetric with a dense layer functioning like a barrier at the side facing the feed solution. In this layer the components are transported by diffusion and viscous flow through pores and pinholes can be neglected. In forward osmosis the movement of water occurs until the osmotic equilibrium is reached or until the chemical potentials on both side of the membrane are equal. Reverse osmosis occurs when the hydrostatic pressure difference applied is greater than the osmotic pressure difference between the feed an permeate solution. This results in a water flux across the membrane with a retention of solutes by the RO membrane. Common membranes materials are cellulose acetate, polysulfone (PS) and PES.

Membrane technologies, as every industrial process, have a number of advantages, but also several drawbacks. They can be implemented in a huge number of separations; they do not require a phase change to achieve the goal and the energy consumptions are quite restrained. Moreover, membranes can be fabricated with very high selectivity for the components of interest and with different typology of material, polymeric and inorganic materials. They are more environmental friendly then conventional industrial processes. On the other hand, membrane processes rarely produce two pure products (there is always a minor amount of contaminants) and they are difficult to stage (most of the membrane processes have only few stages) and scale up. Membranes can also have chemicals incompatibilities for some process solutions; especially polymeric membranes cannot withstand harsh operative conditions such as extremes of pH and temperature. Finally, one of the most significant drawback is fouling; it is difficult to remove and it can affect strongly the permeation rate thus the efficiency of the process.

### 1.7.2 Common membrane configurations

MF, UF, NF and RO membrane technologies are widely used in industrial applications and, according to the purpose, the membranes can be arranged in different configurations. The

membrane configurations refer to the geometry of the filter and to the spatial position with respect to the feed and permeate flows. In most industrial processes, the membrane installations are in modular structure, therefore the configuration influences also the way in which membranes are packed inside the module. There are four types of possible configurations: plate and frame, spiral wound, tubular and hollow fiber. The geometry of the first two is planar, while for the other is cylindrical. Each configuration needs to respect some indispensable characteristics.

1. **Compactness**, allowing the packing of as much membrane surface as possible in a compact volume
2. **Low resistance to tangential flow**, less friction, less energy losses, low pressure drops along the retentate channel
3. **No "dead" regions**, as to have a uniform velocity distribution
4. **High degree of turbulences in the retentate side** to prevent fouling and promote mass transfer
5. **Easy cleaning and maintenance**
6. **Low cost per unit membrane area.**

Here the principal characteristics of the possible membrane configurations are described.

- ***Plate and frame configuration***:

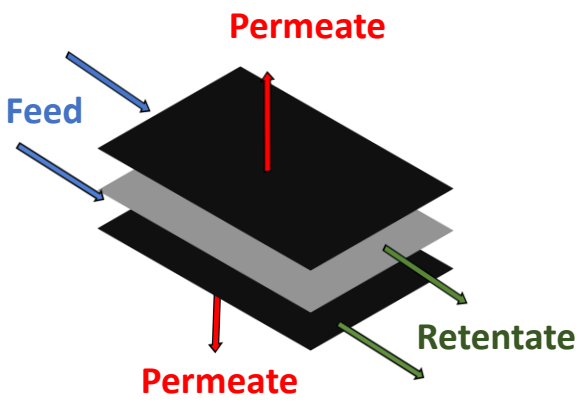


**Figure 1.6**: *Plate and frame configuration.*

The membranes can be squared or circular, arranged in vertical or horizontal stacks. This module cannot withstand high pressure and therefore is limited to MF and UF applications. The surface area to volume ratio is not high. It is the industrial module

that resembles more the configuration used in laboratory. In each feed and permeate compartment a spacer is placed. To avoid channeling (the tendency to by-pass parts of the available membrane area) and establish a uniform flow distribution, baffles are also introduced. The advantages associated to this configuration are the low sensitivity of particulate blocking the feed side and the possibility of using flat membranes without glue usage. On the other hand, it needs several sealings, it has high pressure drops and a low packing density. It is the first earliest membrane configuration proposed but, currently, it has limited applications (mainly in pervaporation and gas separations)

- ***Spiral wound configuration***:

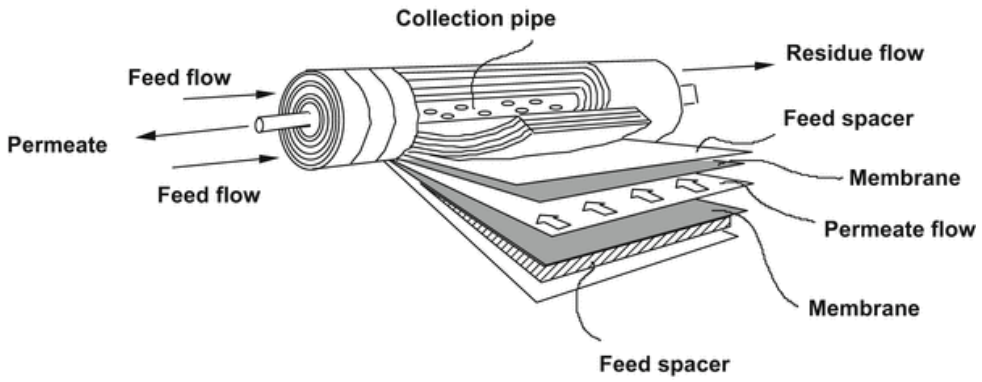


**Figure 1.7***: Spiral wound configuration.*

Two large membrane sheets are heat-sealed on three sides, creating a bag. A spacer (flexible) mesh or a porous support is placed into the bag to create a gap between the two membranes to let the permeate flow. The system is then wounded in a spiral, forming a cylindric module. The bag opening is placed in contact with a central collecting tube for the permeate. The sheet of membrane rolled up are separated by a mesh spacer, providing space for the retentate flow. This kind of configuration has a high surface area to volume ratio.

- ***Tubular configuration***:

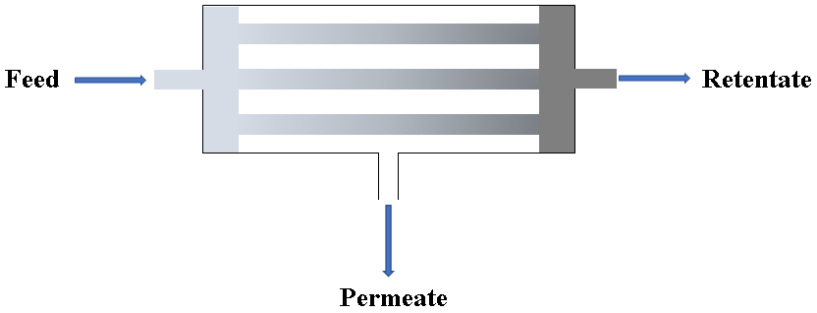


**Figure 1.8**: *Tubular configuration.*

It resembles a shell and tube heat exchanger; the membrane is casted on the inner wall of rigid porous tubes, made of polymeric or ceramic materials. The tubes are connected to two parallel bundles inside the shell. The diameter of the tubes may range from 10 mm to 25 mm. The flow direction is normally inside-out meaning that the retentate flows inside the tubes while the permeate is collected in the shell. The other modality (outside-in) is used to clean and unclog the membranes. They are flexible configurations, with the possibility to preserve a high tangential flow velocity in the feed and, as a consequence, they are suitable for the treatment of solutions with high concentration of suspended solid. They are easy to clean due to their large diameter, but they do not exhibit a high surface area to volume ratio.

- ***Hollow fiber configuration***: it is similar to the tubular configuration but fibers (tubes) are much thinner with diameter varying from 1 mm to capillary size. The small diameter assures sufficient mechanical strength and an external support is not needed. A huge number of fibers are connected to perforated end-plates and the entire bundle is collocated into a jacket. Flow direction can be inside-out or outside-in. These configurations are very compact, with an ultra-high surface area to volume ratio, but they are very propense to clogging and fouling limiting their use to clean solutions with relatively low viscosity.

## 1.8 Adsorption onto porous materials

In this work, the principles of filtration and adsorption were both exploited to confer to a single material the ability to simultaneously remove water and adsorb undesired compounds...

The adsorption process consists in an adhesion between a gas, a liquid or a dissolved solid to a surface (normally a porous surface). The process originates a film of adsorbate onto an adsorbent surface. The bond between the adsorbent and the adsorbate depends on the species involved and, accordingly, the adsorption can be physical (physisorption) characterized by weak interactions like London or Van-der-Waals forces or it can have a chemical nature, comporting the creation of covalent bonds. It may also occur due to electrostatic interactions.

Adsorption is present in a wide range of natural, physical, biological and chemical systems, as well as in industrial applications such as heterogeneous catalysis, cooling processes, water treatment and pharmaceutical applications.

### 1.8.1 Adsorption isotherm models

The adsorption solutes from liquid solutions is described through isotherms, defining the amount of adsorbent as a function of concentrations at a constant temperature. The amount adsorbed is normalized by the mass of the adsorbent used to compare different materials results. There exist a huge number of isotherm models and here are described only the most used one[34]:

- **Langmuir isotherm**: this model is generally used to describe the adsorption of biomolecules on a solid support. It is a semi-empirical model with a kinetic basis and was developed on statistical thermodynamics. It is based on 4 assumptions:
    1. All the adsorption sites are equivalent, and each site can only accommodate one molecule.
    2. The surface is homogenous energetically speaking and adsorbates don't interact.
    3. No phase transition is present.
    4. Only a monolayer is formed in the maximum adsorption situation. Adsorption occurs only on surface sites and not on other adsorbates.

  These assumptions are rarely all true; imperfections on the surface are always present, the adsorbed molecules seldomly are inert and the adsorption mechanism is not the same for the first and the last molecule adsorbed. The last assumption is the most problematic since more molecules tend to be adsorbed on the monolayer.

In the Langmuir model the adsorbent is assumed to be an ideal solid surface composed of a series of independent sites able to bind the adsorbate. The adsorbate binding is treated like a chemical reaction between the adsorbate molecule, $M$, and an empty site, S. This leads to an adsorbed complex, $MS$:

$$M + S \leftrightarrow MS \quad (9)$$

The rate of direct reaction (adsorption) depends linearly on both the concentration of molecules in solution and the residual capacity of the support to adsorb other molecules. Therefore, the reaction can be expressed as follows:

$$R_1 = k_1 c\,(q_{max} - q) \quad (10)$$

Where $R_1$ is the rate of direct reaction, $k_1$ is the kinetic constant for the direct reaction, $c$ is the concentration of molecule in solution, $q_{max}$ is the maximum adsorption capacity of the support and $q$ is the concentration of the complex $MS$ on the solid surface. For the adsorption reaction it is assumed a first rate kinetic order, that is proportional to the concentration of molecules adsorbed on the support, so:

$$R_2 = k_2 q \quad (11)$$

where $R_2$ is the rate of the inverse reaction (desorption) and $k_2$ is the kinetic constant for the inverse reaction. By combining Equation (10) and (11) in a mass balance, Equation (13) is obtained:

$$\frac{dq}{dt} = k_1 c\,(q_{max} - q) - k_2 q \quad (12)$$

At equilibrium the adsorption and desorption rater are equal:

$$k_1 c\,(q_{max} - q) = k_2 q \quad (13)$$

By solving Equation (13) for q, Equation (14) is obtained:

$$q = \frac{q_{max} c}{K_d + c} \quad (14)$$

which represent the adsorption isotherm of the Langmuir model in which $K_d$ is the dissociation constant. $q_{max}$ and $K_d$ are functions of the adsorbate and of the operating conditions (pH, temperature, organic solvent, buffer type)

- **Freundlich and Temkin isotherm**: they are used when the Langmuir model is not adequate to describe the system under investigation. These models are useful when the binding surface is heterogeneous and the adsorption sites are characterized by different binding energies:

$$q_{eq} = k c_{eq}^{n} \quad (15)$$

Equation (15) represent the Freundlich isotherm model where k and n are constants depending on the nature of the substrate and of the adsorbate, while the Temkin isotherm model is described by Equation (16):

$$q_{eq} = \frac{RT}{b_T} \ln (K_T c_{eq}) \quad (16)$$

where $K_T$ is the equilibrium binding constant and $b_T$ is the variation of adsorption energy.

## 1.9 The concept of Mixed Matrix Membranes (MMMs) for water treatment

In previous paragraphs, a description of the membrane technologies used in water treatment is given. An insight of the membrane materials for this application was provided together with their advantages and drawbacks: polymeric membranes are cheap, easy to fabricate, versatile but they have poor chemical and mechanical resistance to harsh operation conditions and low durability, while, on the other hand, ceramic membranes are very resistant to adverse process environments but their production at industrial level is costly and complicated and they are not versatile.

In the last decades, researchers have been trying to combine the features of polymeric and ceramic materials in one single membrane called Mixed Matrix Membrane (MMM). Commonly, objectives such as increases in permeability and selectivity, fouling reduction and specific removal of target components, were achieved by combining two or more processes, developing integrated filtration units. Advancements in materials and membrane technologies have made the process tuning possible and they paved the way for the introduction of MMMs in water filtration applications.

MMMs have also revolutionized other separation areas such has gas separation, blood purification, toxins removal from human plasma, sensors and biosensors. Nevertheless, MMMs are not ready to be scaled-up to industrial processes since is a technology still in development and by now, for water treatment applications, only lab-scale prototypes are available.

### 1.9.1 MMMs for water treatment

Mixed Matrix Membranes are formed by a polymeric matrix in which micro or nano-materials can be dispersed or embedded. These fillers are normally porous and of various

nature typically zeolites, carbon molecular sieves, activated carbon, carbon nanotubes or non-porous materials such as silica, titanium oxide and fullerene. In general, MMMs can potentially offer the stability of a ceramic material together with the fabrication easiness of a polymer. Moreover, they can exhibit higher permselectivity, fouling resistance and chemical strength over a wide range of temperatures and pHs. Several methods were developed over time to synthesize them such as filler dispersion in polymer solutions, in-situ polymerization and sol-gel method. The polymeric matrix governs the permeability, while the filler plays an important role for the separation performance. The filler addition normally modifies the morphology of the membrane with a consequent alteration of the transport phenomena influencing the overall performance of the membrane. Some collateral effects during the preparation of MMMs can occur. The most undesired are the interfacial voids formation, particles aggregation and pore blockage. Therefore, to optimize the synthesis several parameters need to be controlled (polymer concentration, filler concentration, casting and eventual coating techniques)[35].

MMMs can be categorized according to the type of filler present. In following the most common types of MMMs are presented, together with some example of MMMs successfully prepared:

- **Inorganic Filler-based MMMs**: inorganic filler can interact with the matrix forming covalent bonds, hydrogen bonds or simply through Van der Waals forces. Zirconium oxide particle were successfully embedded in polyether sulfone (PES) membrane to increase conspicuously rejection of dye due to the hydrophilic character of zirconium oxide. Several studies have been done on introducing graphene oxide to increase dye rejection; despite the graphene oxide hydrophobic nature, tailoring the casting procedure no significant effects on the overall membrane permeability were recorded. Antimicrobial MMMs were obtained implementing silver nanoparticles: the presence of silver nanoparticles under a thin selective layer enhanced the antifouling properties of the membranes, inhibiting the leaching phenomena and make them suitable for antimicrobial applications. Inorganic fillers are essential part of the MMMs since they strongly contribute to the achievement of the desired characteristics. The principal purposes for which MMMs are employed in for water treatment are: enhancing the flux, improving the selectivity, alleviating fouling and biofouling. One of the most important drawbacks of the addition of an inorganic filler to a polymer matrix is their chemical

incompatibility that may create voids at the polymer-filler interface mining the MMM integrity and selective transport properties.

- **Organic Filler-based MMMs**: they are MMMs in which organic components such as activated carbon, cyclodextrin, polypyrrole, polyaniline, chitosan beads are embedded in a polymeric matrix normally through blending or phase inversion. Organic fillers have more functional groups compatible with the polymer and this makes them more suitable for the embedment. Their capability of linking themselves with hydrophobic surfaces make them a better choice for developing functionalized membranes with enhanced antifouling, rejections and fluxes.

- **Biomaterial-based MMMs**: the incorporation of biofillers enhance MMMs functionalities such as mechanical resistance, fouling resistance and permeability with the advantage that are bio-based materials. They are normally coated on the polymeric substrate or they can be incorporated in vesicles that are coated on the support. Biofiller-based MMMs offer unique ability to control the permeability and recently, their barrier properties towards urea, glucose, glycerol and salts was reported. Nevertheless, intense research is still needed to find more effective and reliable ways to incorporate these fillers in a polymeric support.

- **Hybrid Filler-based MMMs**: this type of MMMs contains two different fillers added to the polymeric phase. These hybrid materials are embedded either to tailor one specific characteristic of the pristine membrane or to increase the overall efficiency of the resulting MMMs. Studies have reported that the incorporation of different iron oxide and polyaniline into PES matrixes increased the copper removal from water while chitosan-montmorillonite enhanced strongly PES fouling resistance. Nevertheless, a surface pore blockage was reported for these hybrid filler-based MMMs indicating that the selection and the composition of the filler is a crucial point in the preparation of these materials.

### 1.9.2 MMMs for adsorption and hemodialysis applications

In addition to the traditional application of MMMs for gas separation and water treatment, an interesting field towards which research has recently moved is the application of MMMs

for adsorption purposes. Traditional adsorbents are generally of particle form; however, either in batch or semi-continuous operation particulate adsorbent encounter several problems. In batch processes, a uniform particle dispersion is difficult to be maintained in large vessels and additional costs for final solid-liquid separation are needed. In semi-continuous operations that implies packed-bed particles, often high pressure drops and clogging are encountered due to the low bed porosity and length. These problems could be exempted with the use of Mixed Matrix Membrane Adsorbers (MMMAs)[36], [37]. The porous polymer matrix provides support and pathways for the solutes to reach the adsorptive sites of the filler. MMMAs can provide uniform packing distribution, bed with high porosity, low pressure drops and small residence time with a consequent benefit in time and energy consumption with respect to conventional packed bed processes. Since the adsorption capacity of the MMMAs depends on the trapped fillers, on the pore size distribution and the surface area, on the ion exchange capability and batch adsorption properties of the particle, is crucial to adequately evaluate these characteristics to achieve the best performance possible. Moreover, a careful evaluation of the mass transport mechanism needs to be performed. The transport within the adsorbent MMMAs can be summarized in 4 steps including the external mass transfer from the bulk solution to the membrane surface (1), diffusion trough the membrane pores in the membrane thickness direction (axial diffusion) (2), radial diffusion in membrane pores to reach the particles (3) and diffusion inside the pores of the adsorbent (4). In pristine particles adsorption the limiting step would be intraparticle diffusion (4) while for the present technology the rate-limiting step is the axial diffusion[38].

One of the main disadvantages of hemodialysis is that the removal of toxins depends only on the membrane pore size (or on the molecular weight of the solute) with a lack of specificity. Moreover, it cannot remove middle molecules and molecule bound to protein efficiently. Modified hemodialysis membranes are proposed to increase membrane pore size and to combine the filtration and adsorption in one single step. A new approach to obtain adsorptive hemodialysis membranes is the MMM approach: functionalized sorbents can be embedded in a biocompatible porous support to combine adsorption, diffusion and convection in a single step. Trapping small adsorbent into the matrix can improve the surface area and shorten the diffusion distance of toxic molecules to active sites. Follow this concept, a MMM based on cellulose acetate with incorporated activated carbon was developed and tested[39]. The flat sheet membranes are prepared by phase inversion

technique and to improve the blood-compatibility and avoid contact between blood and the activated carbon the MMMs are co-casted with a particle free cellulose acetate solution with a top layer free of adsorbent giving rise to double layer MMM adsorber. Results have shown an increase in dynamic creatinine removal and the adsorption contributes to more than 83% of the total removal indicating that the integration of adsorption in dialysis could be effective and MMMs have potentiality for the efficient integration of the two processes.

Dual layer MMM membranes with activated carbon as adsorbent where also fabricated with PES and PVP in a hollow fiber configuration. The membrane consists in an inner selective layer of blended polymers and an outer layer in which activated carbon is confined embedded in a PES/PVP matrix[40]. The inner particle-free layer prevents the direct contact of blood with activated carbon providing excellent membrane blood-compatibility. The results shown that this MMM offers superior endotoxin removal with respect to conventional hemodialyzers and could act as a barrier inhibiting the inflammatory response in case of bacterial contamination.

Future studies would be centered on the application of MMM in portable artificial kidney where spent dialysate should be continuously regenerated and recirculated for a long time. Moreover, MMM for hemodialysis should be also investigated for their application when pure dialysis water is not available as for several developing country assessing, as a consequence, the reduction of waste water and energy consumption associated to their use.

## 1.10 Aim of the project

Hemodialysis is the principal renal replacement therapy for people with a chronic kidney disease waiting for a transplant. As all the extracorporeal treatments, it has several limits in substituting the real organ function and, in addition, it has extremely high operative costs for the health care system with severe environmental drawbacks.

For each person receiving the therapy, 120 L of ultrapure water are needed. Considering that, and according to the 3/4 sessions per week needed by the patients 336 million of ultrapure water are needed per year to prepare the dialysis solution. At the end of the treatment, the fluid full of waste metabolites is discharged and sent to the drain. To produce the 120 L, at least 500 L are treated in a reverse osmosis membrane module comprehensive of softeners, activated carbon filters and deionizers. The reject water during the reverse

osmosis process is sent to the drain even if it could be recycled and used for several purposes[41]. Thus, the overall amount of water consumed to meet the worldwide needs of hemodialysis is 156 billion of liters per year.

The principal aim of the project is therefore to synthesize and characterize novel Mixed Matrix Membrane Adsorbers (MMMAs) for the removal of uremic toxins from aqueous solutions. The concept of Mixed Matrix Membranes, well developed for gas separation application, is here implemented for liquid stream purification. The polymeric matrix gives stability and strength to the system, while the adsorbers have specific affinity for the uremic toxins targeted in this work. Moreover, in collaboration with the Istituto Superior Técnico in Lisbon, hybrid membranes for artificial kidney applications were prepared and specifically characterized for the removal of uremic toxins and for albumin retention in a surrogate system of an artificial kidney (AK). As final result, a fluid mechanics of the membrane module and a new dimensionless mass transfer correlation was obtained. The peculiarities of the new correlation proposed are the operative conditions for which is valid, not present in the contemporary literature, the broad range of solutes for which is usable and the introduction of a Reynolds number accounting for the permeation that is a key parameter influencing the overall mass transport rates.

## References

[1] R. Preidt, 850 million people worldwide have kidney disease, 2018, www.webmd.com, (n.d.). https://www.webmd.com/kidney-stones/news/20180705/850-million-people-worldwide-have-kidney-disease.

[2] dialysis diet, 2020, www.drugs.com, (n.d.). https://www.drugs.com/cg/dialysis-diet.html.

[3] NHS, 2018, www.nhs.uk, (n.d.). https://www.nhs.uk/conditions/dialysis/side-effects/#haemo.

[4] S.A. Sanjad, Overview of Renal Function, Textb. Clin. Pediatr. (2012) 2689–2695. doi:10.1007/978-3-642-02202-9_288.

[5] R. Bellomo, C. Ronco, J.A. Kellum, R.L. Mehta, P. Palevsky, Acute renal failure - definition, outcome measures, animal models, fluid therapy and information technology needs: the Second International Consensus Conference of the Acute Dialysis Quality Initiative (ADQI) Group., Crit. Care. 8 (2004). doi:10.1186/cc2872.

[6] P. Romagnani, G. Remuzzi, R. Glassock, A. Levin, K.J. Jager, M. Tonelli, Z. Massy, C. Wanner, H.J. Anders, Chronic kidney disease, Nat. Rev. Dis. Prim. 3 (2017). doi:10.1038/nrdp.2017.88.

[7] U.S national library of medicine, medlineplus.gov, (n.d.). https://medlineplus.gov/ency/article/007305.htm.

[8] A.S. Levey, J. Coresh, Chronic kidney disease, Lancet. 379 (2012) 165–180. doi:10.1016/S0140-6736(11)60178-5.

[9] A. Dhondt, R. Vanholder, W. Van Biesen, N. Lameire, The removal of uremic toxins, Kidney Int. Suppl. 58 (2000). doi:10.1046/j.1523-1755.2000.07606.x.

[10] R. Vanholder, R. De Smet, G. Glorieux, A. Argilés, U. Baurmeister, P. Brunet, W. Clark, G. Cohen, P.P. De Deyn, R. Deppisch, B. Descamps-Latscha, T. Henle, A. Jörres, H.D. Lemke, Z.A. Massy, J. Passlick-Deetjen, M. Rodriguez, B. Stegmayr, P. Stenvinkel, C. Tetta, C. Wanner, W. Zidek, Review on uremic toxins: Classification, concentration, and interindividual variability, Kidney Int. 63 (2003) 1934–1943. doi:10.1046/j.1523-1755.2003.00924.x.

[11] F. Duranton, G. Cohen, R. De Smet, M. Rodriguez, J. Jankowski, R. Vanholder, A. Argiles, Normal and pathologic concentrations of uremic toxins, J. Am. Soc. Nephrol. 23 (2012) 1258–1270. doi:10.1681/ASN.2011121175.

[12] R.Vanholder, R. De Smet, N. Lameire, Protein-bound uremic solutes: The forgotten toxins, Kidney Int., 59 (2001) 266-270. doi.org/10.1046/j.1523-1755.2001.59780266.x.

[13] R. Vanholder, E. Schepers, A. Pletinck, E. V. Nagler, G. Glorieux, The uremic toxicity of indoxyl sulfate and p-cresyl sulfate: A systematic review, J. Am. Soc. Nephrol. 25 (2014) 1897–1907. doi:10.1681/ASN.2013101062.

[14] G.M. Fleming, Renal replacement therapy review: Past, present and future, Organogenesis. 7 (2011) 2–12. doi:10.4161/org.7.1.13997.

[15] J Kurkus, Nils Alwall-one of precursors of dilaysis treatment, G. Ital. Nefrol., 35, 2018, Supplement 70.

[16] B. H.Scribner, J. E. Z. Caner, R. Buri, W. Quinton, The technique of continuous hemodialysis, ASAIO, 6. 1960, 88-103

[17] A.J. Wing, M. Magowan, Principles of Dialysis, in: Ren. Unit, Macmillan Education UK, London, 1975: pp. 33–50. doi:10.1007/978-1-349-02527-5_3.

[18] A. M. A. Ahmed, Mohd. F. Allam, E. S. Habil, A. M. Metwally, N. A. Ibrahiem, M. Radwan, M. M. El-Gaafary, A. Afifi, M. A. Gadallah, Development of practice guidelines for hemodialysis in Egypt, Indian J. Nephrol., 2010, 4, 193-2020. doi:10.4103/0971-4065.73450

[19] A. R. Nissenson and R. N. Fine, Handbook of Dialysis Therapy (Fifth Edition), 2017

[20] S. Eloot, Experimental and Numerical Modeling of Dialysis, 2004.

[21] K. M. Kim, H. J. Oh, H. Y. Choi, H. Lee, D. R. Ryu, Impact of chrnoic kidney disease on mortality: A nationwide cohort study, Kidney Res. Clin. Pract., 2019, 38, 382-390doi:10.23876/j.krcp.18.0128.

[22] M. Dąbrowska-Bender, G. Dykowska, W. Żuk, M. Milewska, A. Staniszewska, The impact on quality of life of dialysis patients with renal insufficiency. Patient Preference and Adherence. Patient Preference and Adherence [revista en Internet]

2018 [acceso 11 julio 2020]; 12(1):577-583, (2018) 577–583. doi:10.2147/PPA.S156356.

[23] I, C. Yu, R. Chen, J.J. Li, J.J. Li, M. Drahansky, M.. Paridah, A. Moradbak, A.. Mohamed, H. abdulwahab taiwo Owolabi, FolaLi, M. Asniza, S.H.. Abdul Khalid, T. Sharma, N. Dohare, M. Kumari, U.K. Singh, A.B. Khan, M.S. Borse, R. Patel, A. Paez, A. Howe, D. Goldschmidt, C. Corporation, J. Coates, F. Reading, We are IntechOpen , the world ' s leading publisher of Open Access books Built by scientists , for scientists TOP 1 %, Intech. i (2012) 13. doi:10.1016/j.colsurfa.2011.12.014.

[24] E. Ubranézyk, M. Sowa, W. Simka, Urea removal from aqueous solutions-a review, J. Appl. Electrochem., 46 (2016) 1011-1029. doi 10.007/s10800-016-0993-6.

[25] C. Ronco, L. Fecondini, The vicenza wearable artificial kidney for peritoneal dialysis (ViWAK PD), Blood Purif. 25 (2007) 383–388. doi:10.1159/000107775.

[26] V. Gura, C. Ronco, F. Nalesso, A. Brendolan, M. Beizai, C. Ezon, A. Davenport, E. Rambod, A wearable hemofilter for continuous ambulatory ultrafiltration, Kidney Int. 73 (2008) 497–502. doi:10.1038/sj.ki.5002711.

[27] N.A. Bazaev, V.M. Grinvald, S. V. Selishchev, A. V. Kalinov, A. V. Kozachuk, V. V. Kosatkin, F.F. Tyunder, D. V. Federyakin, Exp erimental research of wearable artificial kidney, Vestn. Transplantologii i Iskusstv. Organov. 19 (2017) 46–52. doi:10.15825/1995-1191-2017-3-46-52.

[28] N.J. Ofsthun, A.K. Stennett, An integrated membrane/sorbent PD approach to a wearable artificial kidney, IFMBE Proc. 25 (2009) 729–732. doi:10.1007/978-3-642-03885-3-202.

[29] C. Ronco, The wearable artificial kidney: is peritoneal dialysis the solution?, Contrib. Nephrol. 163 (2009) 300–305. doi:10.1159/000223814.

[30] C. Ronco, A. Davenport, V. Gura, Los dispositivos portátiles miniaturizados el futuro del riñón artificial, Nefrologia. 31 (2011) 9–16. doi:10.3265/Nefrologia.pre2010.Nov.10758.

[31] M. Wester, F. Simonis, K.G. Gerritsen, W.H. Boer, W.K. Wodzig, J.P. Kooman, J.A. Joles, A regenerable potassium and phosphate sorbent system to enhance dialysis efficacy and device portability: An in vitro study, Nephrol. Dial. Transplant.

28 (2013) 2364–2371. doi:10.1093/ndt/gft205.

[32] B. Van Der Bruggen, C. Vandecasteele, T. Van Gestel, W. Doyenb, R. Leysenb, Review of Pressure-Driven Membrane Processes, Environ. Prog. 22 (2003) 46–56.

[33] N.L. Le, S.P. Nunes, Materials and membrane technologies for water and energy sustainability, Sustain. Mater. Technol. 7 (2016) 1–28. doi:10.1016/j.susmat.2016.02.001.

[34] C.T. Chiou, Fundamentals of the Adsorption Theory, Partit. Adsorpt. Org. Contam. Environ. Syst. (2003) 39–52. doi:10.1002/0471264326.ch4.

[35] D. Qadir, H. Mukhtar, L.K. Keong, Mixed Matrix Membranes for Water Purification Applications, Sep. Purif. Rev. 46 (2017) 62–80. doi:10.1080/15422119.2016.1196460.

[36] M. Ulbricht, Advanced functional polymer membranes, Polymer (Guildf). 47 (2006) 2217–2262. doi:10.1016/j.polymer.2006.01.084.

[37] M.E. Avramescu, M. Gironès, Z. Borneman, M. Wessling, Preparation of mixed matrix adsorber membranes for protein recovery, J. Memb. Sci. 218 (2003) 219–233. doi:10.1016/S0376-7388(03)00178-9.

[38] S. Yi Suen, Mixed Matrix Membranes for Adsorption Application, J. Chem. Eng. Process Technol. 06 (2015) 1–2. doi:10.4172/2157-7048.1000e119.

[39] Saiful, Z. Borneman, M. Wessling, Double layer mixed matrix membrane adsorbers improving capacity and safety hemodialysis, IOP Conf. Ser. Mater. Sci. Eng. 352 (2018). doi:10.1088/1757-899X/352/1/012048.

[40] A.F. Ismail, M.N.Z. Abidin, S. Mansur, M.Z. Zailani, N. Said, Y. Raharjo, S.M. Rosid, M.H.D. Othman, P.S. Goh, H. Hasbullah, Hemodialysis Membrane for Blood Purification Process, Elsevier Inc., 2019. doi:10.1016/b978-0-12-812815-2.00009-0.

[41] L. Ponson, W. Arkouche, M. Laville, Toward green dialysis: Focus on water savings, Hemodial. Int. 18 (2014) 7–14. doi:10.1111/hdi.12117.

# 2 MATERIALS AND METHODS

## 2.1 Introduction

A detailed literature review is propaedeutic and necessary to understand the problematics related to hemodialysis and the emerging technologies proposed to improve it performances and to limit its environmental impact. The concept of Mixed Matrix Membranes (MMMs) is becoming a real alternative to be implemented in hemodialyzers, combining filtration ad adsorption in a unique step. Moreover, membrane adsorbers can represent a real breakthrough in chromatography for the removal of contaminants since they offer a more homogeneous stationary phase then the common packed bed column together with lower pressure drops during operation.

Therefore, in this thesis work, several adsorbents were analyzed and characterized for their adsorption properties. First the adsorbent themselves in aqueous solutions of uremic toxins, urea, creatinine and uric acid, and then embedded in a polymeric matrix exploiting the concept of MMMs. These membrane adsorbers were then tested for their batch and continuous removal capacity with a single aqueous toxin solution and in a mixture of the three principal toxins. The objective of this thesis is to develop MMMAs for the regeneration of spent dialysate to reduce water consumption associated to dialysis. Therefore, the MMMAs components were carefully selected also according to the materials toxicity and biocompatibility [1], [2], [12].

The matrix of the MMMAs is made of cellulose acetate, which is a biocompatible derivative of cellulose. Its degree of substitution is around 39% and it does not contain components considerable persistent, bio-accumulable or toxic for the environment. The biodegrading process is feasible but slow. Moreover, the fillers used in the MMMAs are zeolites and activated carbon, which are solid adsorbent commonly used even for body depuration. Therefore, all the major components of the MMMAs can be considered non-hazardous for the environment and for human health.

Moreover, during the period in Lisbon, a surrogate system of an artificial kidney was fully characterized in terms of fluid dynamics and mass transfer to develop a new mass transfer correlation for laminar flow regimes applicable in a range of Schmidt number values related

to the hemodialysis processes. In Lisbon, apart from urea, creatinine and uric acid, para-cresyl sulfate (p-CS) and bovine serum albumin (BSA) were also introduced in the artificial kidney surrogate characterization.

In this chapter a detailed description of the materials and methods used for the synthesis and characterization of the adsorbents and of the membranes used is presented.

## 2.2 Hemodialysis molecules targeted and analysis protocol

Among all the components eliminated and retained during hemodialysis, four characteristic uremic toxins were chosen: urea, creatinine, uric acid and para-cresyl sulfate (pCS). The first three compounds were selected as low molecular weight metabolites present in the spent dialysate solution at highest concentrations, while the last one represents the category of protein-bound uremic toxins.

Bovine serum albumin (BSA) was also taken into consideration to assess the rejection capability of the materials prepared.

Urea, creatinine and uric acid are classified as soluble compounds with low molecular weight, $M_w$ < 500 Da, non protein-bound toxins while pCS exists prevalently bound to albumin making its complete removal barely possible. For each of them, the value of concentration present in the blood of healthy individuals, $c_N$, and the highest concentration possible in hyperuricemia conditions, $c_{MAX}$ were used. According to the different stages of kidney failure affecting the patient, in the spent dialysate is possible to observe concentration of these toxins ranging from $c_N$ to $c_{MAX}$ as listed in Table 2.1.

**Table 2.1***: Urea, creatinine, uric acid, p-CS and BSA characteristic.*

| Toxin | Mw (g/mol) | $c_N$ (mg/mL) | $c_{MAX}$ (mg/mL) | $\lambda_{UV\text{-}VIS}$ (nm) |
|---|---|---|---|---|
| *Urea* | 60.06 | 0.4 | 4.6 | 200 |
| *Creatinine* | 113.12 | 0.012 | 0.24 | 235 |
| *Uric acid* | 168.11 | 0.067 | 0.15 | 290 |
| *p-CS* | 188.2 | • **Total**: 0.0029<br>• **Free**:0.0001 | • **Total**: 0.043<br>• **Free**:0.0026 | 265 |
| *BSA* | 66463 | 35-50 | - | 280 |

The last column of Table 2.1 represents the characteristic absorption wavelength of each compound. It will be used to calculate the concentration with an UV-Vis spectrophotometer. Urea was purchased from Sigma Aldrich, while creatinine and uric acid from Acros Organics.

p-CS was synthesized in the organic chemistry laboratory of the Istituto Superior Técnico in Lisbon, and its characteristic are listed below together with BSA. Being p-CS commonly found attached to albumin, a distinction between the free fraction and the bounded one needs to be considered.

Bovine serum albumin was purchased by Sigma Aldrich with a degree of purity > 98 % and in form of lyophilized powder.

The wavelengths present in the last column of Table 2.1 were determined through pure toxins solution scans with the UV-Vis spectrophotometer Shimadzu UV-1601 to find the wavelengths at which the toxins considered in this work have the maximum absorption. For all the experiments involving an UV-Vis analysis the concentrations were calculated at those wavelengths. Moreover, for each toxin considered an UV-Vis a calibration curve was built to connect the absorbance value obtained during the analysis with the corresponding concentration. The absorbance and the concentration are related through the Lambert-Beer law:

$$A = \varepsilon \cdot c \cdot l \tag{17}$$

where $A$ is the absorbance, $\varepsilon$ is the molar extinction coefficient ($M^{-1}$ $cm^{-1}$), $l$ is the length of the light path (cm) and $c$ is the concentration (M). This relation is linear only at low solute concentration because a high analyte amount exhibits higher intermolecular and electrostatic interaction changing the molar absorptivity of the solution. Thus, calibration curves are needed also to determine the maximum concentration at which is possible to use the Lambert-Beer equation. The slope of the straight line, arising from plotting different concentration values as functions of the absorbance read, is the product $\varepsilon \cdot l$. Thus, with the angular coefficient is possible to correlate $A$ and $c$ and to determine the amount of analyte present in the analyzed solutions.

## 2.3 Solid adsorbents chosen and their characterization

As mentioned in Chapter 1, MMMs with adsorbent particles incorporated could have a tremendous potential in hemodialysis applications, integrating diffusion, convection and adsorption in a single step.

Among all the adsorbent present, three types were the most studied and tested for the adsorption of uremic toxins from water and from physiological solutions:

- ***Activated carbons***: or activated charcoal, it is a form of carbon activated in order to have small, compact pores to increase the surface area. The activation can be done physically through carbonization or oxidation where the pristine materials are processed with hot gases, or chemically, where the carbon substrate is impregnated with an acid, a base or a salt. The chemical activation is the preferred way since it requires lower temperature and shorter time to be completed. Activated carbons are complex products difficult to classify upon their behavior, surface characteristics and other general criteria. However, a broad classification can be done based on their size and industrial applications[1]:
    - *Powdered activated carbons* have the form of a powder and they present a large surface to volume ratio with a small diffusion distance.
    - *Granular activated carbons* have a larger particle size compared to the powdered one thus, they have a smaller surface area. They are normally used for gas and vapor adsorption as well as for water treatment.

- *Extruded activated carbons* are produced extruding a mixture of powdered activated carbon and a binder. Their principle application is in gas separation due to their low pressure drop and high mechanical strength.
- *Bead activated carbons* are made from petroleum pitch and they are known for their low pressure drops, high mechanical strength and low dust content.

- ***Zeolites***: they are aluminosilicate minerals with a micro/nano porous structure. They can be found in nature (over 40 types of different frameworks) or they can be synthesized industrially. Zeolites have a porous skeleton that normally accommodate a wide range of cations ($Na^+$, $K^+$, $Ca^{2+}$, $Mg^{2+}$ and others) which are willing to be exchanged in contact with solutions. Some of the common natural zeolites are analcime, chabazite, clinoptilolite, heulandite and stilbite. They form when volcanic rocks or ashes react with alkaline ground water. They are often contaminated with other minerals, metal, quartz, and therefore their commercial application is not suitable for processes requiring uniformity and purity.

  The zeolite lattice is formed by tetrahedrons $TO_4$ (T= Si, Al, P, etc.) where the oxygen atoms are shared with adjacent tetrahedrons. The tetrahedral units are disposed in more complex geometries, like chains or rings, to create regular structures.

  Zeolites are known to be molecular sieve materials since they have the capability to selectively separate molecules according their size. They are characterized by a regular pore structure of molecular dimensions and the maximum size of the species entering the pores is controlled by the channels' dimensions. The channels are not always cylindrical since the rings present in the zeolite lattice are sometimes not symmetrical due to the strain induced by the bonding between the units needed to create the overall structure. As already mentioned above, zeolites can be produced synthetically; typical procedures involve the heating of aqueous solution of alumina and silica with sodium hydroxide. Synthetic zeolites have the advantage of being uniform and pure and the production process can potentially be tailored to address a variety of goals, according to the application considered.

  Since the principal components involved in the preparation of zeolites are silica and alumina, two of the most present minerals on earth, the potential use of zeolites can be virtually unlimited.

- ***Silicon Dioxide***: it is also known as silica ($SiO_2$) and it is commonly found in nature as quartz. Silica is abundant in nature and it exists as a compound of several minerals or as a synthetic product. It has its principal application in structural materials, microelectronics and in food and pharmaceutical industries. Silicates have a tetrahedral structure with four oxygen atoms surrounding a central silicon atom. They can have a number of crystalline forms (polymorphs) but also different amorphous forms. $SiO_2$ it is a very versatile material that lately gained importance also for adsorption purposes. One of the amorphous form of silicon dioxide, silica gel is a porous material with an irregular tridimensional framework of silicon and oxygen atoms with voids and pores in the nanometer scale. It can be used as desiccant to avoid the growth of mold and spoilage and the decomposition of chemical compounds. It is a common stationary phase for chromatography since its hydroxyl groups can be easily functionalized to address the removal or retention of a specific target component. These modified silica gels can be also exploited in organic synthesis and in purification technologies.

Several studies reported in literature considered the use of activated carbons as adsorbent for biomedical purposes; since the activated carbons adsorption is non-specific, different kind of materials were chosen and tested for uremic toxins removal. Due to their excellent adsorption capacity different types of zeolites such as Linde Type A (LTA), stilbite (STI), silicalite (MFI), mordenite (MOR) and faujasite (FAU) where considered for creatinine, urea, uric acid and p-cresol removal[2]. The adsorption capacity of each material was measured and studied considering as evaluating parameters the channel size, acidity, hydrophobicity, charge compensating cations, hydrothermal treatment and grain size. For initial concentrations close to that of patients with renal failure, it is possible to remove 75% of creatinine (with MOR) and 60% of p-cresol (with MFI), while STI are efficient for the adsorption of urea and uric acid.

Specific type of MFI and MOR were studied for the adsorption of p-cresol and creatinine from aqueous and physiological solutions[3], [4], [5]. The tests were done on ZSM-5 zeolites and on a pure silicalite. MFI-type zeolites are able to adsorb 85% of p-cresol in the uremic concentration range. The adsorption capacity for creatinine of MOR45 was also analyzed and it was found that it is influenced by the presence of albumin. Indeed, the MOR45 capacity of 150 µmol/g without albumin decreased to 100 µmol/g with albumin, respectively. Other studies were focused on the synthesis an amine-functionalized

mesoporous silica via post-grafting method. The material was tested for urea adsorption[6]. It was observed that mesoporous silica and amine-functionalized mesoporous silica present a faster urea adsorption rate and higher binding with respect to activated carbons that are a popular choice as universal adsorbents.

In all the works mentioned above, the properties of the adsorptive particles are crucial for a successful elimination of toxins. Therefore, the performance of the adsorbent can be adjusted tuning the pore size distribution[7].Based on this, a study on the performance of carbon-based sorbents with two well-defined pores size was proposed[8]. Using such adsorbent, it was possible to remove the daily production of creatinine of kidney failure patients, 1800 mg.

Porous adsorbent materials have tremendous potentiality when removal of uremic toxins is concerned. It is possible to functionalize and tailor them to adsorb a specific compound or a series of chemicals. However, several efforts need to be done to exploit their ability in a real hemodialysis process combining the adsorption and filtration in a unique step.

Among all the adsorbents suitable for contaminants removal listed above, two different types of zeolite were chosen for this research project, together with the most common used porous adsorber, activated carbon.

Granules of activated carbon (Draco®KB) were purchased from Sigma-Aldrich, but only the fraction of material with a particle diameter < 53 µm was used for the experiments.

Zeolite Socony Mobile-5, ZSM-5, and a HEU-type of zeolite (ZUF) were selected for as inorganic fillers for uremic toxins adsorption. The first is a synthetic zeolite of the MFI framework family. It is composed of different pentasil units connected by oxygen bridges. The second is a natural zeolite, clinoptilolite, that belongs to the Heulandite framework family and its structure is composed of several tetrahedra in which each oxygen is shared between two neighboring units. ZSM-5 pellets were supplied by ZeoChem AG (ZEOcat Z-400) while ZUF powder was purchased from ZeoBent Handels GmHb.

In Table 2.2, zeolite characteristics are reported.

**Table 2.2**: *Characteristic of the zeolites chosen.*

| Zeolite | Type of structure and general formula | Si/Al ratio |
|---|---|---|
| *ZSM-5* 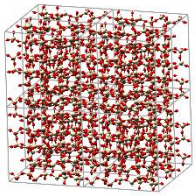 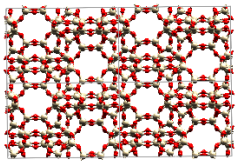 | *MFI* $Na_nAl_nSi_{(96-n)}O_{192}\cdot 16H_2O$ $(0<n<27)$ | >5[4] |
| *Z UF* 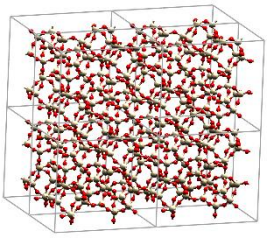 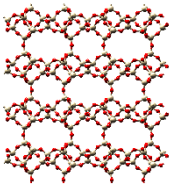 | *HEU* $(Na,K)_6(Si_{30}Al_6O_{72})\cdot 20H_2O$ | 4.0-5.7 |

The Si/Al ratio is a key parameter that affects the zeolite acidity, ion exchange capacity and hydrophobicity. For water decontamination purposes, a high Si/Al ratio is more indicated since low values of these parameter increase the $H^+$ adsorption that may cause zeolite dissolution[9]. The images reported in Table 2.2 are obtained with a molecular dynamic software, MAPS. This allowed the visualization of the pore structure and dimension of the two zeolites considered in this work of thesis.

A structure of activated carbon used a structure is not presented since it is a completely amorphous material with a variable conformation according to the synthesis procedure. It can be considered a non-organized form of graphite with a pore structure that strongly depends on the raw material and the production process used.

### 2.3.1 Particle size distribution and zeolite activation procedure

ZSM-5 pellets and activated carbons granules were grinded to obtain a fine powder sample. After grinding, the particle size distribution analysis for zeolites were carried out with a Laser Particle Sizer analysette® 22 (Fritsch) suitable for solid suspensions with particle size from 0.16 µm to 1100 µm was used. The software connected to the laser directly creates a particle sized distribution graph.

For the activated powdered carbon, a wet sieving procedure was used. The sieves had different mesh size: 106, 90, 75, 63 and 53 µm. A wet procedure is required to avoid electrostatic interactions between the particles and the metal wire of the sieve. The dried samples were weighted, and the information obtained was plotted to identify the amount of carbon obtained for each fraction.

Previous works have underlined that the removal capacity of zeolites towards uremic toxins is limited in absence of an acid dealumination treatment. The procedure consists in a partial or total removal of Al atoms from the zeolite framework under strong acidic conditions through which Brønsted acid sites are created in the surroundings of the framework Al atoms. As a consequence of the dealumination, a polymeric gel of alumina is formed in the channel of the material. This process may also induce the elimination of framework cations, tuning the zeolites pore size as to make them suitable for diffusion of relatively large molecules too[10].

According to the literature, acid activation with 1 M HCl should enhance the adsorption capacity of the materials[11]. The zeolites were washed with demineralized water and dried in the oven at 110-120°C for 2-3 hours. Subsequently, 5 mL of 1 M HCl were added for each gram of material. The suspension was stirred for 48 hours at 90 rpm, then filtered and washed several times to bring the pH back to neutrality. Finally, the wet powder was dried at 110°C.

The particle size distribution analysis was performed also on the modified zeolites to assess eventual changes in particles dimensions.

### 2.3.2 Adsorption kinetics and equilibrium isotherm experiments

Binding kinetics of urea, creatinine and uric acid has been experimentally measured for all the three adsorbents considered. 1.25 g of adsorbent was immersed in a beaker containing 10 mL of the pure toxin solution and kept under mechanical agitation by the action of an orbital shaker. The toxin concentration has been measured at regular

intervals of time by sampling the supernatant obtained after centrifugation of the suspension. The batch characterization of the adsorbents was completed by measuring the static binding capacity at equilibrium: 0.125 g of adsorbent were immersed in 4 mL of pure toxin solution at different concentrations and kept under agitation at 90 rpm for 24 hours. All experiments were performed at room temperature.

The toxin concentration was measured through UV readings at 200 nm for urea, at 235 nm for creatinine and at 290 nm for uric acid using a Shimadzu UV-1601 UV-Visible spectrophotometer.

## 2.4 Membrane synthesis

The synthesis of polymeric membranes is a delicate procedure affected by several parameters that need to be properly chosen. The choice of the solvent, together with the casting conditions are crucial to have a successful membrane preparation process. This work of thesis is focused on one specific material very commonly used to prepare porous membrane for water treatment applications: cellulose acetate (CA).

Cellulose acetate (CA) is an ester of cellulose, obtained by reacting cellulose with acetic anhydride and acetic acid in a sulfuric acid environment. According to the grade of acetylation (varying from 29% to 44.8% normally) mono-, di-, triacetate of cellulose can be produced. In 1865, Schützenberger was the first scientist who first attempt to synthesized cellulose acetate through heating cellulose in a sealed glass tubes with acetic anhydride. A decade later, Franchimont discovered that, using sulfuric acid as catalysts, CA could be prepared at room temperature. In 1894 came out the first patent on cellulose triacetate and enormous efforts were done to make it suitable for photographic film applications and homelike plastic materials. The first important commercial appearance was in 1904 when Miles discovered cellulose diacetate. The primary application was in the aircraft field to substitute the heavy rubber tissue wings. A cellulose diacetate coating on linen tissue gave a light material resistant to water, oil and petrol. It became a quite successful material and its industrial production started already in 1905[12]. After that, CA was mostly used to produce silk-like textiles and only in the 1950’s its potentiality as filtering material was discovered. In the early 1950’s Samul Yuster at the University of California proposed the idea that was possible to produce fresh water from brines: based on thermodynamic

considerations, brines in contact with air or other hydrophobic surfaces will have a layer of almost pure water adjacent to the interface[12]. Therefore, it should be possible to recover this fresh water. To the scope, a plastic film supported by a porous plate was use, and thanks to pressurization of salt the solution the brine was desalinated. This was the first concept of reverse osmosis (RO) processes and commercially available CA films were used for the purpose. After years of attempts, commercially available membrane sheets were considered inadequate for the scope. Fortunately, Loeb and Sourirajan in 1965 developed the first porous asymmetric membrane made of cellulose acetate by non-solvent induced phase inversion (NIPS) starting a real revolution in membrane fabrication for water treatment technologies.

Therefore, cellulose acetate was the first high performance asymmetric membrane prepared and commercialized. CA and its derivatives are suitable for membrane fabrication due to their high salt rejection, low cost, easiness in manufacturing, non-toxicity, biocompatibility and renewability. However, they have some drawbacks like poor resistance to bacteriological agents, harsh cleaning conditions and poor mechanical strength. The most common preparation method for cellulose acetate membrane is the non-solvent induced phase separation (NIPS).

For this thesis, all the membranes prepared are cellulose acetate (CA) based membranes. CA, was purchased from Sigma Aldrich, with an average molecular weight, $M_n$, of 30000 Da, a degree of acetyl substitution approximately of 2.4 and a density of 1.3 g/mL at 25°C. The cellulose acetate structure is reported in Figure 2.1:

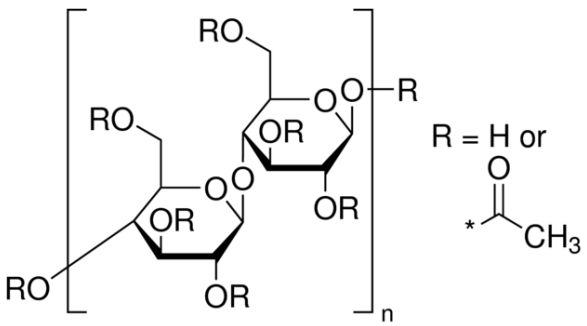


**Figure 2.1***: Cellulose acetate structure.*

For the preparation of the mixed matrix membrane adsorbers for the removal of uremic toxins from aqueous solution, a common NIPS casting technique was used.

For the production of CA membrane for artificial kidneys application, NIPS was coupled with the Sol-Gel process to synthesized CA/$SiO_2$ membrane with a monophasic inorganic/organic hybrid structure. Both the MMMAs and the hybrid membranes were casted with a flat sheet geometry.

### 2.4.1 Synthesis of Mixed Matrix Membrane Adsorbers (MMMAs)

All the membrane production techniques involve a phase separation through which the solid phase separates from the polymeric solution. MMMAs were prepared through the NIPS, according to which the polymer solution is immersed in a non-solvent coagulation bath (typically water) where the solvent/non-solvent exchange takes place. The solvent moves from the solution to the bath while the non-solvent does the reverse path, resulting in the formation of the membrane. It is possible to produce both flat sheet and tubular membranes: the first type is generally prepared on a nonwoven support and the preparation entails the use of a casting knife; however, is also feasible to produce also self-standing films. For the tubular conformation, the polymer and the bore fluid are co-extruded by means of a spinneret giving rise to a self-supporting structure with different diameter (ranging from 0.5 mm to 5 mm normally)[13].

There are several factors influencing the NIPS methods such as the exchange rate of solvent/non-solvent and the velocity of the phase separation. Both of them can strongly modify the membrane morphology. Moreover, thermodynamics plays also an important role in the phase separation process; polymer/solvent/non-solvent interactions can be described by the solubility parameter theory.

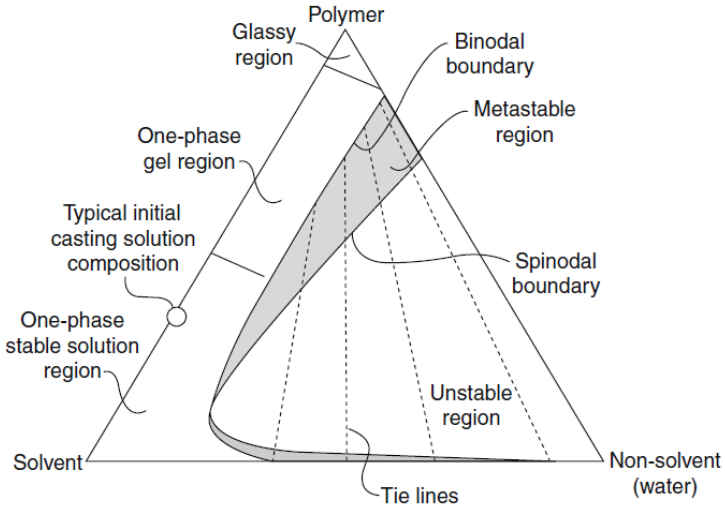


**Figure 2.2***: Phase diagram of a three-component system.*

In the ternary phase diagram (Figure 2.2), the corners represent the pure components and the sides the binary mixtures. The area of the triangle represents points in which ternary mixture is present. Three regions can be distinguished, separated by a binodal and a spinodal boundary: the region on the left of the binodal boundary is a thermodynamically stable one-phase region; between the binodal and spinodal boundaries a metastable region is present which is thermodynamically unstable and no phase separation can occur. On the right of the spinodal boundary, there is the unstable region where phase separation takes place.

The structure of the membrane depends on the thermodynamics and kinetics aspects of the phase separation, but also on the solvent used to dissolve the polymer and on the amount of time the membrane is left in contact with air or with a controlled gas-atmosphere before being soaked into the coagulation bath. The duration of the contact of the surface of the membrane with the atmosphere is responsible for the thickness of the active layer on the top of the membrane. The properties of the active layer are fundamental for achieving the right separation efficiency, therefore it is important to optimize the contact time between the polymer solution and the atmosphere according to the application sought.

In this work, prior to the preparation of mixed matrix membrane adsorbers, pristine cellulose acetate membranes were prepared to tune the procedure and to assess the effect of the filler addition on the membrane removal capacities. For the preparation of the membrane 1-methyl-2-pyrrolidone, NMP (density 1.03 g/mL), purchased by Fluorochem was used as solvent and Poly(ethylene glycol), PEG, of 400 Da (Sigma

Aldrich) was used as pore former. NMP has a very high boiling point, around 202 °C, a post thermal treatment is thus necessary to assure its complete evaporation.
Cellulose acetate membranes were prepared through the phase inversion casting technique [14]. 13.5 wt% of cellulose acetate was poured into NMP and stirred until complete dissolution. Then 8 wt% of PEG 400 was added and the solution stirred overnight to assure a good mixing between the different components. The membranes were casted with a knife with adjustable thickness, BYK-Gardner 2326 fixing the height of the knife to 400 μm. Deionized water was utilized as non-solvent for the phase inversion in a bath, kept at 23°C, where the membrane is immediately immersed after casting. The synthesized membranes were heat-treated for one week in a deionized water bath at 40°C to remove the excess NMP and PEG.
After determining the right casting conditions for the pure cellulose acetate porous membrane, mixed matrix membrane adsorbers, (MMMAs) were prepared according to a procedure similar to the one described above. Different amounts of ZUF (from 5 to 60 wt%), ZSM-5 (from 5 to 30 wt%) and activated carbon (from 5 to 30 wt%) were soaked into NMP and sonicated until a homogenous dispersion was obtained [15]. Subsequently, 10% of the total amount of polymer was added to the solution and stirred up to complete dissolution to prevent aggregation of the zeolite particles. The rest of the polymer was finally added, and the solution was stirred overnight. The casting procedure and the post-casting heat-treatment are the same described for the pristine CA membrane. The MMMAs prepared are 10 x 17cm and have a thickness of approximately 250 μm. The membranes are labelled according to the amount (in wt%) and type of filler added. For instance, MMMA_ZUF-5 is the membrane with 5 wt% of ZUF, MMMA_ZSM5-5 is the membrane with 5 wt% of ZSM-5 and MMMA-AC-5 is the one with 5 wt% of AC.

### 2.4.2 Synthesis of hybrid cellulose acetate/$SiO_2$ for AK applications (CA/$SiO_2$)

Hybrid cellulose acetate/silica membranes were synthesized through coupling the phase inversion technique and the sol-gel process. The sol-gel process is a versatile technique offering a wide range of opportunities to tune the membrane synthesis. It is a common method in material science to fabricate both glassy and ceramic materials. During the process, the solution evolves towards the formation of a gel-like network in which both a liquid and a solid phase are present. Typical precursors for the process are metal alkoxides

and chlorides, which undergo hydrolysis and polycondensation reactions to create a colloid. The term colloid is used to address a broad range of solid-liquid mixtures which contain distinct solid particles dispersed to various degree in a liquid medium. The colloids formation depends strongly on the size of the particles that need to be larger than atoms but small enough to exhibit Brownian motion (which is the random motion of the particles suspended in a fluid resulting from the collision of them with the fluid molecules). Under certain chemical conditions, typically base-catalyzed solution, the particles can grow to a sufficient dimension to become colloids that are subjected to sedimentation and gravity forces. On the other hand, under acidic conditions the interparticle forces have enough strength to cause considerable aggregation and/or flocculation prior to growth.

In membrane science, the incorporation of inorganic materials inside the polymer structure to improve their stability and mechanical properties is a common practice. Conspicuous amount of silica, alumina and other kind of inorganic fillers are mixed with the polymeric matrix to synthesize a better performing material. The presence of these fillers can modify the opacity, conductivity and permeability of the final material. Lately, the use of sol-gel process to produce hybrid inorganic-organic membranes was intensively investigated. Using this method coupled with the phase inversion is possible to grow inorganic component into the polymeric matrix with a very fine dispersion of the inorganic component reaching even molecular level. The polymerization of the inorganic phase occurs by hydrolysis and polycondensation[16].

The incorporation of metal oxide in CA was strongly investigated. Composite CA/niobium oxide were prepared from niobium chloride[16]. The inorganic particles were homogenously dispersed into the matrix. Another oxide used in reinforcing CA was zirconium oxide: the membranes were prepared from the hydrolysis of zirconium tetraisopropoxide to increase the phosphate retention[17]. The most common precursors used in coupling the sol-gel method with the membrane synthesis are the silanes. Tetraethoxysilane (TEOS) is frequently used to prepare CA modified hybrid membrane. After the reaction with TEOS, silica domains were embedded in the polymer matrix[17].

The sol-gel technique coupled with phase inversion has a tremendous potential in tailoring the polymeric membrane characteristic and performances. It is potentially possible, by tuning the sol-gel process and the membrane preparation conditions, to chemically bind the inorganic particle to the polymer matrix obtaining a hybrid structure with homogeneity in

the particle dispersion. Choosing the right precursor, it is feasible to give to the membrane specific affinity towards a target molecule.

In this work, the sol-gel process was carried out under acidic conditions. When the sol-gel hydrolysis and condensation occur under acidic conditions at a pH ~ 3, the condensation reaction rate is proportional to the hydroxide (-OH) group concentration giving rise to the following reaction sequence[18]:

$$\equiv Si - OH + OH^- \xrightarrow{fast} \equiv Si - O^- + H_2O \quad (18)$$

$$\equiv Si - O^- + OH - Si \xrightarrow{slow} \equiv Si - O - Si \equiv +OH^- \quad (19)$$

Under acidic conditions the condensation starts only when hydrolysis (Equation (18)) has taken place. At pH values lower than 3, a complete hydrolysis is achieved bringing to linear or highly branched polymeric structure with nanopores (< 2 nm). Subsequently, the condensation step can occur between silanol group and the polymeric phase, CA, via nucleophilic substitution. After the sol-gel process is concluded, the reaction between the inorganic silanol group and the C-OH or COOH group of CA is expected. This will bring to the formation of Si-O-C bonds. Finally, a symmetric structure with the Si particle bound to the polymeric matrix is obtained. Membranes were prepared using CA (as reported in paragraph 2.4) as polymer, formamide (Carlo Erba) and acetone (Labchem) as solvents, tetraethylortosilicate TEOS (Sigma-Aldrich) as precursor for the sol gel process and nitric acid. $HNO_3$, (JMGS) as acidic catalyst.

In Table 2.3 the specification of the casting solution prepared for the CA/$SiO_2$ hybrid membrane are reported. For simplicity, the membrane prepared are named CA_30 and CA_22:

**Table 2.3***: Membrane casting solutions composition.*

| | | CA_30 | CA_22 |
|---|---|---|---|
| | | Composition | |
| Solutions components | *Cellulose acetate (wt%)* | 16.4 | 16.4 |
| | *Formamide (wt%)* | 29 | 21.3 |
| | *Acetone (wt%)* | 51.1 | 58.8 |
| | *TEOS (wt%)* | 3 | 3 |
| | *Water (wt%)* | 0.5 | 0.5 |
| | *$HNO_3$ (mL)* | 0.20 (4 drops) | 0.20 (4 drops) |

The membrane percentage compositions are given on a hundred grams basis. The only difference in between the two solutions is the percentage of solvents. Formamide is the solvent that gives the porous structure to the membrane, therefore CA_22 will have a tighter pore structure than CA_30. According to the porous membrane characterization they are classified as ultrafiltration membranes.

## 2.5 MMMAs morphology and surface characterization

Morphology and surface properties are crucial parameters to characterize the membrane and to verify if the casting procedure was successful, and if the membrane has the desired characteristics. The membranes morphology is normally inspected through electron microscopy. In this dissertation scanning electron microscopy was used to investigate the MMMAs cross section, and thus their pore structure and to detect the presence of defects on their surfaces.

### 2.5.1 Scanning Electron Microscopy (SEM) and Energy Dispersive X-ray analysis (EDS)

The morphology of membranes was studied by scanning electron microscopy (SEM). Scanning electron microscopy is a powerful technique to image the surface of a sample. It utilizes the interaction between the electrons with the specimen for the generation of images and it has a higher resolution than optical microscope. An SEM has normally, as components, an electron source, a column containing electromagnetic lenses, electron detectors, a sample chamber and a computer display. The electron source is the most important part; even if

conventional emitters are reliable and cheap, field emission electron source (FESEM) is the most used since it has higher magnification and better resolution. Moreover, the elemental composition of the specimen can be calculated with a special detector for X-rays and this is the principle of the EDX.

SEM principles are quite simple: a focused electron beam reacts with the sample and from this interaction secondary electrons (SEs), backscattered electrons and characteristic X-ray are produced and detected with different revelators. Generally, there are two types of interaction that can occurs: elastic and inelastic. During the inelastic interactions, low-energy SEs are emitted from the sample while elastic interaction are generated by the deflection of primary electrons upon contact with the sample's atomic nucleus or by electrons of comparable energy. The deflection is at an angle of 90 degrees and these electrons are called back scattered electrons (BSE). In Figure 2.3 the teardrop-shaped volume of the specimen (interaction volume) is reported together with the type of electrons emitted or deflected for each region.

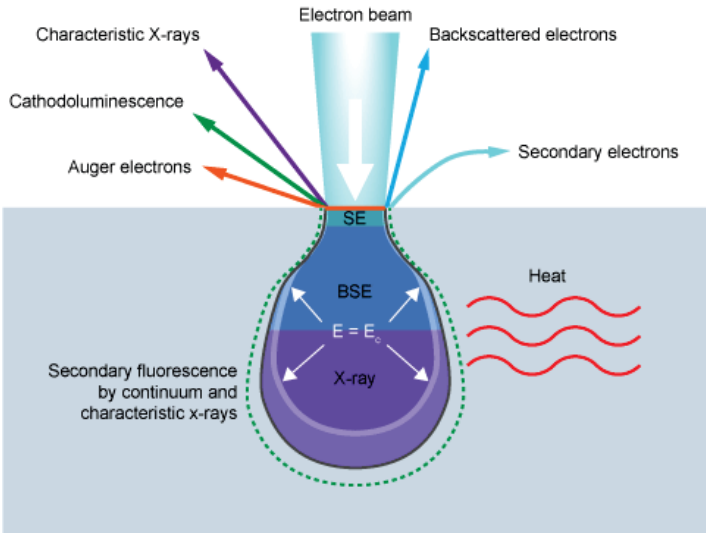


**Figure 2.3**: T*he teardrop-shaped volume of the specimen (interaction volume) with the type of electrons emitted or deflected for each region*[19].

SEM images are processed normally in a SE mode; as the incident electrons have low energy, the detection can be only achieved for few nanometers of the sample surface. Therefore, SE can be useful to image the surface texture and roughness of the specimen. BSE mode of operation involves the revelation of incident electrons with a relatively high

energy (50 eV) and it provides significant information about the structures below the surface of the samples.

The electron source is either a tungsten filament or a solid-state crystal; the tungsten one is the most common due to its low price, high reliability and sustainability for low magnification imaging and X-ray analysis. It has a V shape and it is resistively heated to emit electrons; a particular cylinder (Wehnelt cylinder) is used to produce a focused beam since the tungsten filament when heated produces electrons with spread trajectories.

X-ray spectroscopy is a powerful technique to detect, qualitative and quantitative, the elementary composition of the samples. Upon the collision with an electron beam in a typical SEM, the samples produce characteristic X-rays; since none of the elements have the same X-ray spectrum, it is possible to measure the concentration of that elements in the specimen.

In this thesis, images were taken after metallization with aluminum by a Philips XL 20 SEM microscope (FEI).
The specimens were dried through a surfactant/plasticizer-coating method[20]. It consists of an ambient temperature evaporation of water induced by the submersion of the sample for 40 minutes in an aqueous solution of 4% V/V of a surface-active agent, Triton X-100 (Sigma Aldrich) and of a 20% V/V of plasticizer, glycerol (Sigma Aldrich). After the treatment, MMMAs were hung up in the fume hood to dry for 1.5 hours.
The presence of zeolite in the MMMAs was demonstrated through EDS spectroscopy using a Genesis 2000 (FEI) probe.

### 2.5.2 Contact angle measurements

The contact angle is a fundamental parameter useful to determine the hydrophobicity/hydrophilicity of a materials. The surface wetting properties of the membrane have gained huge importance in the membrane separation field since they can affect the permeate flux, rejection and fouling characteristics of a membrane. The analysis of surface energy and interaction of the liquid with the solid substrate provides information on the wettability or on hydrophilicity/hydrophobicity of the active layer of the membranes[21]. This characteristic can be determined with contact angle measurements. The contact angle is useful to understand the surface

interaction of a three phases system: solid, liquid and air. When a drop of liquid is poured on a flat horizontal surface, the angle formed by the intersection of liquid-air and liquid-solid interface, integrated drawing the tangent line from the contact point between the liquid-air interface, is called contact angle. The interface where the solid, liquid and air are in contact is a three-phase contact line showed in Figure 2.4:

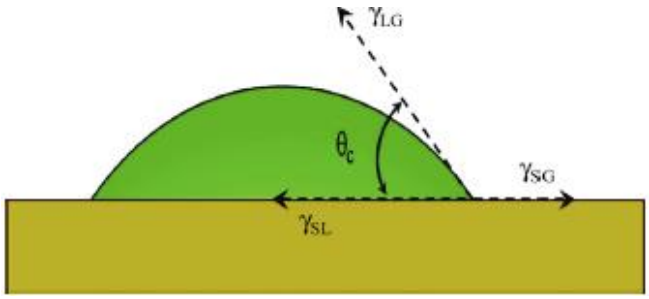


**Figure 2.4**: *Contact angle formed by the liquid spread over a surface. $\gamma_{LG}$ is the surface tension between the liquid and the gas (air), $\gamma_{SG}$ is the surface tension between the solid and the gas (air), $\gamma_{SL}$ is the surface tension between the solid and the liquid and $\theta_C$ is the contact angle.*

The calculation of the contact angle with Young's equation

$$\gamma_{SG} - \gamma_{SL} - \gamma_{LG} cos\theta_C = 0 \quad (20)$$

supposes that the solid surface is an ideal surface meaning that it should be rigid, flat, inert, smooth, homogeneous, insoluble and nonporous. These characteristics are normally not applicable to real surfaces, meaning that the angle value may vary from one point to another. Another important issue is that wetting phenomena are not static; the 3 interfacial tensions are in actual movement and they form what is called the dynamic contact angle. The contact angles expanding over a surface and contracting along the same path are respectively called advancing and receding contact angle. The difference between the 2 values is called hysteresis, that is a fundamental parameter to determine the surface roughness.

MMMAs dynamic contact angles were measured with an Attension Biolin Scientific tensiometer. MMMAs samples were cut in rectangular pieces and hung to an ultraprecise micro-balance while a lift with an extreme high resolution moves up and down a container with the liquid of interest (water). During the dipping phase, the advancing contact angle is measured, while the receding contact angle is measured during the de-wetting process.

Dynamic contact angle measurements can also be useful to assess surface roughness or the presence of contamination. On a contaminated or rough surface, Young's equation (Equation (28)) is valid only locally since the contact angle may vary from place to place on the surface inspected. This means that the adhesion energy varies locally, and the liquid needs to win the energy barriers to wet the surface. This will lead to a contact angle hysteresis that can be measured accounting for the difference between the advancing and receding contact angles.

### 2.5.3 Solvent uptake and density

The water uptake it is a parameter calculated to understand which is the attitude of the membrane in contact with water. It can give information on the swelling behavior of the sample and on the amount of water absorbed at equilibrium conditions.

The membrane water uptake was determined at ambient conditions, the MMMAs samples were first saturated by soaking them for 2 days in deionized water. The MMMAs wet weight, $m_{wet}$ was measured with an analytical balance (Mettler Toledo, precision $10^{-4}$ g). The membranes were then dried overnight in a vacuum oven at 100°C and quickly weighted to estimate the dry weight, $m_{dry}$.

The water uptake, $w_u$, was calculated as follow:

$$w_u = \frac{m_{wet} - m_{dry}}{m_{dry}} \quad (21)$$

Then the density of the hydrated mixed matrix membrane MMMAs, $\rho_{h\text{-}MMMAs}$, was measured with the Density Kit MS-DNY 54 (Mettler Toledo). The hydrated membrane (h-MMMAs) is first weighted in air and then in the auxiliary liquid (ethylene glycol) characterized by a known density. $\rho_{h\text{-}MMMAs}$ is calculated as follow:

$$\rho_{h-MMMAs} = \frac{A}{A-B} * (\rho_w - \rho_{air}) + \rho_{air} \quad (22)$$

where A is the weight of the system in air and B is the weight of the system in ethylene glycol.

The density of the dry MMMAs, $\rho_{MMMAs}$, cannot be measured directly because the membrane is not stable in dry conditions. Therefore, such value was calculated from the density of water $\rho_w$ and that of the hydrated membrane $\rho_{h\text{-}MMAs}$, considering the volume additivity:

$$V_{h-MMMAs} = V_w + V_{MMMAs} \tag{23}$$

$$\frac{m_{wet}}{\rho_{h-MMMAs}} = \frac{m_w}{\rho_w} + \frac{m_{dry}}{\rho_{MMMAs}} \tag{24}$$

$$\rho_{MMMAs} = \frac{\rho_{h-MMMAs} * \rho_w * m_{dry}}{m_{wet} * \rho_w - \rho_{h-MMMAs} * (m_{wet} - m_{dry})} \tag{25}$$

where $\rho_w$ is the water density at ambient temperature (0.997 g/cm$^3$) and $m_w$ is the mass of water adsorbed.

The density measurement in this work of thesis was done as to obtain an indication of the filler distribution uniformity inside the MMMAs. Since the polymer is the lighter phase and the filler the heavier, increasing the adsorber loading an increase in the MMMAs density should be experienced. A property that is normally inspected measuring the density is the interfacial adhesion between the inorganic particles and the polymeric phase. This is common for the characterization of the dense membrane in which a component should preferentially pass or be retained due to the filler presence. If the adhesion at the interface is poor, the sieving effect can be altered, and the separation pursued not achieved.

## 2.6 MMMAs flow and adsorption properties

To assess the MMMAs performances, several tests were performed both in batch and in continuous operation mode. MMMAs hydraulic permeability was measured to evaluate the flow properties while adsorption experiments were done to determine the removal capability of the MMMAs towards single toxin solutions and a for a mixture of urea, creatinine and uric acid.

### 2.6.1 Pure water fluxes and Hydraulic Permeability

The membrane permeability was obtained by measuring the pure water flux though a membrane disc of 6.35 cm diameter using an Amicon® stirred cell. Tests were performed at different pressures, from 0.5 to 1.5 bar. The hydraulic permeability was calculated with Darcy's law (Equation (2)) plotting the water fluxes over the transmembrane pressure.

The apparatus used is reported in Figure 2.5:

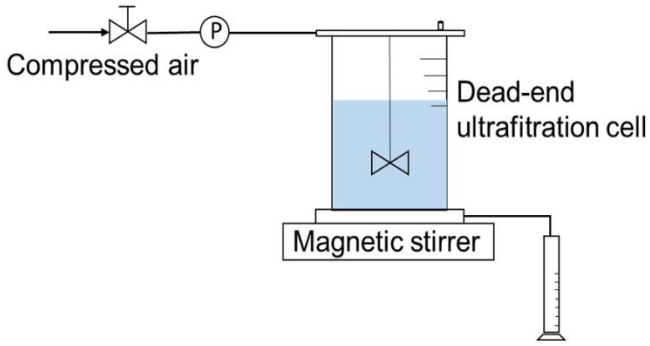


**Figure 2.5***: Ultrafiltration apparatus for the test of hydraulic permeability of MMMAs.*

The apparatus reported in Figure 2.5 is run in a dead-end operation mode, but the continuous stirring applied simulate a cross flow filtration, avoiding solute deposition and thus limiting the occurrence of concentration polarization. Previous work demonstrate that the hydraulic permeability results obtained with this system and with a cross-flow ultrafiltration cell are comparable[22]. The permeate samples are collected till a fixed volume is filled and the water flux is calculated. Then, the water flux is plotted as a function of the transmembrane pressure, TMP:

$$TMP = \frac{P_{Feed\ in} + P_{Feed\ out}}{2} - P_{permeate\ out} \quad (26)$$

Since $P_{permeate\ out}$ is the atmospheric pressure, the TMP is calculate averaging $P_{Feed\ in}$ and $P_{Feed\ out}$. The slope of the linear regression of the plotted date is the hydraulic permeability.

To assess the effect of the pressure on the membranes' flow properties, experiments to monitor the hydraulic permeability in time were done.

### 2.6.2 Single-toxin batch removal capacity

The static binding capacity is a fundamental parameter to assess the adsorption ability of a material. It provides information on the amount of target component removed with respect to the amount of adsorbent used. By normalizing the mass adsorbed over the grams/liters of adsorbent substrate is possible to compare the binding capacity of different materials.

The static binding capacity of the membranes (pure CA and all MMMAs) for the uremic toxins was determined in experiments analogous to the ones performed with the sole filler. Two disks of 15 mm of diameter were immersed in 2 mL of the pure

toxin solution at $c_{MAX}$ and kept under agitation for 24 hours before analysis. Opportune dilutions, according to the calibration curves, where prepared to analyze the feed solution and the solution after the test. Each test was repeated twice to check the reproducibility of the results.

### 2.6.3 Batch removal capacity for a mixture of toxins

One of the purpose of this thesis is to find new adsorbents to remove, at least partially, the uremic toxins present the spent dialysis solution to save water that, in the current process, is sent to the drain. Therefore, it is important to assess the MMMAs performances in contact with a mixture of toxins mimicking the real process situation.

The mixture of urea, creatinine and uric acid was prepared at a concentration equal to $c_{MAX}$ for each toxin and the same experimental procedure described in paragraph 3.5.2 was used. For the analysis, the UV-Vis spectrophotometer was not suitable since both creatinine and uric acid adsorb at 200 nm, which is the unique UV-Vis wavelength at which urea can be properly detected. Therefore, another analytical technique was implemented: High Performance Liquid Chromatography, HPLC. It allows the detection of mixtures of component through a chromatographic column able to separate the solutes present according to the analytes dimension or to the analytes/column interactions. There exists different type of chromatography techniques and the most common are briefly summarized in the following lines:

- **Size Exclusion Chromatography**: it separates particles according to the molecular size.
- **Reversed-Phase Chromatography**: it operates on the principle of hydrophobic interactions between the column packing (stationary phase), the liquid phase circulating in the column (mobile phase) and the analytes.
- **Ion-Exchange chromatography**: the retention is based on the attraction between the ions in solution and the charged sites on the stationary phase
- **Affinity Chromatography**: it is used to purify biological molecules present in a mixture exploiting the high affinity interaction between the target and the stationary phase and the consequent removal of the molecule of interest.

#### *2.6.3.1 High Performance Liquid Chromatography (HPLC) procedure*

In this work, to determine the solutions concentration when a mixture of toxins was used the HPLC technique was utilized. The system used comprehend a separation module, *Waters 2695 Separations Module*, a UV-Vis detector able to monitor simultaneously two different wavelengths, *Waters 2497 Dual λ Absorbance Detector* and a Hydrophobic interaction column XBRIDGE C18, 3.5 μm, purchased from Waters (column dimensions: 4.6 mm x 50 mm) The mobile phase used was a mixture of water, HPLC grade purchased from Merck and acetonitrile supplied by Scharlau. All the tests were run in an isocratic mode with a fixed water/acetonitrile percentage, 98:2. This proportion was found to be the most adequate to have an acceptable peaks resolution. The stationary phase of the column is a C18 chain and it separates thanks to the action of hydrophobic interactions: C18 has stronger affinity towards less polar compounds and normally an aqueous (polar) mobile phase is used to elute the target component. Thus, the more polar toxin will be the first one to exit the column while the less polar will be the last. The topological polar surface area (TPSA) can be an indication of the overall polar atoms present on a molecule surface, thus it can give an indication of the hydrophilic character of the molecule. TPSA[23][24][25] values for creatinine, urea and uric acid are reported in Table 2.4:

**Table 2.4***: Topological surface polar area of the toxins considered.*

| Toxin | TPSA (Å) |
|---|---|
| *Creatinine* | 59 |
| *Urea* | 69 |
| *Uric acid* | 99 |

As is possible to see from Table 2.5 the TPSA is very similar for the three toxins and is a challenge to separate them. After several attempts the 98:2 water/acetonitrile composition was found to be the best one to achieve the goal. The flow rate was kept low, 0.5 mL/min, to minimize the pressure drops along the column.

As for the UV-Vis spectrophotometer, also for these tests, calibration curves were performed, and the experiments were repeated twice to verify the reproducibility of the results.

### 2.6.4 Continuous removal capacity for single-toxin solutions and for a toxin mixture

Continuous adsorption tests were performed to calculate the dynamic adsorption capacity of the MMMAs prepared. This is a fundamental parameter to determine the performances of the MMMAs in real process conditions. To investigate the dynamic behavior of MMMAs a particular set-up is needed. Fast Protein Liquid Chromatography, FPLC, is a liquid chromatographic technique normally used to separate protein mixture. It allows the construction of breakthrough curves from which is possible to calculate the dynamic adsorption capacity of the materials tested. Typically, it is composed by:

- **High precision pumps**: they are normally two-cylinder piston pumps that can guarantee a range of flow rates from few mL per minute for laboratory uses to several liters per minutes for industrial scale applications
- **Injection loop**: is composed of tubing, of a glass cylinder (super loop) that contains the sample solution to be injected in the column. This allow the injection of a known volume of solution.
- **Injection valve**: it is a motorized valve with three different possible position for loading the sample loop, injecting the sample in the column and for connecting the pump to the waste line.
- **Column**: It can be a glass or plastic column packed with the materials chosen for the separation. It is possible to connect also stainless-steel cells in which membrane can be stacked.
- **Flow cell**: The solution exiting the column passes through one or more flow cells to measure the analytes concentration by Uv-Vis absorption. It is equipped also with a conductivity and a pH flow cells.
- **Fraction collector**: It is a rotating rack that can be filled with tubes collecting the fraction of the samples exiting the column in fixed volumes.

As mentioned above, in dynamic experiments, the concentration at the outlet of a fixed bed adsorber is defined by a breakthrough curve. This curve is the time-resolved effluent concentration of the compound under investigation. It is possible, with the auxilium of a dispersion curve that takes into account the system dead volumes, to calculate the amount of analyte adsorbed in flow conditions. The difference between the integrated area beneath the dispersion and the breakthrough curves can be used to determine the dynamic adsorption capacity.

### *2.6.4.1 Fast Protein Liquid Chromatography (FPLC) set-up and procedure*

The FPLC used to calculate the dynamic binding capacity is an AKTA PURIFIER (GE Healthcare) and the scheme of the apparatus and the injection valves position are reported in Figure 2.6 and 2.7:

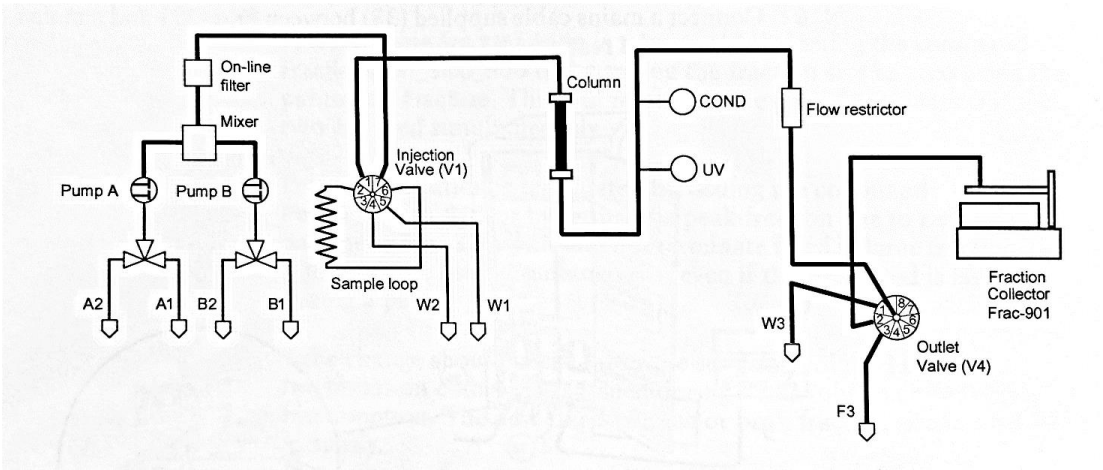


**Figure 2.6***: FPLC components set-up.*

The equipment has two pumps connected to a mixer that allow the injection of different feed solutions. The feed is then sent to the injection valve that has three different operating positions:

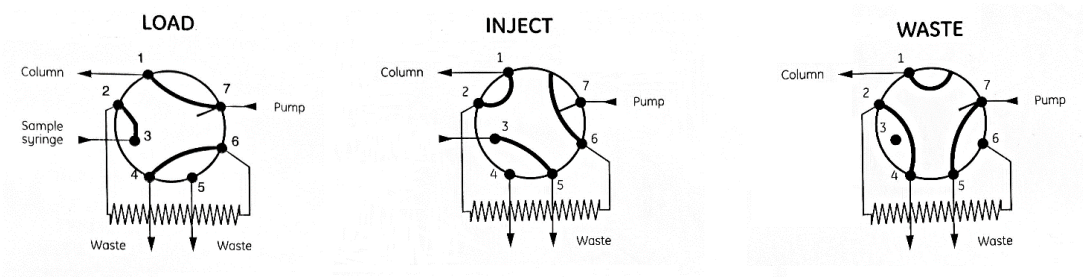


**Figure 2.7***: FPLC injection valve positions.*

In the load one, the solution coming from the pump is directly sent to the column and subsequently to the UV and conductivity detector; this configuration is normally used to clean and stabilize the sample cell before the test; in the injection position the feed solution charge in the loop is sent to the column. The adsorption test is done in this configuration. In the waste valve position, the column is disconnected from the pump and loop can be emptied. The machine is also equipped with an automatic sample collector that can be used to analyze fraction of the solution coming out of the sample cell.

For the FPLC tests, a stainless steel column was packed with disks of 25 mm of the MMMAs synthesized; the MMMAs were stacked with the active layer facing the inlet solution and a flow distributor was used to assure a complete wetting of the membranes. 40 mL of aqueous feed solution were placed in sealed glass cylinder, the super loop, to introduce the sample in the system avoiding the suction of air. Both the loop and the cell were connected to the injection valve. The membrane cell was flushed with deionized water till no air bubbles were detected. The flow rate was fixed to 0.5 mL/min to keep the pressure drop around 0 and the UV-Vis detector was set with the proper wavelength according to the toxins to be detected.

For the tests with the mixture of the three toxins the cell was packed with 22 membranes of 25 mm of diameter. Two MMMAs were chosen according to the performances obtained with the batch and continuous adsorption tests. Since the UV-Vis signal of creatinine and uric acid interferes with the one of urea, was not possible to detect the three toxins outlet concentration. Therefore, samples were taken at fixed time intervals and analyzed at the HPLC with the set-up and procedure described in paragraph 2.6.3.1

As mentioned above, to analyze the data a dispersion curve accounting for the system dead volume is needed. To build this curve a solute that does not interact with the substrate placed in the column is normally used. Acetone, arginine or lysine are generally used but in the case of MMMAs all of them were not suitable for scope: acetone, even in very dilute concentration, is a solvent for cellulose acetate and it alters the membrane conformation while arginine and lysin were adsorbed by the membranes (this was verified with batch adsorption tests). Therefore, NaCl was used as solute to build the dispersion curve.

## 2.7 CA/$SiO_2$ hybrid membranes characterization in a surrogate system of an Artificial Kidney (AK)

CA/$SiO_2$ hybrid membrane were characterized for their morphology, surface characteristics and composition in previous works[18]. Therefore, was not necessary being the synthesis a consolidated process, to repeat the tests.

In this work, the CA/$SiO_2$ membrane were tested to determine the hydraulic permeability, the molecular weight cut-off and rejections towards toxins and proteins in a surrogate system of an artificial kidney. The process scheme is show in Figure 2.8.

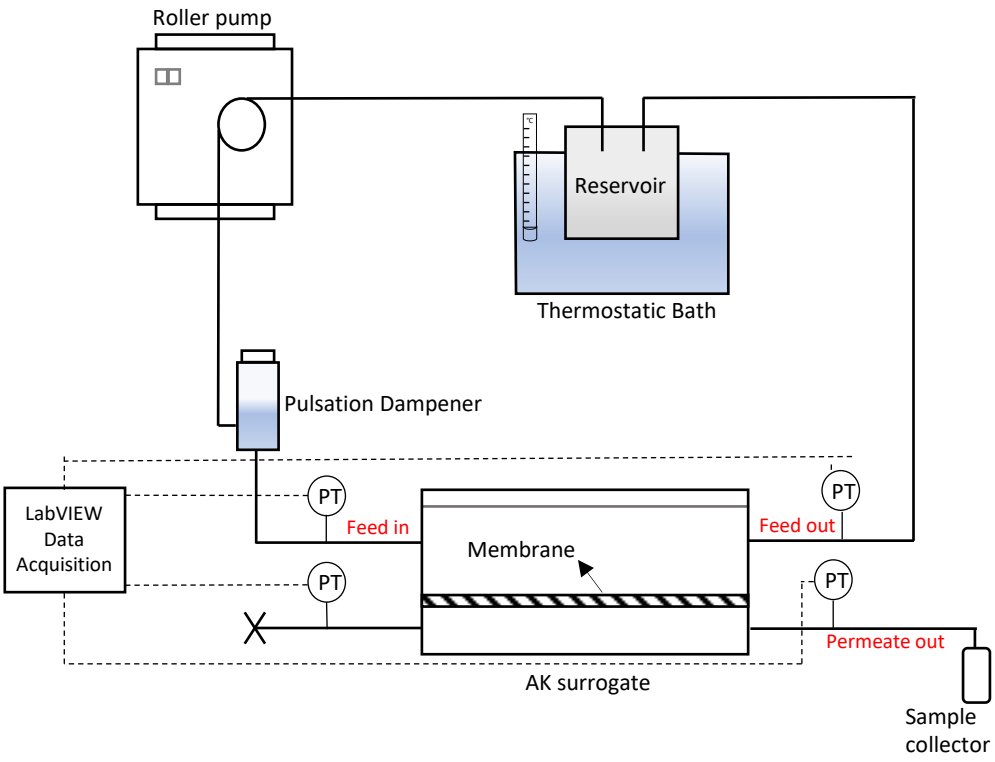


**Figure 2.8***: Scheme of the apparatus used.*

The system is composed of a feed solution reservoir placed in a thermostatic bath to control the temperature, a roller pump, a pulsation dampener to avoid flow intermittences in the membrane cell, the surrogate of the artificial kidney (AK) and four pressure sensors connected to a data acquisition program (LabVIEW). The system is also equipped also to work in dialysis mode, but for the subsequent test described only one feed was used and the bottom left channel was kept closed.

The membrane cell is a surrogate of an artificial kidney. It is made in Plexiglas and the technical draw is reported in Figure 2.9 below:

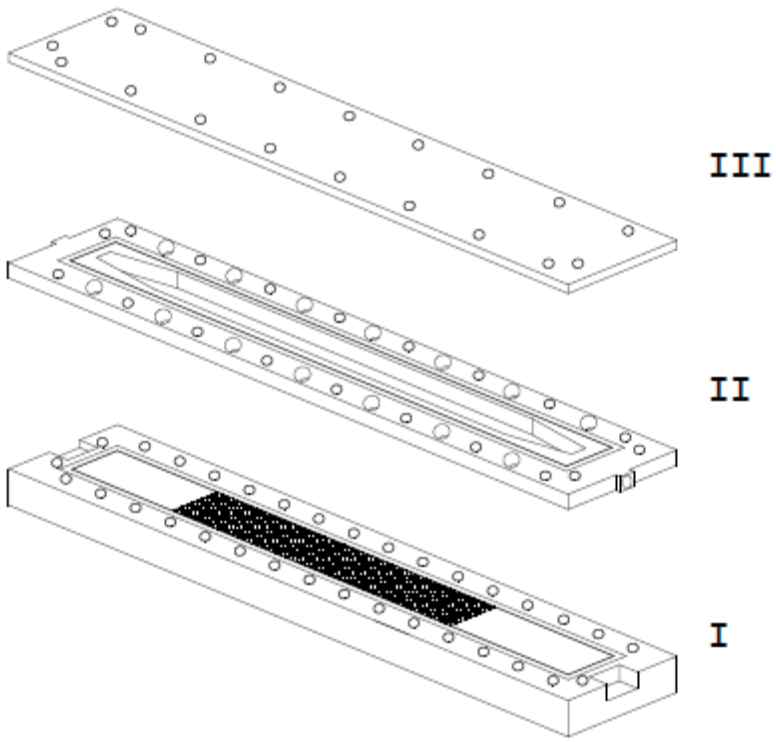


**Figure 2.9***: Prospective draw pf the membrane cell: the surrogate system of an artificial kidney***.**

It is composed of four parts: two sealing pieces on the top and at the bottom, one part defining the feed channel and a porous support piece on which the membrane is posed. The perforated area on the membrane holder is a rectangle of 60 $cm^2$ of dimension, with holes of 1 mm of diameter distanced 1.5 mm. Therefore, the overall active area for permeation is 20.9 $cm^2$. The cell has a slit geometry and it is projected to assure a complete developed laminar flow once the fluid reaches the perforated area. The membrane needs to be cut sufficiently big to be placed beneath the O-ring to avoid leakages.

Prior to start the tests, the roller pump needed to be calibrated. An acetate sheet was placed in the membrane holder part to avoid permeation and effectively determine the flow rate given by each pump position. The pressure was always monitored to already have an indication to the inlet and outlet pressure corresponding to an assigned flowrate. Nine different pump positions were set, and the samples collected at fixed time intervals and weighted to determine the mass. After, data were elaborated, and the pump calibration was determined.

When a membrane is installed in the cell, a compaction process is needed. Since the hybrid membrane are compressible, this procedure allows the membrane to assume a stable configuration that must be kept for all the experiment duration.

### 2.7.1 Permeation towards reference solutes: Molecular Weight Cut-Off (MWCO)

One parameter to determine the membrane performance is the Molecular Weight Cut-Off (MWCO). It is defined as the molecular weight for which 90% of the solute is retained. Even if membranes were fully characterized in previous work and the casting procedure well established, is common practice to assess this parameter again.

In Table 2.5 the reference solutes used to determine the MWCO of CA_30 and CA_22:

**Table 2.5***: Reference solutes used for MWCO calculation.*

| | |
|---|---|
| *CA_30* | PEG 10 kDa |
| | PEG 20 kDa |
| | PEG 35 kDa |
| *CA_22* | PEG 1 kDa |
| | PEG 10 kDa |
| | PEG 20 kDa |

Tests were performed at 90 mL/min with a concentration of 0.6 mg/mL and samples collected and analyzed through Total Organic Carbon measurements. TOC is a measure of the total amount of carbon in organic compounds in pure water or aqueous solution. It is an analytical technique to determine the concentration of a target compound, Since the PEG concentration cannot be directly determined by UV-Vis spectrophotometry, a TOC analyzer machine (TOC-VWS Shimadzu) was used to measure and to calculate the PEG rejection coefficient.

Like for every analytical technique, a calibration curve for all the PEG considered were performed. TOC analysis is very sensitive, therefore extreme caution is needed in preparing the samples. TOC analyzer used a catalytic oxidation combustion technique at high temperature (720°C) to convert organic carbon into carbon dioxide, $CO_2$. The $CO_2$ generated is then measured with a non-dispersive infrared sensors. The solution is automatically injected using a syringe into the machine and the infrared signal is automatically integrated and converted in concentration values.

Rejection coefficients, f, are then calculated and plotted in a $ln(f/(1-f))$ vs molecular weight graphs. Data are linearly fitted and the MWCO is determined through graphic extrapolation of the intersection between the linear regression and the value of $ln(f/(1-f))$ corresponding to 90%.

### 2.7.2 Hydraulic Permeability and Apparent rejections coefficient experiments

The pure water flux was measured to determine the value of hydraulic permeability of CA_30 and CA_22. The roller pump was set to 9 different positions and the permeate sample collected at fixed time interval and weighted. The transmembrane pressure (TMP) was calculated with Equation (26):

Also for this set-up, since $P_{permeate\ out}$ is the atmospheric pressure, TMP is calculated by averaging $P_{Feed\ in}$ and $P_{Feed\ out}$. Then the water fluxes calculated are plotted as function of the TMP and the slope of the linear regression is the hydraulic permeability.

Uremic toxins and BSA rejection tests were done always collecting the permeate sample at fixed time intervals, weighting the amount of solution permeated and analyzing the concentration (opportunely diluted) at the UV-Vis spectrophotometer. Experiments were conducted for different solute concentrations and for different feed flowrates ranging from 40 mL/min to 143 mL/min. The system was equilibrated for 30 minutes before starting the test and after every change in flow rate the pressure was let stabilize. Feed solution samples were taken at the beginning of the test, and before and after each experiment (for all feed flow rates).

In Table 2.6 are reported the solute concentrations at which rejections experiments were performed:

**Table 2.6***: Uremic toxins and BSA concentrations used in apparent rejection experiments.*

| Solute | Concentrations (mg/mL) |
|---|---|
| *Urea* | 4 |
| | 0.5 |
| *Creatinine* | 0.24 |
| | 0.012 |
| *Uric Acid* | 0.03 |
| | 0.003 |
| *p-CS* | 0.2 |
| | 0.1 |
| | 0.05 |
| *BSA* | 10 |
| | 5 |
| | 1 |
| | 0.2 |

Solutes concentrations were determined, and apparent rejection coefficients were calculated.

## 2.8 Fluid mechanics characterization of a surrogate system of an artificial kidney (AK)

Fluid mechanics is the field of physics in which fluid behavior is studied. In this chapter basic equations of fluid mechanics are mentioned since they are propaedeutic for the derivation of the Hagen Poiseuille equation for an impermeable slit which is used for the fluid mechanics characterization of the surrogate system of an artificial kidney (AK). The basic equations governing the fluid mechanics are the Navier-Stokes equations. They are three partial differential equations which describe the motion of viscous fluid substances and they mathematically express the conservation of momentum and the conservation of mass for Newtonian fluids. The Navier-Stokes equations are useful to describe the physics of many phenomena of scientific and engineering interest. One analytic solution of the Navier-Stokes equations is the 2-dimensional Hagen Poiseuille flow equation:

$$p_1 - p_2 = \frac{32\mu VL}{D^2} \quad (27)$$

In a Poiseuille flow the fluid moves through long, straight and rigid channel thanks to a pressure difference imposed between the two ends of the channel and it is valid for channels with circular cross-sections. However, especially in laboratory environments and in microfluidics, it is frequent to deal with other channel geometries like micro-channels with a rectangular cross-section. Therefore, an analogue of Equation (27) for slit geometries must be derived to be used in this work for the fluid mechanics characterization of a surrogate system of the artificial kidney (AK). Previous studies [26] pointed out the surface phenomena gain importance in scaling down the system to micro and mini-channels. Such is the case of pressure drops due to surface roughness that become even more complex when suction through permeable walls is present (such as membrane processes like the surrogate system of an artificial kidney presented in this thesis). The flow in mini-channels/slits with suction, with the global deformation of the velocity profile due to permeation may have a tremendous importance in a wide range of industrial and biomedical applications since it affect the global mass transport process.

### 2.8.1 Analog of Hagen-Poiseuille equation for an impermeable slit (rectangular section)

As it is mentioned above, the Hagen-Poiseuille flow equation is derived for circular, straight channels. Unfortunately, there exist no analytical solution of the Poiseuille flow problem for rectangular cross-section. Despite the high symmetry of the geometry, the best way to solve it analytically is through a Fourier sum. The geometry taken into consideration is reported in Figure 2.10

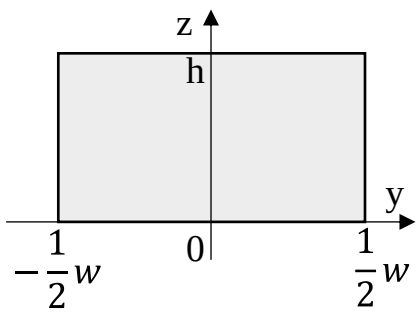


**Figure 2.10***: Rectangular channel with a cross-section height h and width w used to derive the Poiseuille flow equation for a slit.*

In the following equation and considerations, the width of the channel is always considered larger than the height, w > h. The starting Navier-Stokes equation and the associated boundary conditions are:

$$\left[\partial_y^2 + \partial_z^2\right] v_x(y,z) = -\frac{\Delta P}{\rho L}\ for -\frac{1}{2}w < y < \frac{1}{2}w, 0 < z < h \quad (28)$$

$$v_x(y,z) = 0\ for\ y = \pm\frac{1}{2}w, z = 0, z = h \quad (29)$$

Using Fourier series expansions, and considering the ratio $h/w \rightarrow 0$ as an approximation, the value of the flow rate Q for rectangular cross sections becomes:

$$Q \approx \frac{h^3 w \Delta P}{12\rho L}\left[1 - 0.630\frac{h}{w}\right], for\ h < w \quad (30)$$

This is the equation used to calculate the theoretical pressure drop in a channel with a rectangular geometry, and it is used to compare the results obtained in the following experiments. This relation is valid for turbulent flow regime[27].

### 2.8.2 Evaluation of permeation effect on the velocity profile

Little attention is given to the influence of permeation rates on the flow field in hemodialyzers, particularly on the potentially blood-traumatizing shear stresses developed on the membrane surface. Pressure drop can be representative for these forces and in this work its quantification is performed in a surrogate of an artificial kidney system mimicking tangential fluid velocities and membrane removal rates with circulating water.

The two flat-sheet ultrafiltration membranes prepared CA_30 and CA_22 are tested in the surrogate of an AK set-up. The channel in which the fluid flows is reported in Figure 2.11:

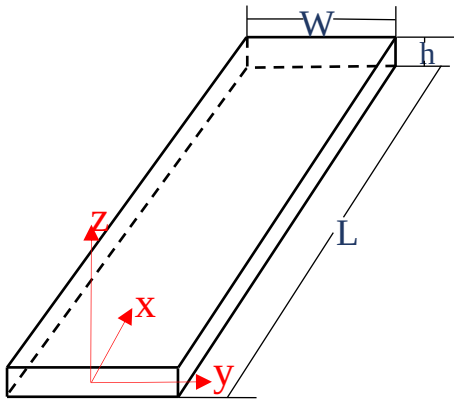


**Figure 2.11***: Feed channel geometry and axis.*

It is a slit with a channel height, h, of 600 µm, a width, W, of 3 cm and a length, L, of 25 cm. The set-up is the one reported in Figure 2.8 and the feed (water) from a 5 L tank is pumped through the slit at volumetric flow rates ranging from 40 mL/min to 145 mL/min. Samples of the permeate and of the retentate are collected and weighted at a fixed time interval. The pressure gradient, ΔP, along L is registered. Tests were done both with the ultrafiltration membrane (permeable walls) and with an acetate sheet (impermeable walls). Since the pressure sensors are measuring exactly the pressure drop across the membrane, to calculate the real pressure loss all the ΔP related to the accidentalities present are discounted from the value registered by the sensors.

Changes in tubes diameter, presence of fittings and tapered inlet and outlet geometries are accounted and thanks to the Bernoulli equation are subtracted from the value of ΔP given by the sensors:

$$\frac{P_A - P_B}{\rho g} + z_A - z_B + \frac{v_A^2 - v_B^2}{2g} - 4f\frac{L_{AB}}{D_{AB}}\frac{v^2}{2g} - k_{i,AB}\frac{v^2}{2g} = 0 \qquad (31)$$

This is the Bernoulli equation for a given part AB of the system. $P_A - P_B$ is the pressure difference in Pa for that part, $z_A - z_B$ is the height difference in m, $v_A^2 - v_B^2$ is the velocites difference while $4f\frac{L_{AB}}{D_{AB}}\frac{v^2}{2g}$ and $k_{i,AB}\frac{v^2}{2g}$ are the distributed (m) and the concentrated (m) pressure losses, respectively. The first takes into account the ratio between the length and the diameter of the portion considered while the second considers the decrease of driving force related to accidentalities, k.

For the experiments, Bernoulli equation was solved for each part of the system involving a change in tube section from the pressure sensors to the membrane cell.

In Table 2.7 are reported the k values used for each accidentality considered:

**Table 2.7***: Types of accidentality present in the system from the pressure sensor to the membrane cell and their values.*

| Type of accidentality | k |
|---|---|
| *Fitting between tubes* | 0.56 |
| *Inlet Fitting* | 0.4 |
| *Outlet Fitting* | 0.6 |
| *Tube section reduction* | 4.8 |

For the conical (tapered) inlet and outlet inside the membrane cell no k was find already tabulated, thus was calculated using the equations reported in Table 2.8:

**Table 2.8**: *Local pressure drop correlations for conical (tapered) geometries.*

| Tapered expansion (inlet) | Tapered reduction (outlet) |
|---|---|
| 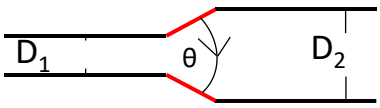 | 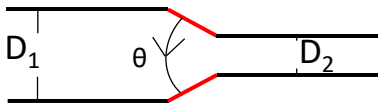 |
| $\boldsymbol{k = 2.6 sin\left(\frac{\theta}{2}\right) \cdot 2 \cdot \left[1 - \left(\frac{D_1}{D_2}\right)^4\right]}$ | $\boldsymbol{k = 1.6 sin\left(\frac{\theta}{2}\right) \cdot \left(1.2 + \frac{160}{Re}\right) \cdot \left[\left(\frac{D_1}{D_2}\right)^4 - 1\right]}$ |
| For Re < 2500 and θ < 45° | For Re < 2500 and θ < 45° |

The value of $\boldsymbol{\theta}$ was determine with the mechanical drawing of the cell (Figure 2.9) and it is 27°.

According to Equation (30), which can be used in this case since h << W, the uncertainty on $\Delta P$ is a function of the variables present[28]:

$$\frac{\sigma_{\Delta P}}{\Delta P} = \sqrt{\left(\frac{\sigma_\mu}{\mu}\right)^2 + \left(\frac{\sigma_L}{L}\right)^2 + \left(\frac{\sigma_Q}{Q}\right)^2 + \left(\frac{\sigma_W}{W}\right)^2 + \left(3\frac{\sigma_h}{h}\right)^2} \quad (32)$$

Since $h/w \rightarrow 0$ this term has been neglected. For the sake of simplicity, it is possible to assume that the uncertainty on the physical properties (viscosity) is neglected since the temperature of the solutions is controlled and kept constant. Since W and L can be measured easily a 2% of uncertainty was considered for these two terms. From the pump calibration, a 5% of uncertainty was associated to Q. It was supposed that the highest uncertainty present is the one connected to the height of the channel since it is difficult to be determined.

Therefore, a 10 % of error was account for it. Replacing these values in Equation (32) yields to:

$$\frac{\sigma_{\Delta P}}{\Delta P} = 18\% \quad (33)$$

which is the error considered for the theoretical pressure drop graphs.

The $\Delta P$ uncertainty on the experimental values, on the other hand, depends on the sensor precision (high accuracy ±1 mmHg) and mainly on the channel height and on the local pressure drop uncertainties. The correlation used to account for the local pressure drops from the sensor to the cell are applicable for the turbulent flow regime, therefore, being the experiments in laminar flow conditions, to be conservative a 20% overall $\sigma\Delta P$ was considered.

## 2.9 Mass transfer characterization of a surrogate system of an artificial kidney (AK)

Before going into the detailed description of the methodology used for the mass transfer characterization of the system considered, an overview on the transport mechanism governing UF and NF membranes needs to be done[29].

The selectivity of an UF membrane is exclusively based on stereochemical principles while for NF membranes, there is also solute diffusion across the polymeric matrix. For both processes (UF and NF), as first approximation to simplify the analysis, if neutral solutes are used, it is possible to neglect solute-solute and solute-membrane interactions and to assume that the fluxes and rejections depend on stereochemical impediments and on hydrodynamic forces. The separation efficiency of NF and UF membranes does not depend only on membrane characteristics but also on the transport phenomena occurring in the fluid phase that wets the membranes.

### 2.9.1 Convective transport through a porous membrane layer

The pressure-driven convective flow is the most common model used to describe flow in a capillary tube; it has as core mechanisms, the sieving process, which is the base of both microfiltration and ultrafiltration processes. It consists in rejecting the molecules with a size greater than the membrane pores. Two different approaches are used to describe the

permeability across porous layers when the membrane can be considered an arrangement of near-spherical particles, the Carman-Kozeny equation can be applied:

$$J = \frac{\varepsilon^2}{K \cdot \mu \cdot S^2 \cdot (1-\varepsilon)^2} \frac{\Delta P}{l_{pore}} \tag{34}$$

where $J$ is the permeate flux (m/s), $\varepsilon$ is the porosity, $\mu$ is the dynamic viscosity (kg/(m·s)) of the permeate, $K$ is the permeability of the porous medium, $S$ is the specific area per unit volume ($m^2/m^3$), $l_{pore}$ is the thickness of the porous layer (m) and $\Delta P$ is the pressure difference between the feed and the permeate side of the membrane (normally in bar). $K$ is a function of the pore size distribution, of the membrane porosity and of the viscosity of the treated solution. In the other approach, the laminar flow through capillaries can be defined with a differential momentum balance equation, Newton law of viscosity. After the integration, the Hagen-Poiseuille equation for porous media is derived. It describes the convective velocity through porous membrane according to Equation (35):

$$J = \frac{\varepsilon \cdot d_{pore}^2}{32 \cdot \mu \cdot \tau} \frac{\Delta P}{l_{pore}} \tag{35}$$

where $\tau$ is the tortuosity of the pores and $d_{pore}$ (m) the pore diameter. In addition, Darcy law (Equation (2)) can be used as basic equation to relate the fluid flow rate to the hydraulic permeability and the driving force governing the process for the porous medium

### 2.9.2 Useful dimensionless number and parameters

Dimensionless number are often used in fluid mechanics and mass transport as tools to reduce the amount of experimental data required to correlate physical phenomena to scalable systems. The classical transport phenomena of mass, momentum and energy are principally analyzed by the ratio of effective diffusivities in each transport mechanism. Six dimensionless number give the relative importance of different phenomena such as inertia, viscosity, conductive heat transport and diffusive mass transport. Below there is a list of the most important numbers that will be necessary to the following chapters:

- ***Reynolds number***: it correlates inertial and viscous forces

  $$Re = \frac{\rho \cdot v \cdot L}{\mu} \tag{36}$$

where $\rho$ in kg/m$^3$ is the density of the fluid, $v$ is the velocity of the fluid in m/s, $\mu$ its viscosity in kg/(m s) and L the characteristic length in m of the considered phenomenon.

- ***Schmidt number***: it relates the viscous to mass diffusion rates

$$Sc = \frac{\mu}{\rho \cdot D} \quad (37)$$

where $\rho$ in kg/m$^3$ is the density of the fluid, $\mu$ its viscosity in kg/(m s) and D is the mass diffusivity in m$^2$/s.

- ***Péclet number***: it is defined as the ratio between the advective transport and diffusive rates

$$Pe = \frac{L \cdot u}{D} \quad (38)$$

where $L$ is the characteristic dimension of the system in m, $u$ is the local fluid velocity in m/s and D is the mass diffusion coefficient in m$^2$/s.

- ***Sherwood number***: it represents the ratio of the convective mass transfer to the rate of diffusive mass transport and it is the analog of Nusselt number for mass transfer

$$Sh = \frac{h \cdot L}{D} \quad (39)$$

where $\rho$ in kg/m$^3$ is the density of the fluid, $v$ is the velocity of the fluid in m/s, $\mu$ its viscosity in kg/(m s), L the characteristic length in m of the considered phenomenon, D is the mass diffusivity in m$^2$/ss and $h$ is the mass transport coefficient in m/s.

The are several parameters defining the performances of a membrane: the hydraulic permeability and the rejection coefficients. There exist two types of rejection coefficients: one is the observed or apparent rejection coefficient, f, that is normally calculated during filtration experiment taking into account the solute concentration in the feed solution and the solute concentration in the permeate solution, while the other is known as the real rejection coefficient, f ', which is dependent on the solute concentration on the membrane surface and on the solute concentration in the permeate. Normally membrane filtration processes are affected by accumulation of solutes on the membrane surface. This leads to a concentration gradient from the bulk of the feed solution to the surface of the membrane; this phenomenon is known as concentration polarization that is a precursor of fouling. It influences the transport mechanism across the membrane and therefore, to define membrane selectivity in presence of concentration polarization, the intrinsic rejection coefficient is needed.

### 2.9.3 Mechanisms in the fluid phase adjacent to the membrane

During membrane separation processes, the solvent is the preferential component that permeates; this induces the formation of a concentration gradient of the solute from the bulk of the solution to the membrane surface. This phenomenon is known as concentration polarization and it is object of an intense investigation due to its practical importance in reducing the operation efficiency of industrial processes. In Fig. 2.12 concentration polarization is schematically depicted:

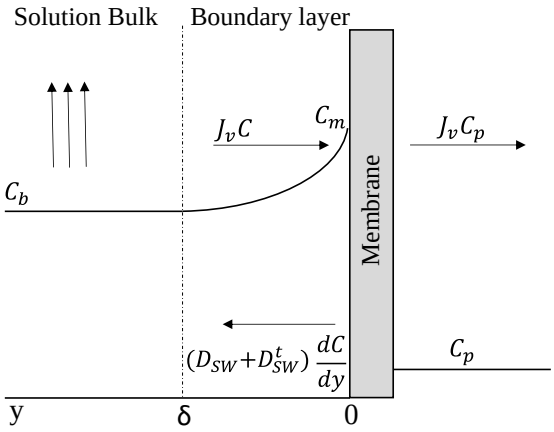


**Figure 2.12**: *Concentration profile in the layer adjacent to the membrane.*

During the sixties, several scientists [30][31][32][33]investigated the mass transport in the boundary layer close to the membrane for turbulent flow in a steady state regime. At high values of the Schmidt number and for partial intrinsic rejections, they obtained the following expression for the mass flux of solute, $J_s$, from the bulk of the solution to the membrane surface:

$$J_s = (D_{SW} + D_{SW}^t)\frac{dC}{dy} + J_v C = J_v C_p = (1 - f')J_v C_m \quad (40)$$

where $D_{SW}$ is the molecular diffusivity, $D_{SW}^t$ is the turbulent molecular diffusivity, $C$ is the solute concentration, $J_v$ is the permeation volumetric flux, $C_m$ and $C_p$ are the solute concentration at the membrane-feed interface and in the permeate respectively, and $f'$ is the intrinsic rejection coefficient defined as:

$$f' = \frac{C_m - C_p}{C_m} \quad (41)$$

When in Equation (41) instead of the concentration on the membrane surface, $C_m$, the concentration of the feed solution (bulk concentration, $C_b$) is used, the apparent rejection coefficient, f, is calculated and this is easily obtainable from experimental results:

$$f = \frac{C_b - C_p}{C_b} \tag{42}$$

In Equation (42) the first term takes into account the molecular and turbulent diffusion, while the second term is related to the convective contribution.

When the membrane is tested only with pure water, the concentration polarization phenomenon is not present, and the volumetric permeate flux is proportional to the transmembrane pressure difference (TMP) and to a proportionality constant $L_p/\mu$ defined as the permeability coefficient of the solvent (with $L_p$ hydraulic permeability). When the permeation of solution with low molecular weight solutes is concerned, the formation of the concentration gradient across the membrane generates an osmotic pressure gradient, Δπ, that makes the effective hydraulic pressure decrease resulting in a decrease of permeate flux. In these circumstances, the volumetric permeate flux is:

$$J_v = \frac{L_p}{\mu}\{\Delta P - [\pi(C_m) - \pi(C_p)]\} \tag{43}$$

During ultrafiltration of solutions containing macromolecules is common to attribute the decrease in flux to the appearance of an additional resistance to transport related to the layer of concentration polarization on the membrane surface. When the concentration of macromolecule gel formation is reached, the resistance is the highest and there is no increase in flux with the increase of the applied pressure. This model is known as the model of resistances in series in the fluid phase close to the membrane and the mechanism is reported in Figure 2.13:

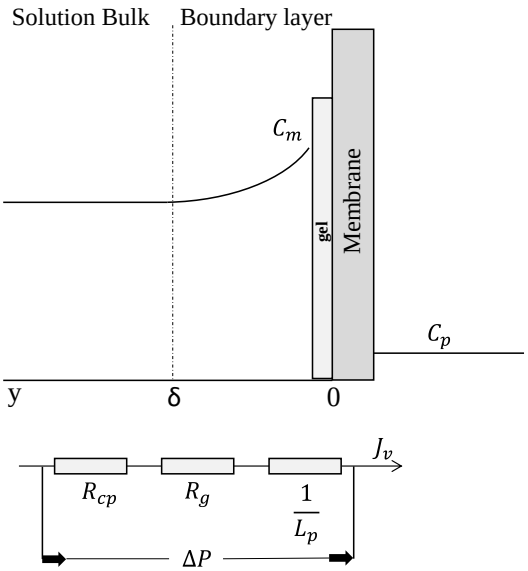


**Figure 2.13***: Illustration of the resistances in series model in the boundary layer adjacent to the membrane.*

The model of the resistance in series is described by Equation (44):

$$J_v = \frac{\Delta P}{\mu(1/L_p + R_{cp} + R_g)} \tag{44}$$

where $1/L_p$, $R_{cp}$ and $R_g$ are the resistance of the membrane, of the polarization layer and of the gel, respectively.

The integration of Equation (40) brings to different solutions according to the conditions considered.

#### *2.9.3.1 The film theory*

The film model assumes that in turbulent flow, in the membrane-feed solution interface, exists a fluid layer of constant thickness, δ, that is not affected by the turbulences. So, $D_{SW}^t$ can be approximated to zero and, therefore, the flow there is predominantly laminar[34]. In this layer the transport properties can thus be considered constant. Integrating Equation (40) with these boundary conditions:

$$C = C_m \; when \; y = 0 \tag{45}$$

$$C = C_b \; when \; y = \delta \tag{46}$$

the following equation is obtained:

$$\frac{C_m - C_p}{C_b - C_p} = e^{\frac{J_v}{D_{SW}/\delta}} \tag{47}$$

Introducing in Equation (47) Equations (41) and (42), the dependence between f and f':

$$f = \frac{f'}{f' + (1+f')exp\left[\frac{J_v}{D_{SW}/\delta}\right]} \tag{48}$$

Equation (48) can be considered the basic equation for concentration polarization, being it the starting expression for a conspicuous part of the models describing the process. They normally differ only for the calculation of the thickness of the layer adjacent to the membrane, δ. The complexity of Equation (48) is in the determination of the thickness of the layer adjacent to the polarization layer. To overcome the problem, the simple technique adopted by the film model is that, in this situation of low mass transfer (common in ultrafiltration, nanofiltration and reverse osmosis), the diffusive contribution is predominant[29]. So, defining the mass transfer coefficient, k, as the proportionality constant between the flux across the interface feed-membrane and the concentration difference $C_b - C_m$:

$$J_s = k(C_b - C_m) \tag{49}$$

the total flux is approximated with the diffusive flux obtainable integrating the Fick's law with the boundary layer defined in Equations (45) and (46),

$$\frac{D_{SW}}{\delta}(C_b - C_m) \approx k(C_b - C_m) \tag{50}$$

obtaining the relation between the mass transfer coefficient and the thickness of the concentration polarization layer:

$$k = \frac{D_{SW}}{\delta} \tag{51}$$

#### *2.9.3.2 Revision on mass transfer coefficients*

Due to the difficulties in the determination of the boundary layer thickness, $\delta$, it is normal practice in engineering to use mass transfer coefficients, k, to calculate the concentration at the interface. The goal is to correlate mass transfer coefficients with other variables. From the flux and mass transfer coefficient definition is visible that k varies with the

interface geometry, with the flow regime of the fluid adjacent to it and with the fluid transport properties:

$$k = k\ (geometry, \langle u \rangle, D_{SW}, \mu)$$

Is easier to work with dimensionless variables and, with the help of experimental observations, correlations of dimensionless numbers have been developed for different standard cases of turbulent flow. Common formulations for the correlation are of the type:

$$Sh = a\ Re^{b}\ Sc^{c} \qquad (52)$$

where a, b and c are characteristic constants of a given interface geometry, a type of flow regime of the fluid adjacent to the interface and of the transport properties of the fluid respectively.

In Table2.9 they are divided in 4 categories according to what they are based on:

**Table 2.9**: *Mass transfer correlations for Newtonian fluid for turbulent flow regime in pipes or between parallel planes.*

| Equation | Working conditions | Authors |
|---|---|---|
| *1) Based on momentum, mass and heat transfer analogies* | | |
| $\boldsymbol{Sh = 0.023 Re^{0.8}\ Sc^{0.33}}$ | $Re > 10^5, Sc > 0.5$ | Chilton-Colburn[35] |
| $\boldsymbol{Sh = 0.34 Re^{0.75}\ Sc^{0.33}}$ | $10^4 < Re < 10^5, Sc > 0.5$ | Dittus-Boelter[36] |
| $\boldsymbol{Sh = \frac{(f_a/2)\ Re\ Sc}{1 + 5\sqrt{f_a/2}\,(Sc - 1)}}$ **$f_a$ is the drag force** | | Prandtl-Taylor[37] |
| $\boldsymbol{Sh = \frac{(f_a/2)\ Re\ Sc}{1 + 5\sqrt{f_a/2}\,[Sc - 1 + ln(1 - 5\,Sc)/6]}}$ | | Von Kármán[38] |
| $\boldsymbol{Sh = 0.021 Re^{0.8}\ Sc^{0.36}}$ | $0.5 < Sc < 5$ | Kays[39] |
| $\boldsymbol{Sh = 0.082 Re^{0.8}\ Sc^{0.33}}$ | $10^4 < Re < 10^6$ | Calderbank-Moo-Young[40] |
| $\boldsymbol{Sh = 0.012(Re^{0.87} - 280)\ Sc^{0.4}\left[1 + (d_t/l)^{2/3}\right]}$ **l is the tube length and $d_t$ the tube diameter** | $15 < Sc < 500$ | Gnielinski[41] |
| $\boldsymbol{Sh = 0.079\ Re\ \sqrt{f_a}\ Sc^{1/3}}$ | $Re > 10^5, Sc > 100$ | Churchill[42] |
| 2) Based on turbulent diffusivity model | | |
| $\boldsymbol{Sh = 0.023 Re^{0.875}\ Sc^{0.25}}$ | $300 < Sc < 700$ | Deissler[43] |
| $\boldsymbol{Sh = 0.00149 Re^{0.88}\ Sc^{0.33}}$ | $Sc > 100$ | Notter-Sleicher[44] |
| $\boldsymbol{Sh = \frac{9}{14.5(2\sqrt{3}\,\pi)} Re\sqrt{f_a} Sc^{0.33}}$ | High Sc | Lin et al.[45] |
| 3) Based on the penetration surface renovation | | |

| | | |
|---|---|---|
| $\boldsymbol{Sh = 0.107\ Re^{0.9}\ Sc^{0.5}}$ | $0.5 < Sc < 10$ | Einstein-Li[46] Pinczewski-Sideman[47] |
| $\boldsymbol{Sh \propto Re^{0.9}\ Sc^{0.3}}$ | | Ruckenstein[40] |
| $\boldsymbol{Sh = 0.102\ Re^{0.9}\ Sc^{0.3}}$ | $Sc > 1000$ | Pinczewski-Sideman[47] |
| $\boldsymbol{Sh = 0.00929(e/d_t)^{0.15}\ Re\ Sc^{1/2}(1.11 + 0.44Sc^{-1/3} - 0.7Sc^{-1/6})}$ | Rough tubes | |
| 4) Empiric correlations | | |
| $\boldsymbol{Sh = 0.023\ Re^{0.83}\ Sc^{0.44}}$ | $0. < Sc < 2.5$ | Gilliland-Sherwood[48] |
| $\boldsymbol{Sh = 0.0096\ Re^{0.931}\ Sc^{0.346}}$ | $10000 < Re < 100000$ $430 < Sc < 10000$ | Harriott-Hamilton[49] |
| $\boldsymbol{Sh = 0.827A^{1/3}\ (f_a/2)^{1/2}\ Re\ Sc^{1/3}}$ **Experimental test of a turbulent diffusivity** | $3000 < Re < 80000$ $800 < Sc < 15000$ | Mizushina et al.[50] |

Commonly, for laminar flow, the Sc number exponent remains 1/3, while the exponent of the Reynolds number is normally between 1/3 and 1/2, lower than the one of turbulent flow (> 0.75). For Re ≤ 1700, 1/3 as exponent is adequate, while from experimental results with a higher Reynolds number, 1/2 as exponent is more accurate. Due to the variety of the correlations present in the literature and the huge number of factors involved in mass transfer, it is difficult to choose the right correlation for the system under investigation. Therefore, it is important to experimentally determine the mass transfer coefficients, especially when flat sheet or tubular permeation are concerned.

#### *2.9.3.3 Other parameters influencing the mass transport*

The mass transfer in membrane processes is strongly dependent on the variation of fluid properties (viscosity, density and diffusivity) on the concentration of solutes and on the membrane surface roughness. Moreover, it is linked to the magnitude of the intrinsic mass transfer capability; this contribution can be consistent when high values of membrane permeability and elevated operating pressure are concerned.

- **Effect of fluid properties variation**

  The formation of the concentration profiles on the membrane surface are responsible for the variation of the physical properties of the solution (viscosity,

density and diffusivity) in the diffusion boundary layer, where concentration polarization is present. Depending on operative conditions (normally on the circulation velocity) and on the permeating solution, the variation of these properties can be high or low influencing the mass transfer or, in extreme cases, by altering the rheology of the solution. In these situations, fluids can modify their behavior and change from Newtonian to non-Newtonian in the polarization layer. These properties, that can undergo modifications, are expressed in the Schmidt number. Thus, the parameter accounting for the variation is a dimensionless number calculated as the ratio of the Schmidt number for the properties of the feed solution and the Schmidt number obtained with the concentration on the membrane surface, $C_m$, elevated to an exponent. The exponent can vary according to the system considered, but for conical cells in which the fluid enters transversally to the membrane area it is possible to set this exponent to 0.14[51].

- **Effect of membrane rugosity**

  The membrane rugosity influences the friction factor and, therefore, the mass transfer. Especially in turbulent flow regime and for high values of the Schmidt number, the effect of membrane roughness can be considerable due to the smaller thickness of the polarization layer with respect to the thickness of the momentum mass transfer layer. The membrane rugosity, $e$ , can be determined experimentally with scanning electron microscopy and then converted in dimensionless rugosity, $e^+$:

  $$e^+ = e\,\frac{u^*}{\nu} \tag{53}$$

  where $\nu$ is the cinematic viscosity and $u^*$ is the friction velocity $u^* = \sqrt{\tau_m/\rho}$ with $\tau_m$ stress at the wall (membrane). This dimensionless roughness allows for consideration of the rugosity in the mass transport.

- **Effect of mass transfer magnitude**

  The magnitude of mass transfer influences positively the transport since it alters the structure of the turbulence layer close to the membrane surface and this resulting in a decrease of the boundary layer adjacent to it. From the definition, the mass transfer coefficient is the relation between the diffusive flux near the interface and a concentration gradient:

  $$J_s - J_v C_m = k^*(C_b - C_m) \tag{54}$$

where the first term represents the diffusive flux contribution given by the difference between the total flux and the convective flux and $k^*$ represent the mass transfer coefficient for high mass transfer, so for high fluxes. In normal situation, the convective contribution can be neglected and therefore Equation (54) becomes Equation (49). It exists a relation between the mass transfer coefficient k[29], with $k^*$:

$$k^* = \frac{J_v}{1-\exp\left(-J_v/k\right)} \tag{55}$$

By analyzing Equation (55) it is possible to notice that at low mass transfer $k^*$tends to $k$, once that $J_v$ is really low and the exponential can be solved with a series:

$$\lim_{J_v \to 0} k^* = \frac{J_v}{1-(1-J_v/k)} = k \tag{56}$$

Considering that membranes with high porosity permit higher solute fluxes towards the interface and, therefore, a higher accumulation of rejected material leads to superior mass transfer from the membrane surface to the bulk of the feed solution. Consequently, is possible to relate the magnitude of mass transfer with the porosity and the permeability of the membranes.

By analyzing the complexity of the variables intervening in mass transfer, the best solution is to calculate the mass transfer coefficient and the relative correlation for the system considered, taking into account the geometry and the operating conditions.

### 2.9.4 Mechanisms in the membrane

The mechanisms involved in preferential permeation, or selectivity, in RO membranes are normally different from the mechanisms involved in UF membranes. In RO the mechanism of diffusion through a polymeric matrix is governed by the solution-diffusion model[30], while, in UF, the permeation is exclusively controlled by the stereochemical model. In the case of NF membranes, the two mechanisms are both involved.

#### *2.9.4.1 Stereochemical permeation model*

In UF, NF and RO operations the rejection of solutes is due to stereochemical hindrances, that can be coupled with other solute-membrane interactions like electrostatic forces, London forces, Van der Waals or acid-base interactions. Deriving from the rejection mechanism, the parameter that normally characterizes the membrane is, apart from the

hydraulic permeability, the mean pore radius; it defines the distance that influences the intensity of the interaction membrane-solute. If highly diluted solutions of neutral and spherical solutes are used, in a first approximation is possible to neglect the solute-solute interactions and solute-membrane interactions and to assume that fluxes and rejections are governed by stereochemical hindrances and hydrodynamic forces. The use of this model for UF, NF and RO membranes is a tentative to give a unified approach to the modeling of membrane separation processes in which a pressure gradient is involved. It is normally used, when it is possible to determine the mean pore radius through reference solute rejection experiments.

It is difficult to describe desalination through RO with the stereochemical model, since it is necessary to introduce other membrane-solute interactions and they are characterized by very small pore dimensions. The aim of this model, when RO is concerned, is not to characterize the membrane but to find a parameter that helps in the prediction of the membrane, behavior for the permeation of aqueous solutions.

### 2.9.5 New integrated model of mass transport and ultrafiltration

The methodology used for the characterization of the surrogate of an artificial kidney set-up in terms of mass transport is explained in this paragraph. Even if in the literature several mass transport dimensionless correlations are present, none of them is adequate to investigate the solute transfer in a slit configuration, in laminar flow conditions, and that takes also into account permeation. With the rejection experiments results obtained for uremic toxins and BSA at different flow conditions, a new mass transfer dimensionless correlation is obtained. The correlation is of the type $Sh = Sh\ (Re, Sc, Re_p)$ that relates the dimensionless mass transfer coefficient or the Sherwood number, $Sh$, to Reynolds, Schmidt and a Reynolds number associated to permeation, $Re_p$.

The integrated model couples the equations of mass transport in the phase adjacent to the membrane surface with the one related to the transport through the membrane. As already mentioned, the mass transfer in the phase adjacent to the membrane is described by the concentration polarization model with the determination of the mass transfer coefficients through experimental correlation of the Sherwood number. On the other hand, the mass transfer through the membrane is described by the stereochemical model. Since the stereochemical model hypothesizes that the membrane is porous, the integrated model is

normally used to characterize the porous structure of the membrane through the determination of the mean pore radius. But, when the mean pore radius is known[52] (as it is the case of this work), the model can be used to determine the solutes-membrane interactions. It can be even adapted to predicts UF, NF or RO operations.

However, in this thesis, the model is used to determine a new mass transfer dimensionless correlation accounting for the permeation effect.

#### *2.9.5.1 Methods for the experimental determination of mass transfer coefficients*

In ultrafiltration the equation describing the film model (Equation (48)) can be more conveniently re-written as:

$$ln\left(\frac{1-f}{f}\right) = ln\left(\frac{1-f'}{f'}\right) + \frac{1}{k}J_v \qquad (57)$$

that if plotted as $ln\left(\frac{1-f}{f}\right)$ vs $J_v$ gives a straight line with a slope corresponding to $\frac{1}{k}$ and an intercept equal to $ln\left(\frac{1-f'}{f'}\right)$. It is known that the apparent rejection coefficient, f, varies with the membrane, with the solute-solvent system and with the operative conditions such as pressure, feed velocity and also with the effect of external and internal diffusion. The same can be said for the permeate flux, $J_v$. While the intrinsic rejection coefficient, f', depends on the membrane, on the pressure and on the solute but it is independent from the external diffusion effects.

The effect of the solute is accounted by the Schmidt number, the circulation regime in the layer adjacent to the membrane and in the feed is characterized by Reynolds, while the permeation through the membrane can be taken into account with a dimensionless number involving the membrane permeability, $Lp^+$. In this work, a Reynolds number of permeation, $Re_p$ has been used instead of $Lp^+$, the dimensionless parameters are defined as follows:

$$L_p^+ = \frac{L_p}{R_m} \qquad (58)$$

where $R_m$ is the mean pore radius (m) obtained with the stereochemical models in previous works[52].

$$Re_p = \frac{\rho \cdot v_p \cdot D_p}{\mu} \qquad (59)$$

where $v_p$ is the permeation velocity (m/s) and $D_p$ is the mean pore diameter (m)

To calculate the mass transfer coefficient with the integrated method, there exist three different approaches:

- ***Pressure variation method***: the mass transfer coefficient, k, is a function of the feed circulation velocity, of the system geometry and of the binomial solute-solvent, and it can also vary with the transmembrane pressure (TMP). In ultrafiltration, as first approximation, it is possible to consider k independent from the TMP[53]. If this approximation is valid, the dominant contribution to the flux is given by convection. Fixing Re, Sc and $Lp^+$ or $Re_p$ and varying the TMP generates a series of data that follows Equation (57). Therefore, the k can be calculated with the slope of the linear regression of the data fitted with Equation (57).
  By applying the same procedure for each circulation velocity imposed, of solutes or membrane, it is possible to obtain experimental values of k, $k_{exp}$ at different Re, Sc and $Lp^+$ or $Re_p$. By calculating the Sherwood number, $Sh_{exp}$, with $k_{exp}$ and using the least square method to minimize the sum of the difference between the squared $Sh_{exp}$ and the squared Sh calculated as a function of Re, Sc and $Lp^+$ or $Re_p$, it is possible to obtain an experimental correlation of the type:
  $$Sh = aRe^b Sc^c L_p^{+\,d}\ (or\ Re_p^d) \qquad (60)$$
  The last term is normally ignored, but in UF can assume an importance since it counts for the dependency of k from the membrane filtration capacity. This can be considered a different form [54] to describe mass transport in presence of permeable walls, where suction and membrane porosity play an important role in the occurrence of elevated mass transfer rates from the membrane to the bulk solution.

- ***Velocity variation method***: it consists in elaborating the results of $J_v$ and f obtained by varying the feed circulation velocity. For a given solute, in Equation (57) k can be considered as the product of a constant (function only of the feed circulation velocity) and the circulation velocity (or Reynolds number) elevated to an exponent, b, that does not depend on the solute:
  $$k = c \cdot \langle v \rangle^b \qquad (61)$$
  From the representation of $ln\left(\frac{1-f}{f}\right)$ vs $\frac{J_v}{\langle v \rangle^b}$, where b is previously decided, it is possible to determine the intrinsic rejection coefficient (from the interaction with

the y axis) of the chosen solute and the velocity constant from the slope of the linear regression. With the slope is possible to calculate the mass transfer coefficient k. This method needs the decision of b a priori and it is normally done on the basis of common exponents in typical mass transfer correlations. For turbulent flow a common value for b is 0.5[35][37], while for the laminar flow regime is 0.33

#### *2.9.5.2 Determination of a new dimensionless mass transfer correlation*

The most common hemodialyzer geometry is the hollow fiber configuration and several studies had been done on the mass transfer in such hemodialysis machine. Local average Sherwood number and dialyzer efficiency were used to assess the mass transfer and the results were compared with Sherwood numbers for different boundary conditions. It was concluded that the use of mass transfer coefficients is adequate to model the actual working conditions under the hypothesis of uniform wall mass flux[55]. However, a slightly different viewpoint was proposed in the study of mass transfer in various hollow fiber geometry where it is affirmed that mass transfer coefficients in commercial modules agree with literature correlations at high flows, but are smaller at low flow rates[56].

Unfortunately, less efforts were done to investigate adequately the mass transfer in a plate dialyzer and to develop a dimensionless mass transfer correlation accounting also the permeation phenomenon. In face of these considerations, the present paragraph is reported the methodology used to evaluate the mass transport in a surrogate system of an artificial kidney (AK) according to different transmembrane pressures (TMP) and feed circulating velocities ($v$), leading to the calculation of a mass transfer coefficient, k, for each operative condition. A case specific mass transfer correlation valid for a range of Schmidt number, $384<Sc<7881$, and a range of Reynolds number, $33<Re<114$.

Here, since the only parameter that was possible to control was the feed circulation velocity (at which is already associated a TMP) the method used to determine the experimental correlation is the velocity variation method. The experimental set-up, operative conditions and concentration used are the ones reported in paragraph 2.7

The system considered is completely different from the ones that were studied for this type of mass transfer correlation until now. The surrogate system of an artificial kidney works in conditions far away from the conventional ultrafiltration and nanofiltration processes,

both in terms of feed circulation velocities and transmembrane pressure. Thus, the correlation proposed in this work is:

$$Sh = a\ Re^{b}\ Sc^{c}\ {Re_p}^{d} \tag{62}$$

The coefficients *a*, *b*, *c* and *d* were calculated by fitting the model correlation to experimental mass transfer coefficients. The best sets of parameters were obtained by varying the constants and minimizing the sum of the squares of the deviation between the experimental, $Sh_{exp}$, and calculated, $Sh_{calc}$, Sherwood numbers and fitting the data with a multilinear regression

To determine the experimental mass transfer coefficient *k* the following approach was used:

$$k = C^{*} < v >^{0.33} \tag{63}$$

and therefore Equation (57) can be re-written as:

$$\ln\left(\frac{1-f}{f}\right) = \ln\left(\frac{1-f'}{f'}\right) + \frac{1}{C^{*}}\frac{J_{\mathrm{v}}}{<v>^{0.33}} \tag{64}$$

In Equation (63) $C^{*}$ is a constant while *u* is the feed circulation velocity and 0.33 is a tipical exponent of the Reynolds number for fully developed laminar flow, which was supposed to be the case in this work of thesis.

As a results, the linear regression of the experimental values of $ln\left(\frac{1-f}{f}\right)$ plotted versus $\frac{J_{\mathrm{v}}}{<v>^{0.33}}$ yields to a straight line whose slope is $\frac{1}{C^{*}}$. Thanks to this representation, the experimental mass transfer coefficients are computed with Equation (63). Moreover through the intercept, the intrinsic rejection coefficient, f', can be estimated. A scheme of the algorithm used to determine the experimental mass tranfer coefficients and $Sh_{exp}$ is shonw in Figure 2.14:

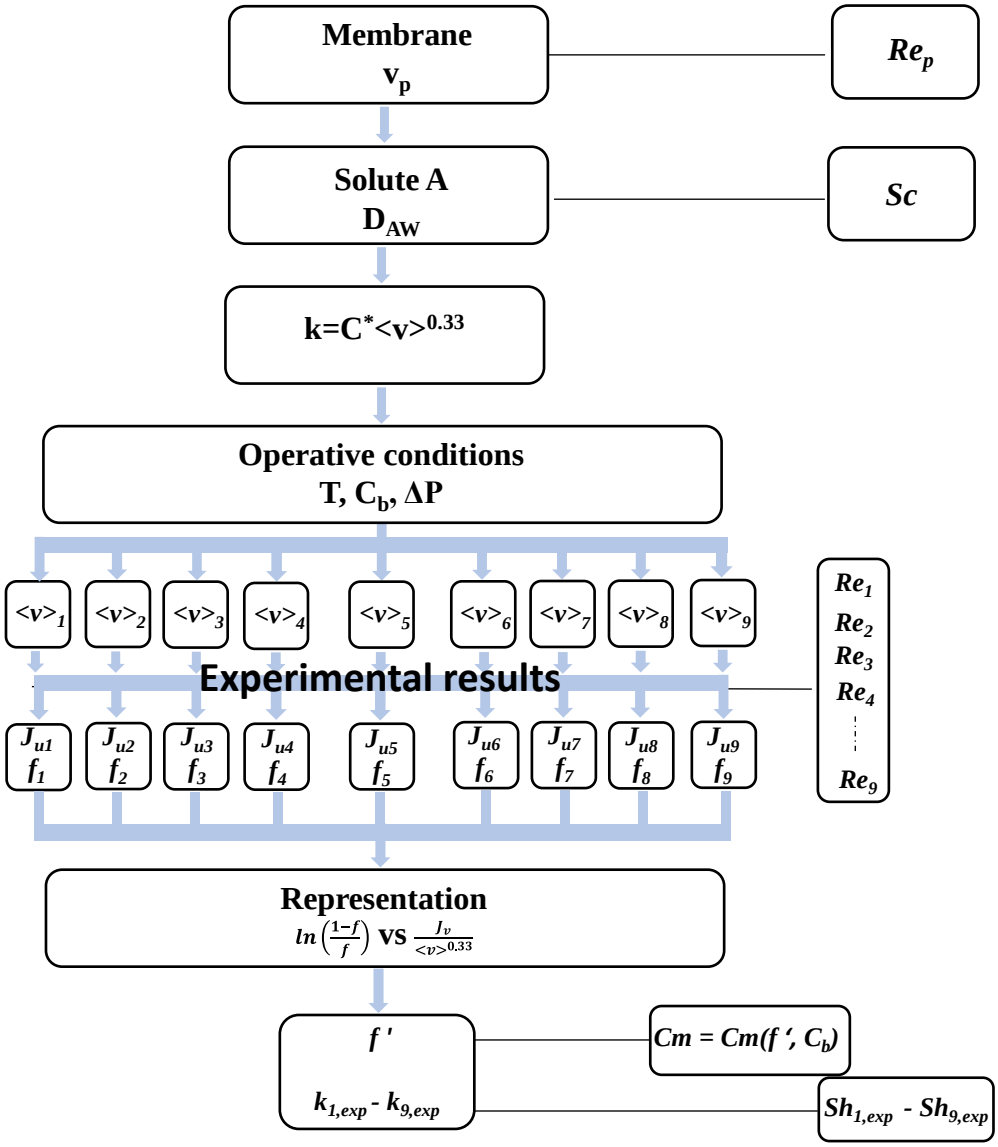


**Figure 2.14**: *Algorithm used to calculate the parameters for the experimental mass transfer correlation.*

After the obtainment of the experimental Sherwood number, the least square method was used to minimize the sum of the squared difference between the $Sh_{exp}$ and the $Sh_{corr}$. The algorithm utilized to fit the data is a multilinear regression.

## References

[1] J.A. Menéndez-Díaz, I. Martín-Gullón, Types of carbon adsorbents and their production. Actived carbon surfaces in environmental remediation., 2006. doi:10.1016/S1573-4285(06)80010-4.

[2] V. Wernert, O. Schäf, H. Ghobarkar, R. Denoyel, Adsorption properties of zeolites for artificial kidney applications, Microporous Mesoporous Mater. 83 (2005) 101–113. doi:10.1016/j.micromeso.2005.03.018.

[3] D.F. Stamatialis, B.J. Papenburg, M. Gironés, S. Saiful, S.N.M. Bettahalli, S. Schmitmeier, M. Wessling, Medical applications of membranes: Drug delivery, artificial organs and tissue engineering, J. Memb. Sci. 308 (2008) 1–34. doi:10.1016/j.memsci.2007.09.059.

[4] D. Bergé-Lefranc, C. Vagner, R. Calaf, H. Pizzala, R. Denoyel, P. Brunet, H. Ghobarkar, O. Schäf, In vitro elimination of protein bound uremic toxin p-cresol by MFI-type zeolites, Microporous Mesoporous Mater. 153 (2012) 288–293. doi:10.1016/j.micromeso.2011.11.024.

[5] D. Bergé-Lefranc, H. Pizzala, J.L. Paillaud, O. Schäf, C. Vagner, P. Boulet, B. Kuchta, R. Denoyel, Adsorption of small uremic toxin molecules on MFI type zeolites from aqueous solution, Adsorption. 14 (2008) 377–387. doi:10.1007/s10450-007-9093-6.

[6] W.K. Cheah, Y.L. Sim, F.Y. Yeoh, Amine-functionalized mesoporous silica for urea adsorption, Mater. Chem. Phys. 175 (2016) 151–157. doi:10.1016/j.matchemphys.2016.03.007.

[7] S. Harm, D. Falkenhagen, J. Hartmann, Pore size ??? A key property for selective toxin removal in blood purification, Int. J. Artif. Organs. 37 (2014) 668–678. doi:10.5301/ijao.5000354.

[8] D. Pavlenko, D. Giasafaki, G. Charalambopoulou, E. Van Geffen, K.G.F. Gerritsen, T. Steriotis, D. Stamatialis, Carbon Adsorbents with Dual Porosity for Efficient Removal of Uremic Toxins and Cytokines from Human Plasma, Sci. Rep. 7 (2017) 1–7. doi:10.1038/s41598-017-15116-y.

[9] M.W. Munthali, M.A. Elsheikh, E. Johan, N. Matsue, Proton adsorption selectivity

of zeolites in aqueous media: Effect of Si/Al ratio of zeolites, Molecules. 19 (2014) 20468–20481. doi:10.3390/molecules191220468.

[10] H.L. Jamieson, H. Yin, A. Waller, A. Khosravi, M.L. Lind, Impact of acids on the structure and composition of Linde Type A zeolites for use in reverse osmosis membranes for recovery of urine-containing wastewaters, Microporous Mesoporous Mater. 201 (2015) 50–60. doi:10.1016/j.micromeso.2014.09.017.

[11] K. Valdiviés-Cruz, A. Lam, C.M. Zicovich-Wilson, Full Mechanism of Zeolite Dealumination in Aqueous Strong Acid Medium: Ab Initio Periodic Study on H-Clinoptilolite, J. Phys. Chem. C. 121 (2017) 2652–2660. doi:10.1021/acs.jpcc.6b09794.

[12] P. Rustemeyer, History of CA and evolution of the markets, Macromol. Symp. 208 (2004) 1–6. doi:10.1002/masy.200450401.

[13] F. Tasselli, Encyclopedia of Membranes, Encycl. Membr. (2015) 1–3. doi:10.1007/978-3-642-40872-4.

[14] E. Saljoughi, M. Sadrzadeh, T. Mohammadi, Effect of preparation variables on morphology and pure water permeation flux through asymmetric cellulose acetate membranes, J. Memb. Sci. 326 (2009) 627–634. doi:10.1016/j.memsci.2008.10.044.

[15] P. Ahmadiannamini, S. Eswaranandam, R. Wickramasinghe, X. Qian, Mixed-matrix membranes for efficient ammonium removal from wastewaters, J. Memb. Sci. 526 (2017) 147–155. doi:10.1016/j.memsci.2016.12.032.

[16] R.A. Zoppi, M.C. Gonçalves, Hybrids of cellulose acetate and sol-gel silica: Morphology, thermomechanical properties, water permeability, and biodegradation evaluation, J. Appl. Polym. Sci. 84 (2002) 2196–2205. doi:10.1002/app.10427.

[17] C.A. Borgo, Y. Gushikem, Zirconium phosphate dispersed on a cellulose fiber surface: Preparation, characterization, and selective adsorption of Li+, Na+, and K+ from aqueous solution, J. Colloid Interface Sci. 246 (2002) 343–347. doi:10.1006/jcis.2001.8045.

[18] G. Mendes, M. Faria, A. Carvalho, M.C. Gonçalves, M.N. de Pinho, Structure of water in hybrid cellulose acetate-silica ultrafiltration membranes and permeation

properties, Carbohydr. Polym. 189 (2018) 342–351. doi:10.1016/j.carbpol.2018.02.030.

[19] A. Montone, SEM THE INSTRUMENT, (2017).

[20] K. D. Vos, F. O. Burris, Drying cellulose acetate reverse osmosis membrane, 1969, Volume 8.

[21] B. Ladewig, M.N.Z. Al-Shaeli, Membrane Characterization Techniques, (2017) In: Fundamentals of Membrane Bioreactors. Springer Transactions in Civil and Environmental Engineering. Springer, Singapore. http://doi-org-443.webvpn.fjmu.edu.cn/10.1007/978-981-10-2014-8_5

[22] Mirko Minervini, A membrane bioreactor for enzyme recovery from saccharification, n.d. https://amslaurea.unibo.it/id/eprint/17746.

[23] National Center for Biotechnology Information (2020). PubChem Compound Summary for CID 588, Creatinine. Retrieved October 27, 2020 from https://pubchem.ncbi.nlm.nih.gov/compound/Creatinine.

[24] National Center for Biotechnology Information (2020). PubChem Compound Summary for CID 1176, Urea. Retrieved October 27, 2020 from https://pubchem.ncbi.nlm.nih.gov/compound/Urea

[25] National Center for Biotechnology Information (2020). PubChem Compound Summary for CID 1175, Uric acid. Retrieved October 27, 2020 from https://pubchem.ncbi.nlm.nih.gov/compound/Uric-acid

[26] V. Magueijo, V. Semiao, M. Norberta de Pinho, Effects of ultrafiltration permeation rates on the hydrodynamics of a minichannel/slit laminar flow, Chem. Eng. Sci. 61 (2006) 7139–7150. doi:10.1016/j.ces.2006.07.041.

[27] F.M. White, Fluid Mechanics 8th in SI units, McGraw Hill Education Ltd, Asia, 2016.

[28] J.C.M. and J.N. Miller, Statistics of analytical chemistry, Ellis Horwood PTR Prentice Hall, New York, 1993.

[29] R.B Bird, W. E. Stewart, E. N Lightfoot, Transport phenomena, John Wiley and Sons, Inc. New York, .1960.

[30] H.K. Lonsdale, U. Merten, R.L. Riley, J. Jay, Transport Properties of Cellulose Acetate Osmotic Membranes, 9 (1965) 1341–1362. doi.org/10.1002/app.1965.070090413.

[31] H.J. Merk, Mass transfer in laminar boundary layers calculated by means of a perturbation method. *A*ppl. sci. Res. 8 (1959) 237–260. doi.org/10.1007/BF00411753

[32] A. I. Johnson, A. Hamielec, D. Ward, A.Golding, End effect corrections in heat and mass transfer studies. Can. J. Chem. Eng., 36 (1958) 221-227. doi:10.1002/cjce.5450360507.

[33] A. I. Johnson, C. W. Bowman, Mass transfer in a bubble column. Can. J. Chem. Eng., 36 (1958) 253-261. doi:10.1002/cjce.5450360606.

[34] H.-H. Fernholz, Boundary Layer Theory: (8th (English) Springer-Verlag Berlin, Heidelberg, New York, 2000.

[35] T.H. Chilton, A.P. Colburn, Prediction from Data on Heat Transfer and Fluid Friction, Ind. Eng. Chem. 26 (1934) 1183–1187. doi:10.1615.

[36] F.W. Dittus, L.M.K. Boelter, Heat transfer in automobile radiators of the tubular type, Int. Commun. Heat Mass Transf. 12 (1985) 3–22. doi:10.1016/0735-1933(85)90003-X.

[37] M.F. Edwards, Heat and Mass Transfer., Chem. Eng. Res. Des. 65 (1987) 495–498.

[38] A.I. Schäfer, N. Andritsos, J. Anastasios, E.M. V Hoek, R. Schneider, Chapter 8 Fouling in Nanofiltration, 2004.

[39] R.E. Lundberg, P.A. McCuen, W.C. Reynolds, Heat transfer in annular passages. Hydrodynamically developed laminar flow with arbitrarily prescribed wall temperatures or heat fluxes, Int. J. Heat Mass Transf. 6 (1963) 495–529. doi:10.1016/0017-9310(63)90124-8.

[40] Y. Kawase, M. Moo-Young, Correlations for liquid-phase mass transfer coefficients in bubble column reactors with newtonian and non-newtonian fluids, Can. J. Chem. Eng. 70 (1992) 48–54. doi:10.1002/cjce.5450700108.

[41] Z. Duan, New correlative models for fully developed turbulent heat and mass

transfer in circular and noncircular ducts, J. Heat Transfer. 134 (2012). doi:10.1115/1.4004855.

[42] S.W. Churchill, H.H.S. Chu, Correlating equations for laminar and turbulent free convection from a vertical plate, Int. J. Heat Mass Transf. 18 (1975) 1323–1329. doi:10.1016/0017-9310(75)90243-4.

[43] G.B. van den Berg, I.G. Rácz, C.A. Smolders, Mass transfer coefficients in cross-flow ultrafiltration, J. Memb. Sci. 47 (1989) 25–51. doi:10.1016/S0376-7388(00)80858-3.

[44] C.A. Sleicher, A.S. Awad, R.H. Notter, Temperature and eddy diffusivity profiles in NaK, Int. J. Heat Mass Transf. 16 (1973) 1565–1575. doi:10.1016/0017-9310(73)90184-1.

[45] H.T. Lin, C.M. Wu, Combined heat and mass transfer by laminar natural convection from a vertical plate, Heat Mass Transf. 30 (1995) 369–376. doi:10.1007/BF01647440.

[46] V. Gekas, K. Ölund, Mass transfer in the membrane concentration polarization layer under turbulent cross flow. II. Application to the characterization of ultrafiltration membranes, J. Memb. Sci. 37 (1988) 145–163. doi:10.1016/S0376-7388(00)83069-0.

[47] V. Schlüter, W.-D. Deckwer, Gas/liquid mass transfer in stirred vessels, Chem. Eng. Sci, 47 (1992) 2357-2362. doi.org/10.1016/0009-2509(92)87060-4.

[48] E.R. Gilliland, T.K. Sherwood, Diffusion of Vapors into Air Streams, Ind. Eng. Chem. 26 (1934) 516–523. doi:10.1021/ie50293a010.

[49] P. Harriott, R.M. Hamilton, Solid-liquid mass transfer in turbulent pipe flow, Chem. Eng. Sci. 20 (1965) 1073–1078. doi:10.1016/0009-2509(65)80110-5.

[50] J. Facão, A.C. Oliveira, Heat and mass transfer in an indirect contact cooling tower: CFD simulation and experiment, Numer. Heat Transf. Part A Appl. 54 (2008) 933–944. doi:10.1080/10407780802359104.

[51] A.M. Brites, M.N. de Pinho, Mass transfer in ultrafiltration, J. Memb. Sci. 61 (1991) 49–63. doi:10.1016/0376-7388(91)80005-Q.

[52] M.J. Beira, M.P. Silva, M. Condesso, P. Cosme, P.L. Almeida, M.C. Corvo, P.J. Sebastião, J.L. Figueirinhas, M.N. de Pinho, Molecular order and dynamics of water in hybrid cellulose acetate–silica asymmetric membranes, Mol. Phys. 117 (2019) 975–982. doi:10.1080/00268976.2018.1537526.

[53] T. Matsuura, S. Sourirajan, Reverse osmosis separation of hydrocarbons in aqueous solutions using porous cellulose acetate membranes, J. Appl. Polym. Sci. 17 (1973) 3683–3708. doi:10.1002/app.1973.070171211.

[54] V Geraldes, V. Semiao, M. N. de Pinho, Flow and mass transfer modelling of nanofitlration, J. Mem. Sci. 191 (2001) 109-128. doi: 10.1016/S0376-7388(01)00458-6

[55] C. Gostoli, A. Gatta. Mass transfer in a hollow fiber dialyzer. J. Memb. Sci., 6 (1980) 133–148. doi.org/10.1016/S0376-7388(00)82156-0.

[56] S.R. Wickramasinghe, M.J. Semmens, E.L. Cussler, Mass transfer in various hollow fiber geometries, J. Memb. Sci. 69 (1992) 235–250. doi:10.1016/0376-7388(92)80042-I.

# 3 EXPERIMENTAL RESULTS AND DISCUSSION

## 3.1 Introduction

In this chapter, the experimental results and the relative discussion are presented. In the first part of work focused on the recycling of the spent dialysate, the fillers selected together with the MMMAs prepared were characterized for their adsorption properties. MMMAs were also tested for their flow properties and to assess their morphology, water uptake, density and contact angle.

The hybrid CA/$SiO_2$ ultrafiltration membranes synthesized in Lisbon for the characterization of a surrogate system of an artificial kidney were tested for their MWCO, hydraulic permeability and rejections capability towards urea, creatinine, uric acid, p-cresyl sulfate and BSA. These experiments were propaedeutic for the fluid mechanics and mass transfer characterization

## 3.2 Adsorbents particle size distribution and adsorption properties

The adsorbents particle size distribution was determined following the procedure described in paragraph 2.3.1. ZUF and ZSM-5 particle size analysis was carried out automatically with a laser while the AC one was done manually with sieves with different mesh dimensions.

In Figure 3.1, 3.2 and 3.3 are reported the particles mean dimension and the effects on it of the dealumination treatment (orange and blue series represent the particle size distribution before and after the dealumination process, respectively):

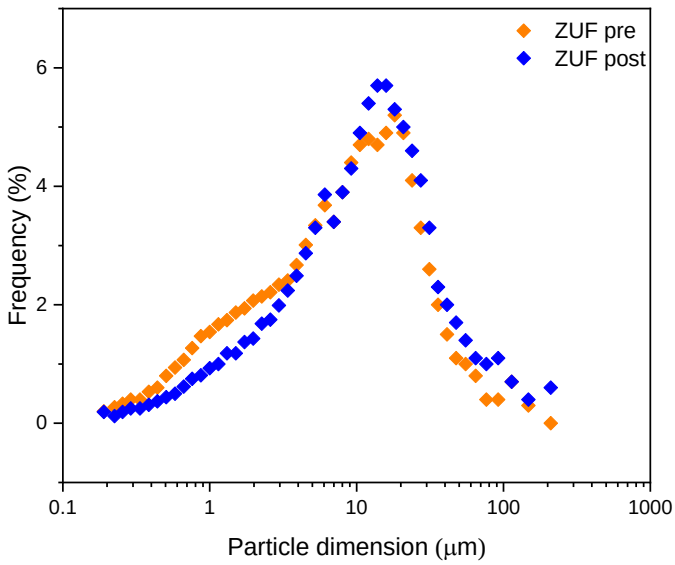


**Figure 3.1**: *ZUF particle size distribution before and after the dealumination process in HCl.*

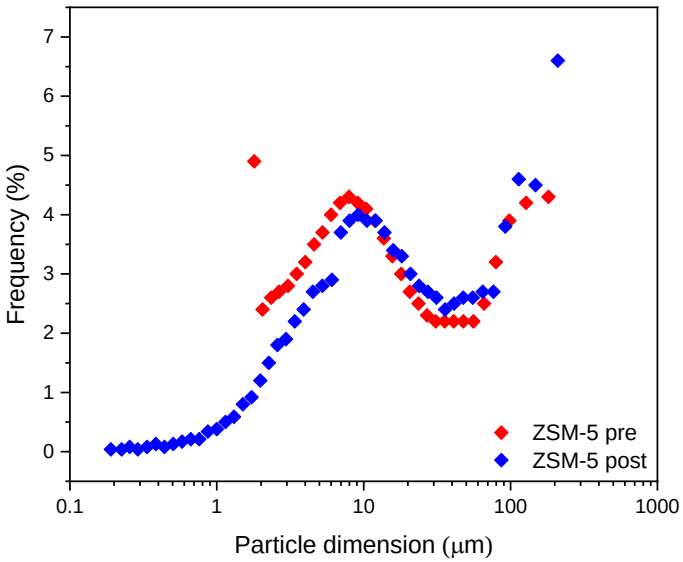


**Figure 3.2**: *ZSM-5 particle size distribution before and after the dealumination process in HCl.*

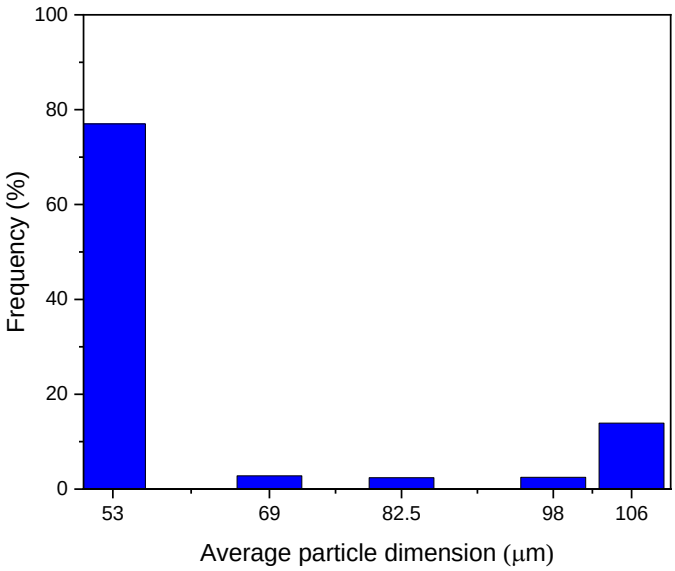


**Figure 3.3**: *AC particle average dimensions.*

The granulometric analysis shows that for activated carbon the fraction remaining after grinding and sieving is the one with diameter ≤ 53 µm. For both zeolites, a mean particle size of around 10 µm was obtained, while for the zeolites primed with HCl a reduction in the number of particles with size smaller than 10 µm after the treatment was observed. Only the fraction of activated carbon with a particle dimension smaller than 53 µm was used for the tests carried out in the following chapters and for the preparation of the MMMAs. While the zeolites, having already a small average particle dimension, were used as provided, but after the HCl priming.

### 3.2.1 Adsorption kinetics

The adsorption kinetics of the three fillers was determined for each toxin considered according to the procedure described in paragraph 2.3.1. The amount adsorbed is reported as a function of the tests duration to determine the time needed for the adsorption

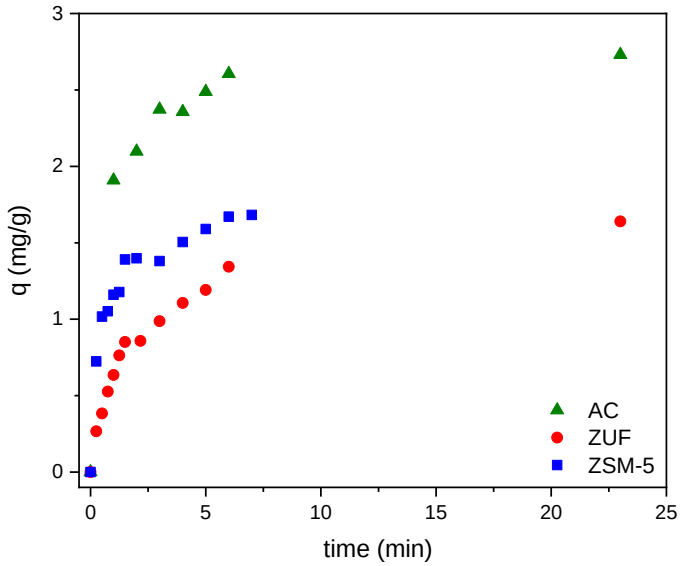


**Figure 3.4**: *Urea adsorption kinetics.*

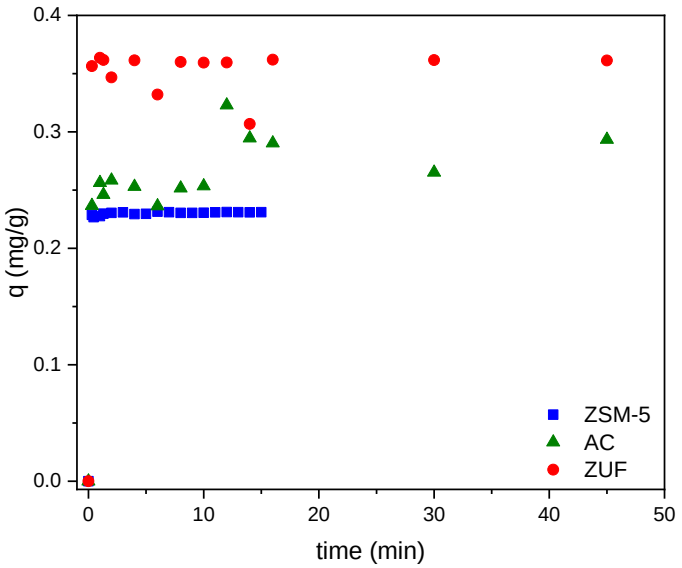


**Figure 3.5**: *Creatinine adsorption kinetics.*

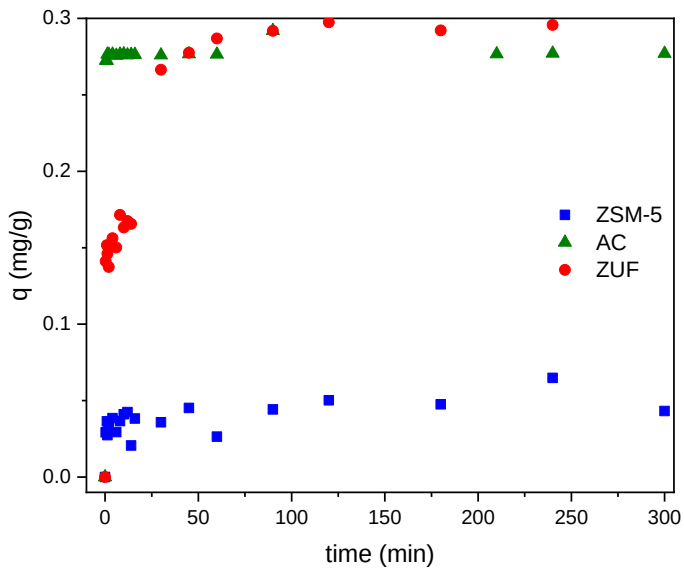


**Figure 3.6**: *Uric acid adsorption kinetics.*

The adsorbents are endowed with different affinity for each toxin; indeed activated carbon is the most suitable adsorbent for urea and creatinine, while ZSM-5 has the highest adsorption capacity for uric acid. Even if the steady state value is different for the different toxins, the adsorption kinetics is quite fast for uric acid and creatinine, where the first minute of test is crucial since the adsorption sites available on the material surface saturate very fast. Whereas, for urea a slower kinetics is reported. This can be attributed to its size, being urea the smallest uremic toxin considered, and thus. it can penetrate the big pores fast, but it has also accessibility to the smaller ones where the transport is diffusion limited. Small nanopores are not accessible for the other two bigger toxins due to steric hindrance.

### 3.2.2 Equilibrium isotherms

Since the goal of this project is the removal of uremic toxins from water, the static binding capacity of the adsorbents is explored in a range of toxin concentration going from $c_N$ to $c_{MAX}$ and the relative isotherms are reported in Figures 3.7, 3.8 and 3.9. The procedure followed is described in paragraph 2.3.1

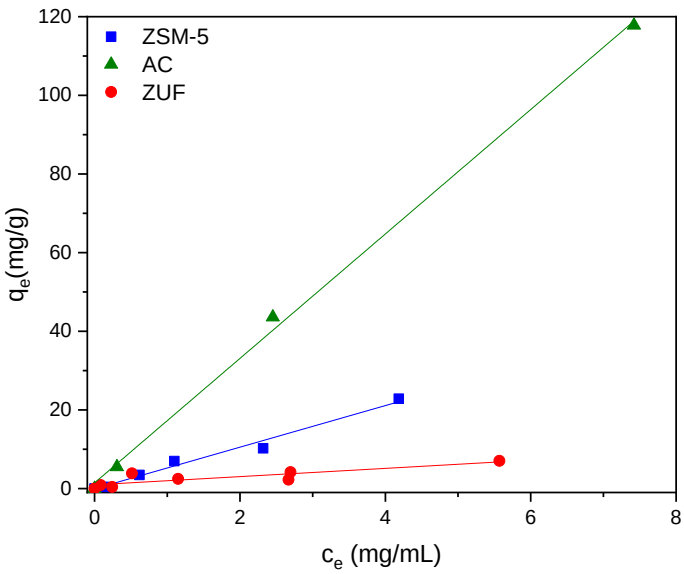


**Figure 3.7***: Urea adsorption isotherm.*

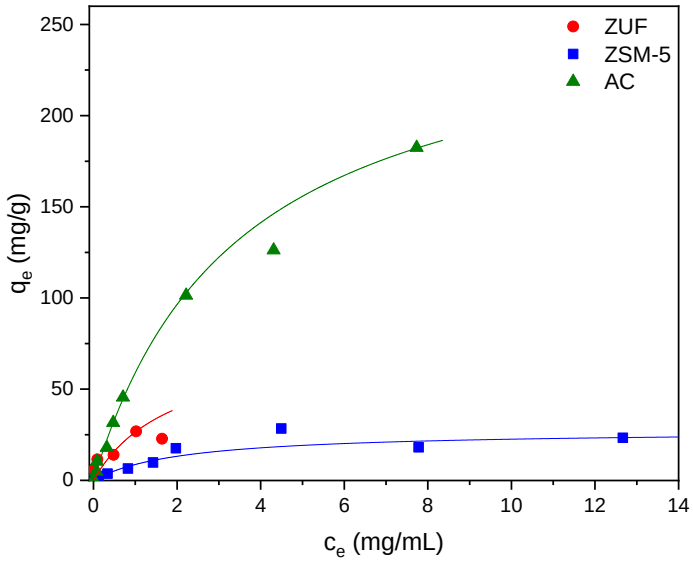


**Figure 3.8***: Creatinine adsorption isotherm.*

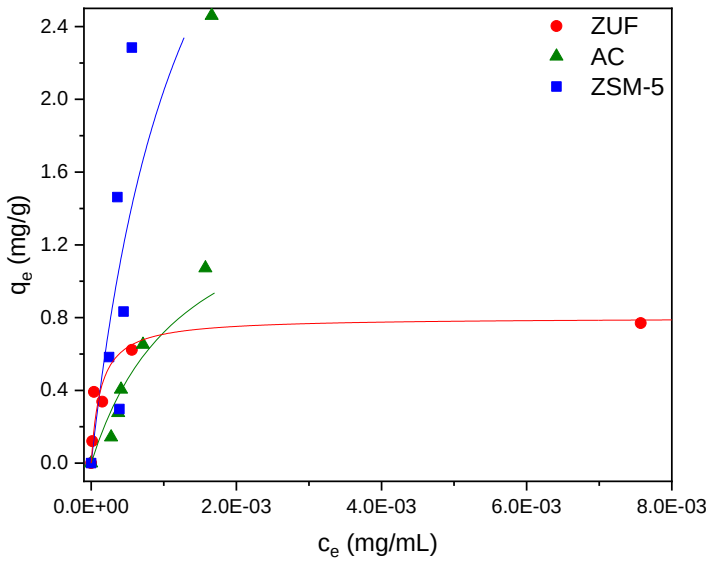


**Figure 3.9**: *Uric acid adsorption isotherm.*

The Langmuir isotherm fits well the experimental data obtained for creatinine and uric acid, while the adsorption of urea shows a linear behavior in the concentration range inspected. To better evaluate the performance of a particular adsorbent, the adsorption isotherm for the fillers with the different toxins were reported.

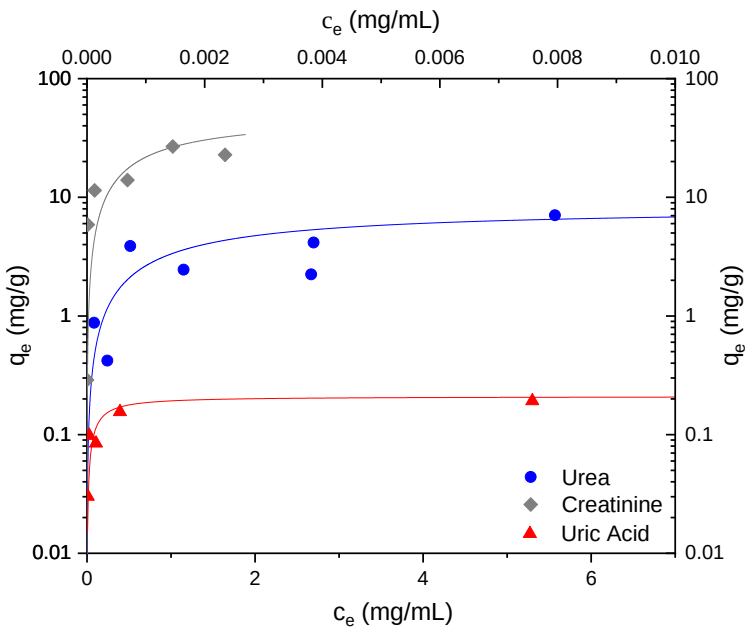


**Figure 3.10**: *ZUF logarithmic adsorption isotherm.*

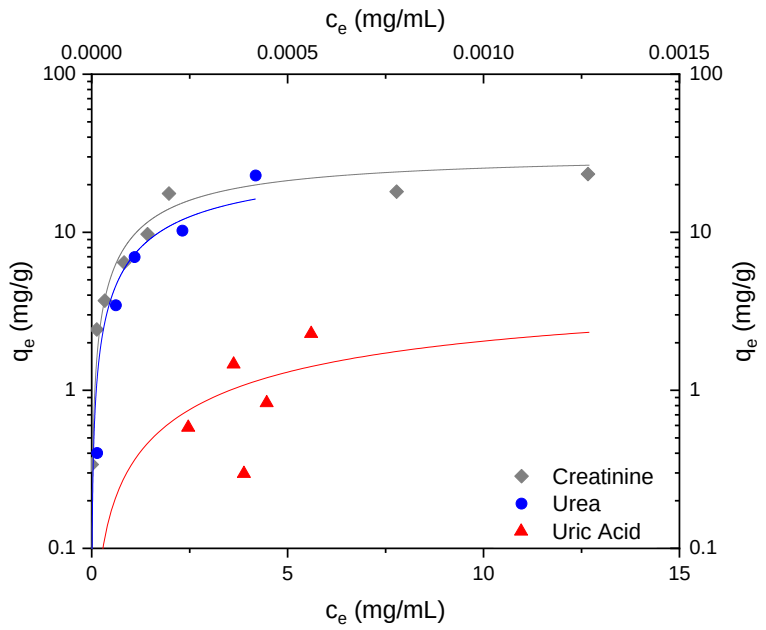


**Figure 3.11**: *ZSM-5 logarithmic adsorption isotherm.*

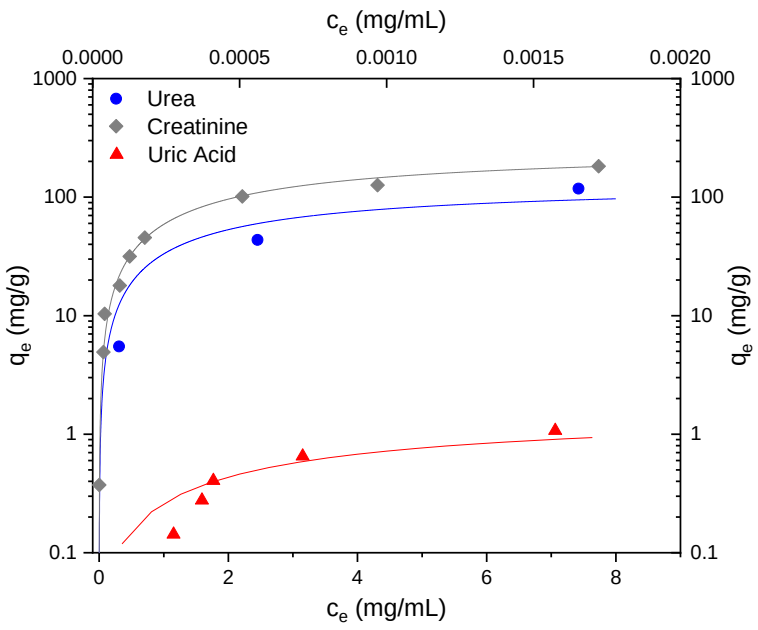


**Figure 3.12**: *AC logarithmic adsorption isotherm.*

In Figure 3.10, 3.11 and 3.12, the y-axis is reported in a logarithmic scale to have a better visualization of the results obtained, since the sorption levels of the various materials differ very much one from the other. Creatinine is the toxin removed in larger amount by all the three adsorbents considered, followed by urea and uric acid. Since the concentrations of uric acid are far below from the one of urea and creatinine, its results are reported on the secondary x and y axis.

## 3.3 MMMAs synthesis, morphology and surface characterization

MMMAs were prepared following the procedure described in paragraph 2.4.1 In Figure 3.13 the membrane aspect is shown.

**Figure 3.13**: *Pure cellulose acetate membrane aspect.*

The active layer of the membrane is distinguishable from the porous bottom one due to its opacity. The dimension of the MMMAs prepared allowed cutting of membrane pieces both for the flow experiments and for the batch adsorption tests. An increase in filler loading gives a change in color and opacity as show in Figure 3.14:

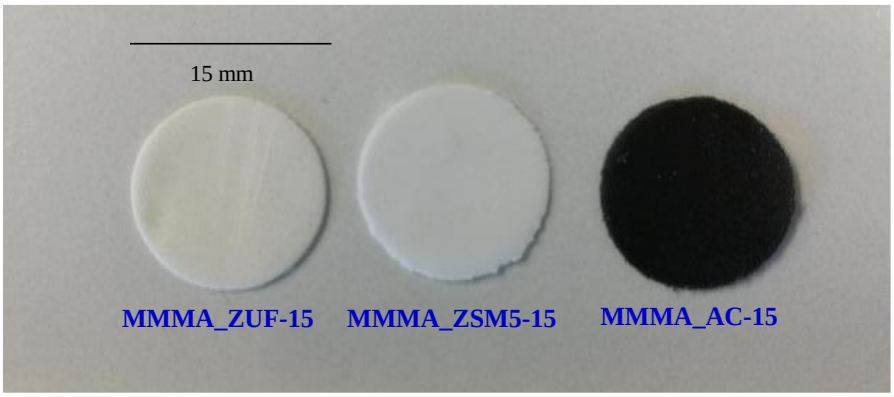


**Figure 3.14**: *Pictures of MMMA_ZUF-15, MMMA_ZSM5-15, MMMA_AC-15.*

The MMMAs are brittle with low resistance to stretching, but they have an appropriate resistance to compression, which is an important feature for the application sought. The filler loading was increased up to a percentage for which was still feasible casting the membrane. Enhancing the adsorbent mass percentage was expected to enhance the filler

surface area available for adsorption and, as a consequence, the MMMAs removal performances.

### 3.3.1 SEM and EDS

Asymmetric mixed matrix membranes were successfully prepared as it is shown in the SEM images reported in Figure. 3.15:

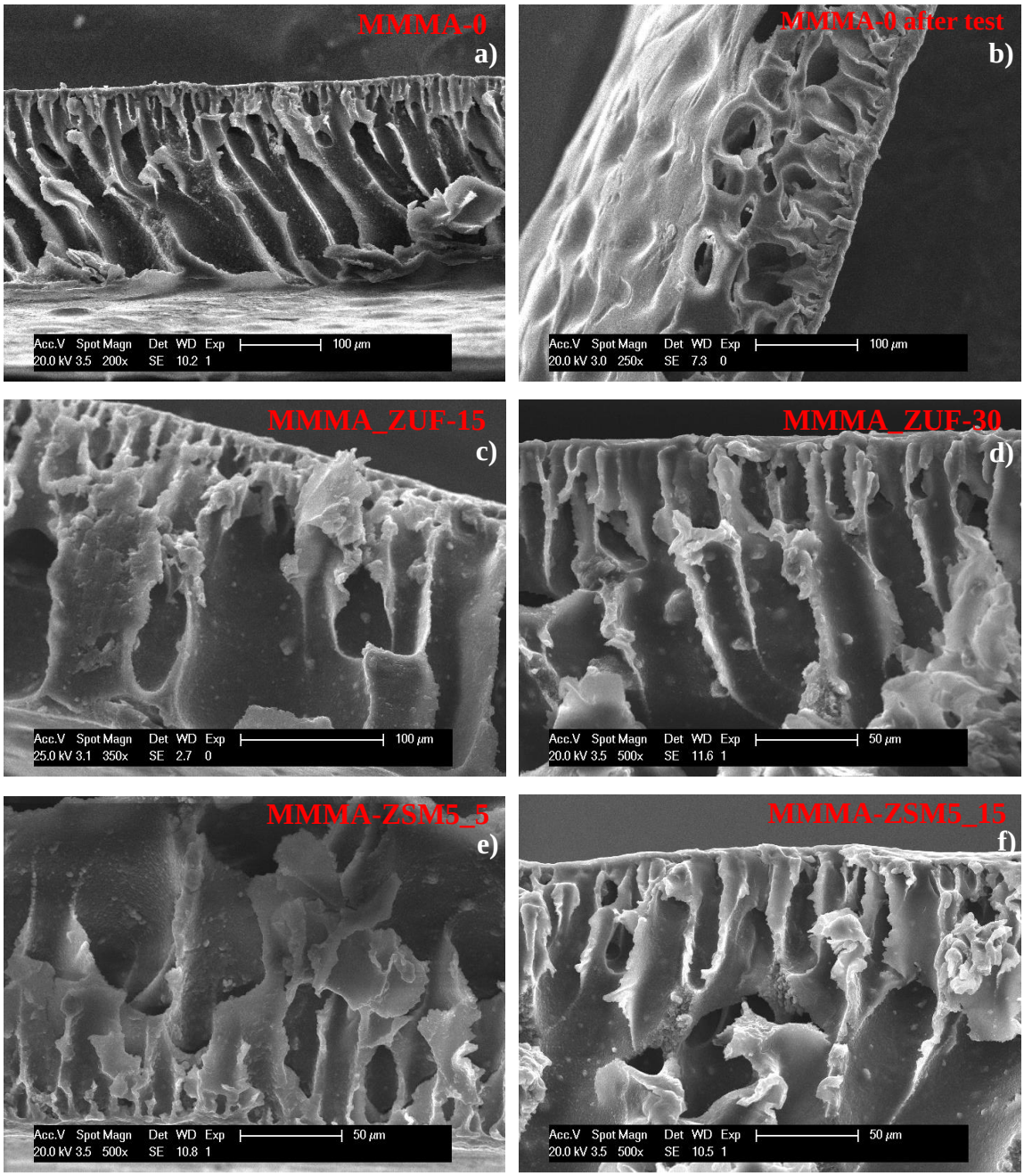

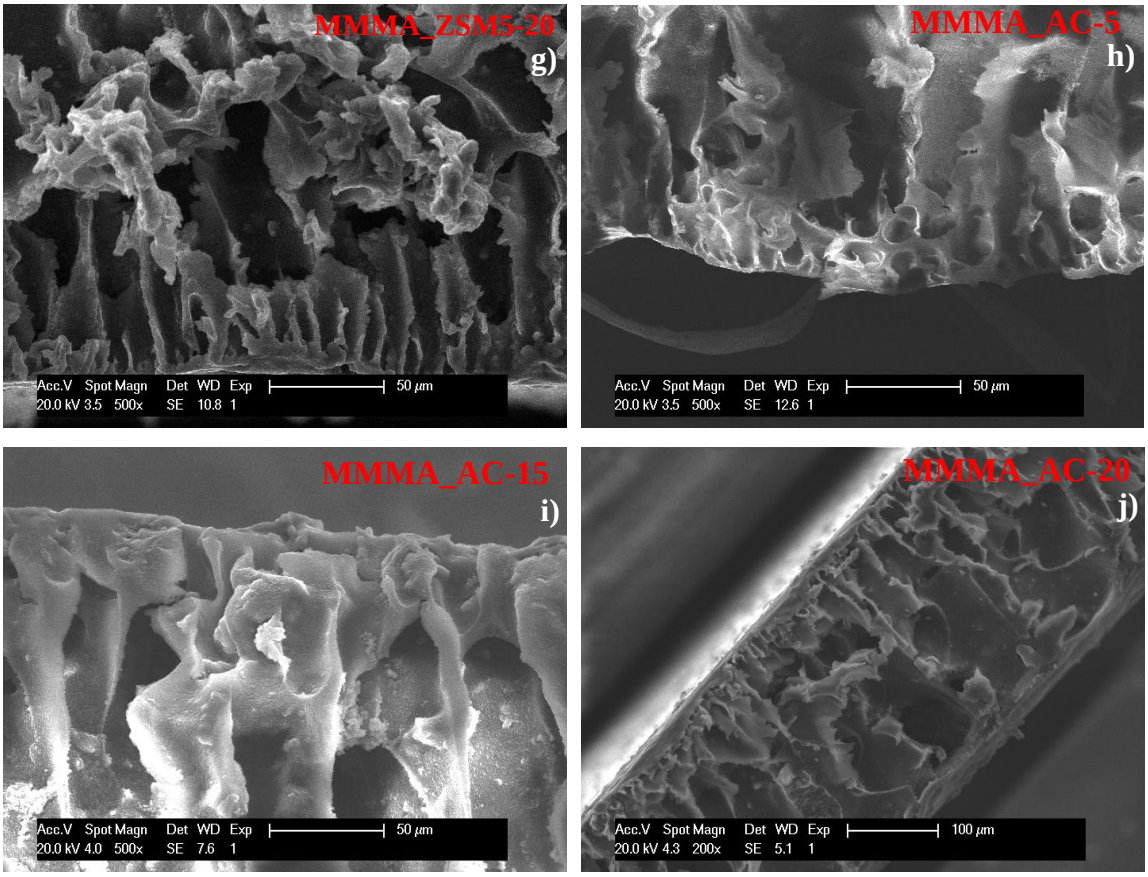


**Figure 3.15**: *SEM images of the MMMAs prepared: a) SEM of the pure cellulose acetate membrane; b) SEM of the pure Cellulose Acetate membrane after being compacted; c) MMMA_ZUF-15; d) MMMA_ZUF-30; e) MMMA_ZSM5-5; f) MMMA_ZSM5-15; g) MMMA_ZSM5-20; h) MMMA_AC-5; i) MMMA_AC-15; j) MMMA_AC-20.*

The pores are well defined and evenly distributed along the plain membrane reported in Figure 3.15 a). It is possible to distinguish the surface that was in contact with the air during the casting procedure (thin layer with small pores), and the surface that was in contact with the glass plate (thick layer with big channels). The SEM images show that increasing the fillers loading in the casting solution does not significantly influence the pores conformation in the MMMAs.

Indeed, the pores maintain their definition even though there is a third component in the casting solution (filler) that may alter the surface tension of the system, which is a key parameter in the formation of asymmetric membranes. From Figure 3.15 f), MMMA_ZSM5-15, it can be noted how the structure of the membrane is very similar to MMMA_ZUF-15 shown in Figure 3.15 c). The pores shape and distribution are almost identical due to the similar chemical structure of the two fillers. In Figures 3.15 h) to 3.15 j) the activated carbon-based membranes are represented: here the shape of the pores is less defined with respect to the zeolite-based membranes. This could be linked to the different affinity between the two

phases, polymer and filler, due to the diverse chemical nature of the fillers considered, zeolite and activated carbon.

To verify the presence of zeolites inside the mixed matrix membranes an EDS was performed on the pure ZUF and on specific areas on the SEM images reported in Figure 3.16. Since the membrane casting procedure was identical for all the three series of MMMAs prepared, MMMAs based on ZUF were taken as example to assess the presence of the filler inside the matrix. Unfortunately, the EDS technique cannot be used to identify AC presence since it is well embedded in the polymer matrix and the peak related to carbon would be comprehensive of the signal of the cellulose acetate backbone and therefore, they are not distinguishable.

The spots on which the EDS was performed are reported in Figure 3.16:

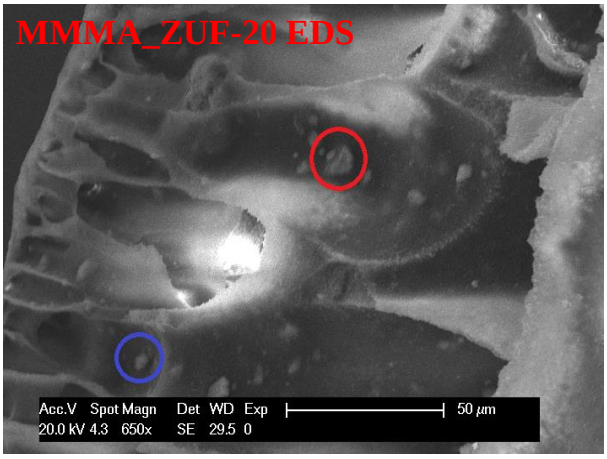


**Figure 3.16**: *SEM image of MMMA_ZUF-20 on which EDS was performed (blue and red circles).*

In Figure 3.17 and 3.18 a) and b) are reported the EDS on the pure ZUF and on the MMMA_ZUF-20:

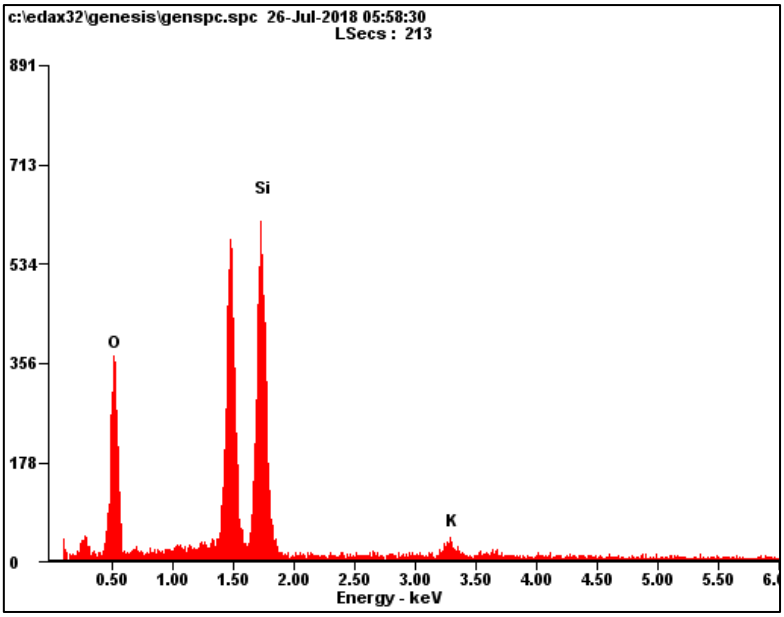


**Figure 3.17**: *EDS of ZUF.*

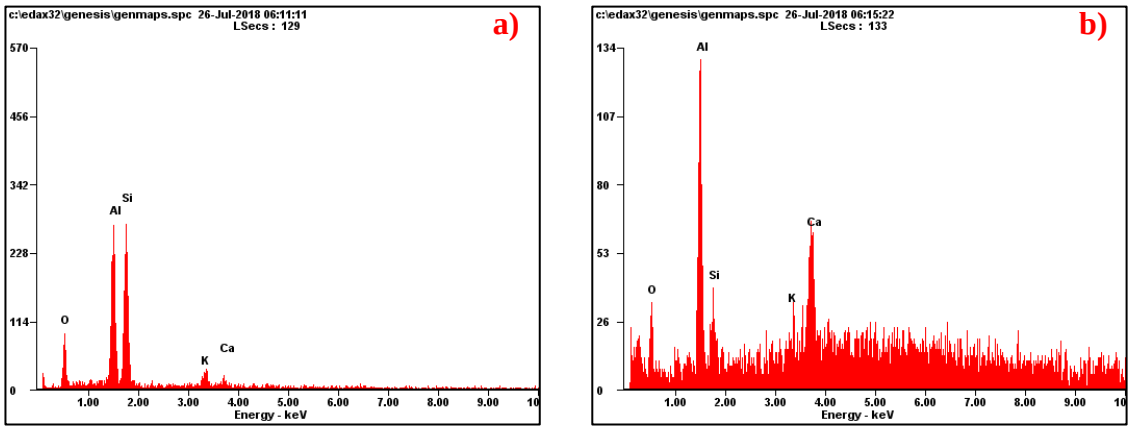


**Figure 3.18**: *EDS on MMMA_ZUF-20: a) red circle; b) blue circle.*

The results of the analysis on the circled spots in Figure 3.16 confirm the presence of the zeolites in the MMMAs. The EDS reports the presence of silicon (Si), aluminum (Al), oxygen (O), potassium (K) and calcium (Ca); these elements identify the presence of ZUF, as it is noticeable in in Table 2.1 in which the ZUF composition is reported. The Al signal is due both to the presence in the aluminosilicate lattice and to the metallization. Therefore, it cannot be considered a relevant signal for the presence of the zeolite. For ZSM-5-based MMMAs the EDS was not performed since the SEMs showed the presence of the same granules observed in the ZUF.

### 3.3.2 Solvent uptake and densities

Water uptake and density measurements were done according to the procedure described in paragraph 2.5.3. The effect of the filler loadings on the ability of the MMMAs to adsorbed water is reported in Figure 3.19.

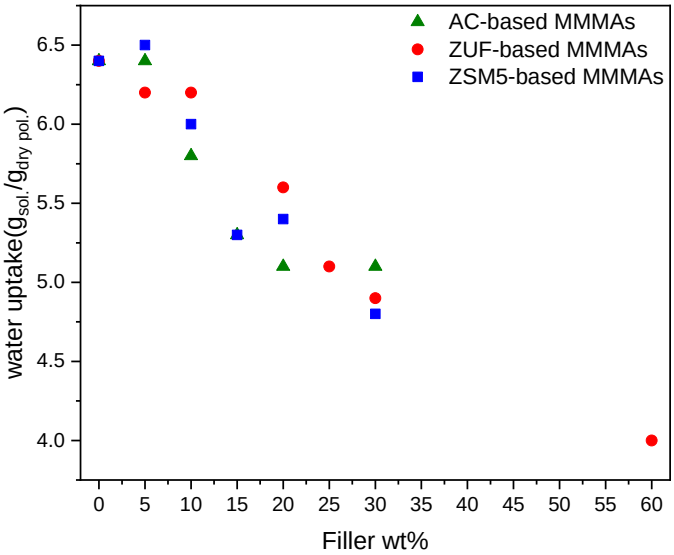


**Figure 3.19**: *MMMAs water uptake.*

The water uptake of the MMMAs, in grams of solvent per gram of dry polymer, decreases with the increase in filler loading, as shown in Figure 3.19. The dealumination process described in paragraph 2.3.1 has increased the Si/Al ratio of the zeolites ZUF and ZSM-5 and, as a consequence, the hydrophobicity of the adsorbent materials. At high filler loadings the strong hydrophobicity of the fillers overcome the hydrophilicity of the polymeric matrix resulting in a lower water uptake of the composite material. For AC, the water uptake behavior is comparable with the one of zeolites since the surface of activated carbon is intrinsically hydrophobic.

In Figure 3.20 MMMAs density are reported. As already mentioned in paragraph 2.5.3, these tests were done to obtain an indication of the filler effectively present in the MMMA. The polymer-filler adhesion, which is normally inspected with these measurements, was not the objective of these experiments.

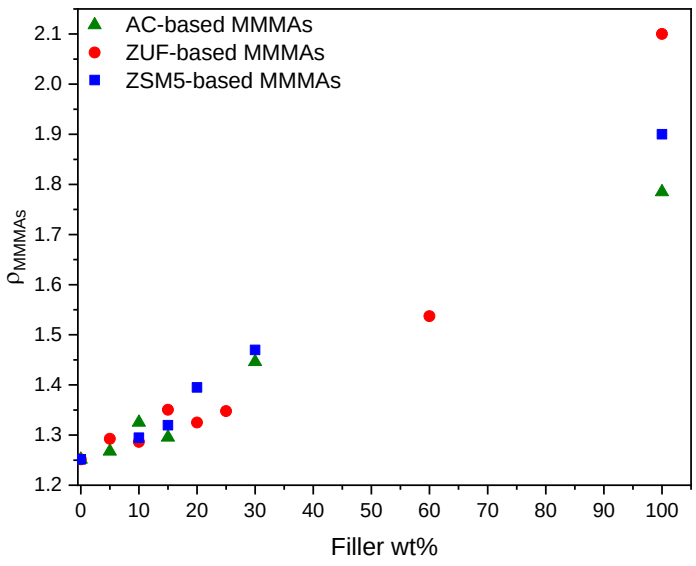


**Figure 3.20**: *MMMAs densities.*

In Figure 3.20 MMMAs densities are reported. The experimental point at 0 wt% of filler corresponds to the plain cellulose acetate membrane, while the one at 100 wt% represent the filler density value as obtained from the literature [1][2][3] Since the fillers are denser than the polymer, the MMMAs density increases with the filler loading. Therefore, ZUF-based membranes should have the highest densities, fixing the filler wt%, but this is not observed for all the membrane prepared. A plausible explanation for this discrepancy resides in the membrane preparation procedure: even if the filler dispersion in the casting solution is quite uniform, some adsorbent particles may cluster and precipitate or they may stick to the wall of the bottle used to prepare the mixture. Moreover, the dispersion of the filler cannot be controlled during the solution spreading and membranes could have zones with non-uniform filler loading.

### 3.3.3 Contac angles

Advanced and receding contact angle measurements give an indication of the superficial behavior of the MMMAs in contact with water. In Table 3.1 the results obtained for all the MMMAs tested are reported:

**Table 3.1**: *MMMAs advancing and receding contact angles.*

| MMMAs | Advancing contact angle (°) | Receding contact angle (°) |
|---|---|---|
| *MMMA-0* | 63±1 | 64±1 |
| *MMMA_ZUF-5* | 62±0.79 | 64±0.48 |
| *MMMA_ZUF-10* | 66±0.20 | 66±0.07 |
| *MMMA_ZUF-15* | 64±0.28 | 64±0.28 |
| *MMMA_ZUF-25* | 61±0.19 | 62±0.17 |
| *MMMA_ZUF-30* | 63±0.27 | 63±0.13 |
| *MMMA_ZUF-60* | 64±0.11 | 65±0.06 |
| *MMMA_ZSM5-5* | 62±0.33 | 63±0.33 |
| *MMMA_ZSM5-10* | 65±0.15 | 66±0.14 |
| *MMMA_ZSM5-15* | 65±0.24 | 66±0.17 |
| *MMMA_ZSM5-20* | 64±0.14 | 65±0.14 |
| *MMMA_ZSM5-30* | 64±0.10 | 65±0.18 |
| *MMMA_AC-5* | 63±0.40 | 63±0.17 |
| *MMMA_AC-10* | 65±0.19 | 66±0.11 |
| *MMMA_AC-15* | 64±0.15 | 64±0.09 |
| *MMMA_AC-20* | 63±0.28 | 64±0.23 |
| *MMMA_AC-30* | 63±0.12 | 64±0.15 |

The results show a very similar behavior among the MMMAs prepared. The values are the same for the advanced and receding angles, 64°± 1.3°. This indicates that, at least on the surface, the hydrophilicity of the pure cellulose acetate membrane is preserved. The presence of the adsorbents does not affect the wettability of the active membrane layer. and, since the advancing and receding contact angles are practically the same, hysteresis is not observed. Dynamic contact angle hysteresis is a measure of the surface roughness, its absence indicates that the surface of the MMMAs can be considered smooth without remarkable irregularities.

## 3.4 MMMAs flow and batch adsorption properties

### 3.4.1 MMMAs water fluxes and hydraulic permeability

MMMAs pure water fluxes and hydraulic permeabilities were calculated with the apparatus shown in Figure 2.5 and according to the procedure described in paragraph 2.6.1. The

results reported correspond to the water fluxes measured after 90 minutes of membranes conditioning at 1.5 bar.

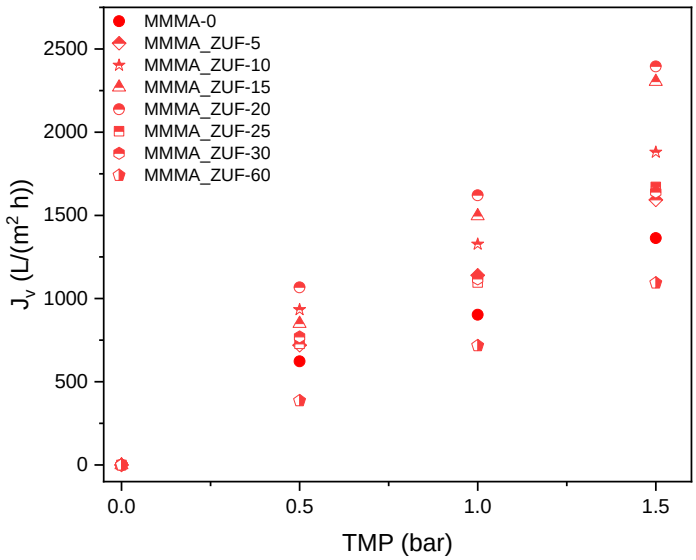


**Figure 3.21**: *ZUF-based MMMAs water fluxes.*

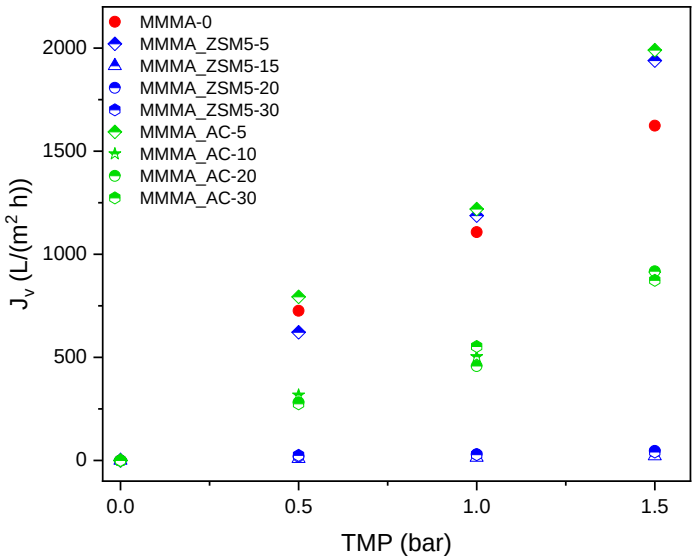


**Figure 3.22**: *ZSM5-based and AC-based MMMAs water fluxes.*

**Table 3.2**: *MMMAs hydraulic permeabilities.*

| MMMAs | Lp (L/(h m$^2$ bar) |
|---|---|
| *MMMA-0* | 906 |
| *MMMA_ZUF-5* | 1082 |
| *MMMA_ZUF-10* | 1286 |
| *MMMA_ZUF-15* | 1486 |
| *MMMA_ZUF-20* | 1597 |
| *MMMA_ZUF-25* | 1102 |
| *MMMA_ZUF-30* | 1103 |
| *MMMA_ZUF-60* | 729 |
| *MMMA_ZSM5-5* | 1260 |
| *MMMA_ZSM5-15* | 14 |
| *MMMA_ZSM5-20* | 13 |
| *MMMA_ZSM5-30* | 15 |
| *MMMA_AC-5* | 1260 |
| *MMMA_AC-10* | 576 |
| *MMMA_AC-20* | 564 |
| *MMMA_AC-30* | 571 |

In Figure 3.21 and 3.22 the water fluxes of MMMAs are reported. With the linear regression of these results, the hydraulic permeabilities, shown in Table 3.2, are calculated. The membranes were tested in a low pressure range, from 0.5 to 1.5 bar, since the aim of the project is to implement these MMMAs into the dialysis process. To allow ultrafiltration across the dialyzer and avoiding counter diffusion of solutes from the spent dialysate towards the blood, a transmembrane pressure, TMP, is needed, and this is achieved applying a negative suction pressure to the dialysate compartment. Normal values of TMP for a high flux dialyzer are around 260 mmHg [4]. Thus, membranes endowed with high water permeability at low transmembrane pressure are preferable to avoid high energy consumption. Moreover, the MMMAs prepared are quite brittle and the use of a higher pressure may damage their structure. The hydraulic permeability of the ZUF-based MMMAs, is enhanced by the presence of the filler, and increases with its content up to a weight fraction of 20%. This behavior can be explained by the fact that zeolites are porous materials and they contribute to increase the void fraction of the system, while, for plain CA membranes, the void fraction is only given by the pore volume. The decrease of permeability, above 20 wt% of ZUF content, could be due to the increase of hydrophobicity of the system: pristine ZUF is a quite hydrophilic material (low Si/Al ratio) but after the dealumination process, the Si/Al is increased and thus is hydrophobicity. So, there is more resistance to the water flux and, therefore, the hydraulic permeability experienced a decrease. This more hydrophobic behavior it is also confirmed by the water uptake results

(Figure 3.19). The different behavior of the other series of MMMAs (ZSM5-based and AC-based) can be explained with the much higher hydrophobicity of ZSM-5 and AC with respect to ZUF. Even if the water uptake behaviors are similar, during the flow tests the water is forced to pass through the limiting membrane layer and it cannot enter the membranes structure also from the bottom part (characterized be big open pores), as it happens during the water uptake measurements, since it is calculated after soaking the membrane in a water medium until the equilibrium is reached. Moreover, ZSM-5 was difficult to suspend in the casting solutions and clusters were always present. Big aggregates present in the final membranes can cause an additional resistance to the flow of water, leading to overall lower fluxes.

Figure. 3.23 and 3.24 show how the hydraulic permeability varies within the test duration at fixed operative conditions. Samples were taken at the beginning of the experiment, after 30 minutes and then every hour for a total duration of 210 min.

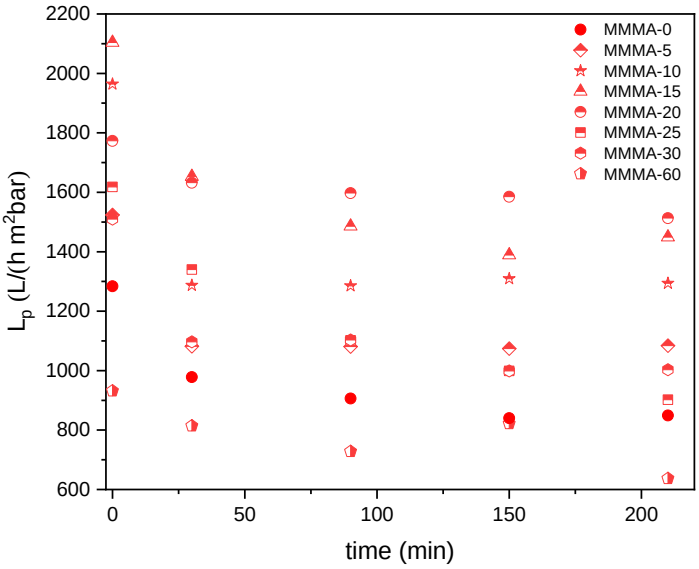


**Figure 3.23**: *ZUF-based MMMAs permeability in time.*

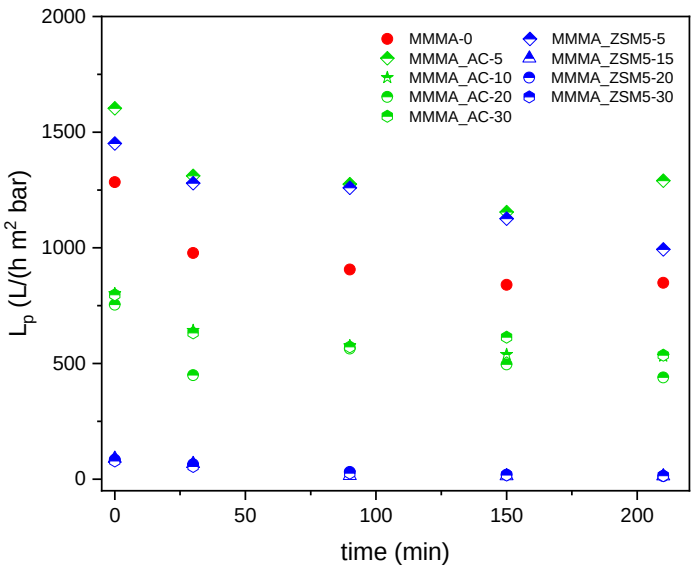


**Figure 3.24**: *ZSM5-based and AC-based permeability in time.*

The hydraulic permeability decreases in the first 90 minutes, but then it stabilizes, and the decrease is less pronounced until the end of the experiment. This behavior is observed in all membranes and is likely due to the change in the pore shape and conformation under the action of the transmembrane pressure; the membrane is compressed, and the pores squeezed until they reach, after 90 min, a stable configuration. This process leads to a decrease in the hydraulic permeability until a stable value is attained.

### 3.4.2 MMMAs batch adsorption properties with single toxin solutions

The membranes were tested for their batch adsorption properties according to the procedure described in paragraph 2.6.2. The results are reported in terms of toxin removal that is defined as the ratio between the mass of toxin adsorbed by the membrane to the mass of toxin in the feed solution:

$$\%_{removed} = \frac{m_{of\ toxin\ adsorbed}}{m_{of\ toxin\ in\ the\ feed\ solution}} \times 100 \qquad (65)$$

The membrane volume used was the same for all experiments, while for the fillers the amount of solid material is different, therefore the value measured for the plain fillers is only reported as a qualitative comparison.

In Figure. 3.25, 3.26 and 3.27 the removal capacity of the MMMAs tested for urea, creatinine and uric acid are reported:

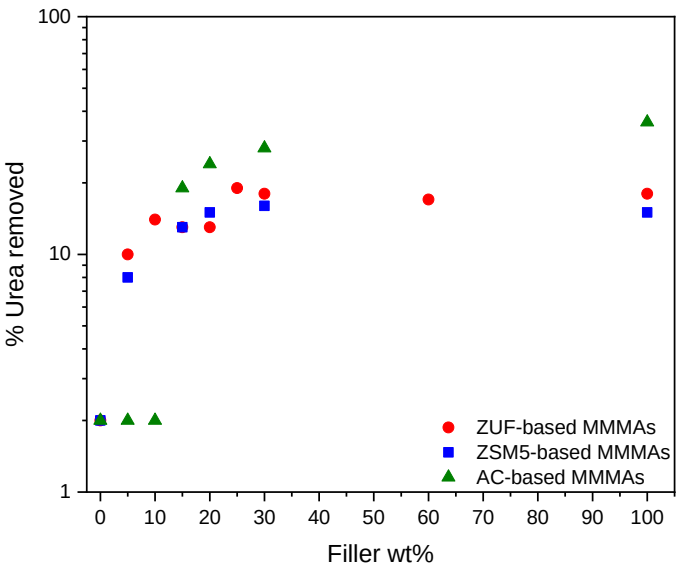


**Figure 3.25**: *Urea percentage removed according to the fillers loading.*

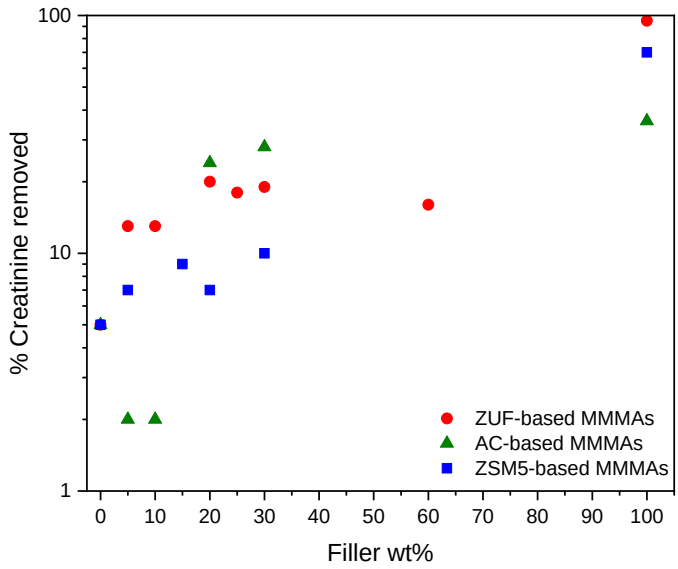


**Figure 3.26**: *Creatinine percentage removed according to the fillers loading.*

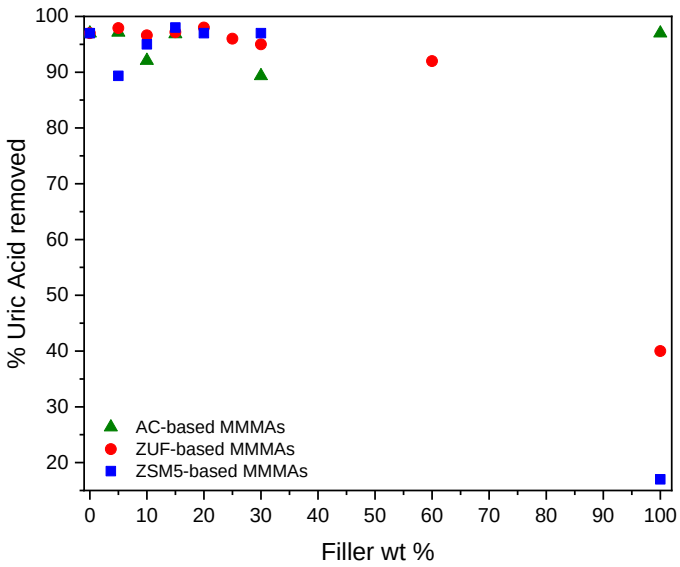


**Figure 3.27**: *Uric acid percentage removed according to the fillers loading.*

The removal of uric acid is high in the plain cellulose acetate membrane, in AC and in the different MMMAs, with factors ranging from 90 to 98%. The addition of zeolites does not enhance the removal capacity of CA membranes, due to the fact that such adsorbents have low removal for uric acid; moreover, the zeolites decrease the water uptake of the membranes. Activated carbon has a removal capacity similar to that of the plain CA membrane, and MMMAs comprising AC do not show a significant toxin removal improvement, but rather a slight decrease, due to the reduction of water uptake caused by AC. An additional explanation can be associated to the ability of uric acid to establish hydrogen bonds with the polymeric matrix. Its hydrogen bond donor count is the highest among the 3 toxins [5][6][7] and this promotes favorable interactions with the polymer that exhibit a high hydrogen bound acceptor count [8]. This can further explain the slightly different removal capacity with the increase of filler amount in the MMMAs.

The situation is completely different for creatinine and urea, where the removal of the plain CA membrane is very low compared to that of all the different MMMAs. Specifically for urea, adding the adsorbent to the membrane improves the removal capacity from 2% to factors as high as 19% when adding ZUF, 22% when adding ZSM-5, 28% when adding AC. In the case of creatinine, the best combination is the one formed by CA with ZUF, followed by AC and ZSM-5 with factors that increase from 5%, for the plain membrane, to 20%, 9% and 21% when adding ZUF, ZSM-5 and AC, respectively. However, in this case the removal enhancement is lower than

expected, at least when adding zeolites to the polymer, as they have a high removal capacity for this toxin. Such behavior is probably due to the fact that the whole porosity of the adsorbent is not accessible once combined with the polymer that may partially block the filler nanopores.

Nevertheless, MMMAs enhance the removal of urea and creatinine with respect to the plain CA membrane and this is noticeable also from the next three graphs reporting the mass adsorbed ($m_{ads}$) of toxins for each filler:

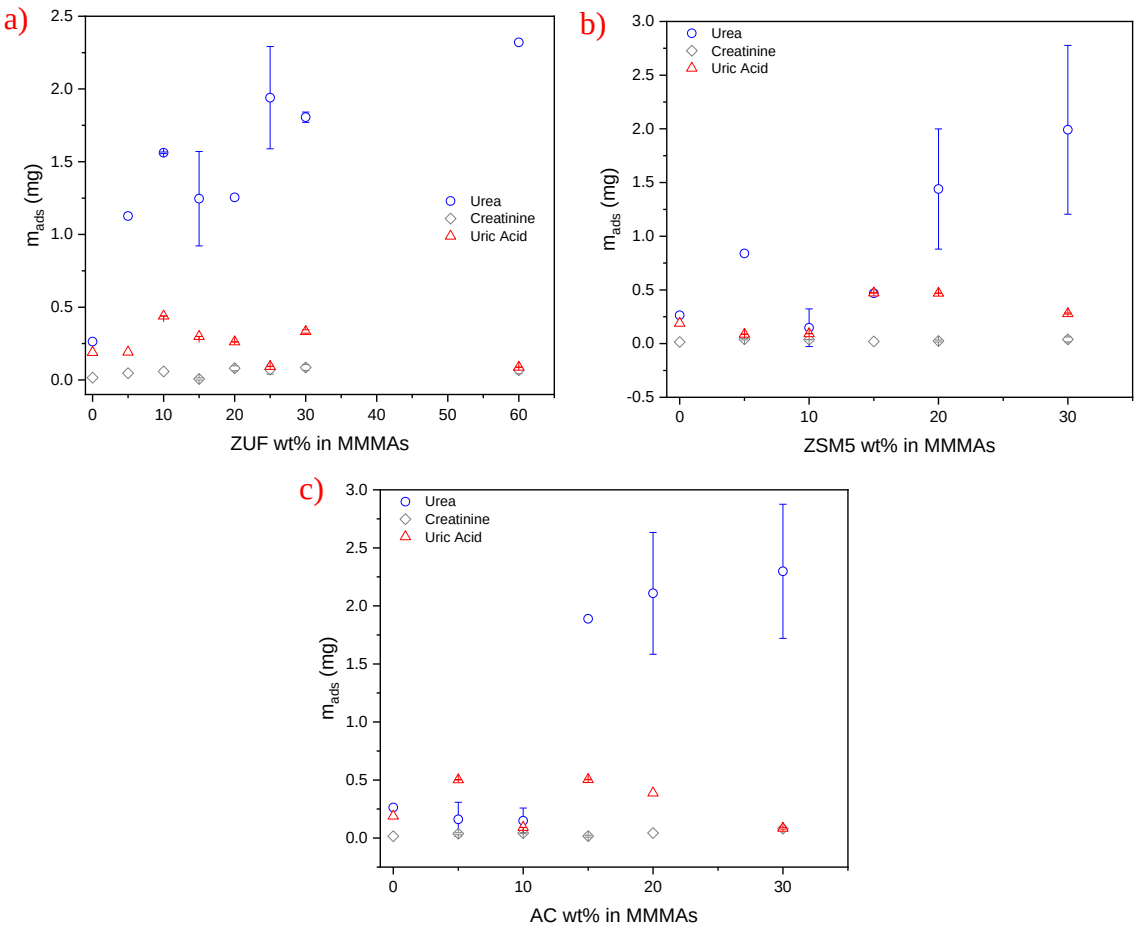


**Figure 3.28**: *Urea, creatinine and uric acid mass adsorbed ($m_{ads}$) for each series of MMMAs: a) ZUF-based MMMAs; b) ZSM5-based MMMAs and c) AC-based MMMAs.*

The increase of the filler loading enhances the performances of the MMMAs as it is shown in Figure 3.28. All the MMMAs adsorb an higher mass of urea, since it is the one present in higher concentrations, while for uric acid and creatine the $m_{ads}$ are lower. The performance could be further improved by increasing the filler loading in the polymer matrix and/or by optimizing the preparation protocol.

### 3.4.3 MMMAs batch adsorption properties with a mixture of toxins

Batch adsorption experiments were conducted following the procedure described in paragraph 2.6.3. The toxin mixture was prepared considering the maximum concentration, $c_{MAX}$, of the three solutes present in patients with and End Stage Renal Disease (ESRD) (Table 2.1). Figure 3.29 a), b) and c) report the MMMAs performances in contact with a mixture of urea, creatinine and uric acid.

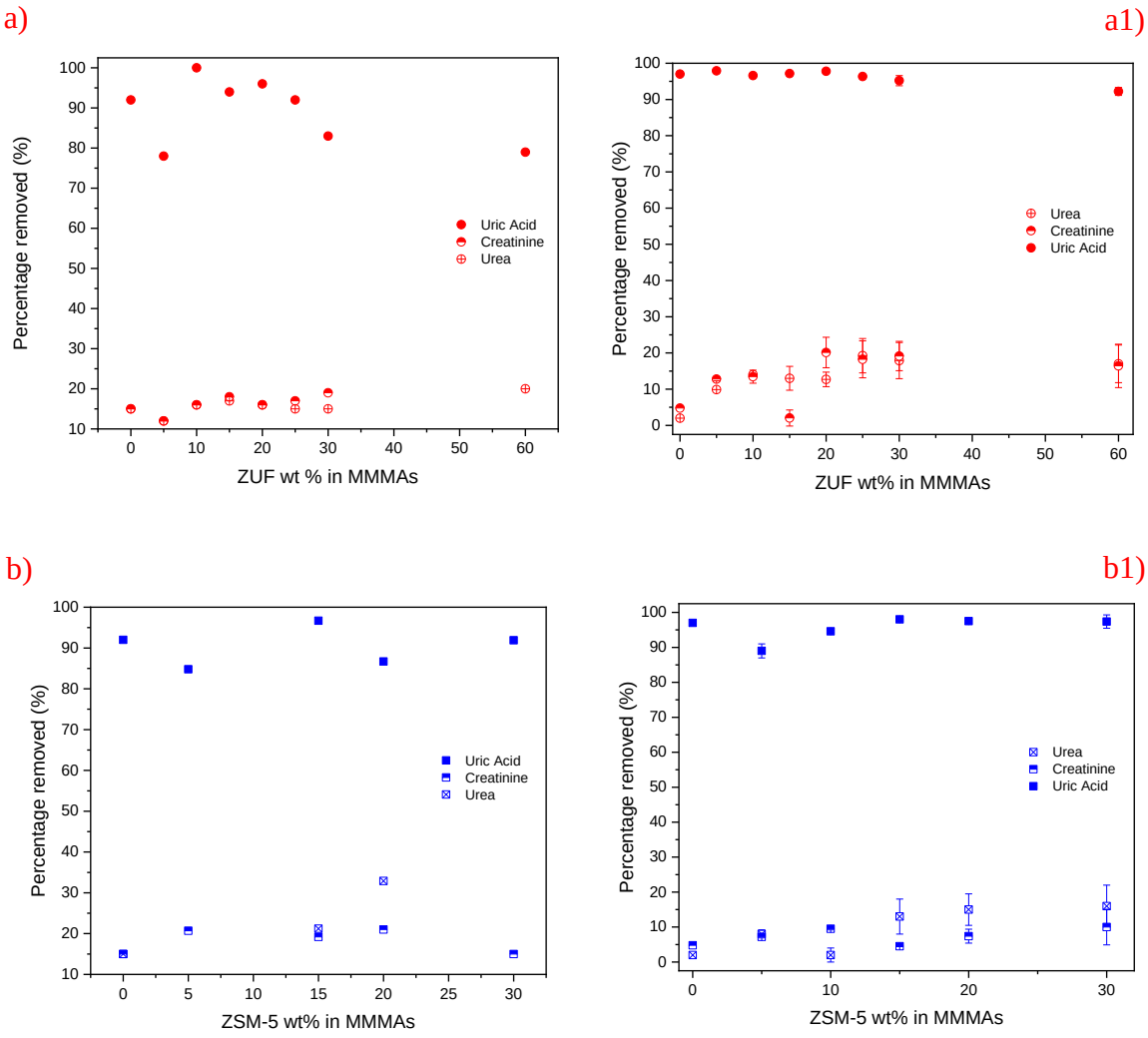

c) c1)

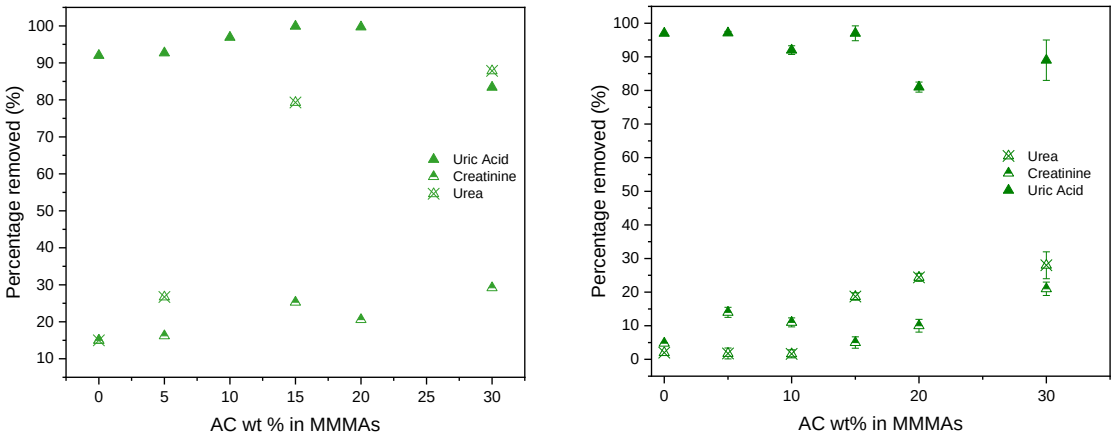


**Figure 3.29**: *Percentage adsorbed of urea, creatinine and uric acid from a mixture of toxins in graph a), b) and c); percentage removed of urea, creatinine and uric acid from single toxin's solutions in graph a1), b1) and c1).*

The results are compared with the one obtained in batch adsorption tests with a single toxin solution. It is possible to see how the performances are equivalent indicating that the MMMAs do not lose their adsorptive capacity in contact with multicomponent solutions. Uric acid is almost completely removed while for urea and creatinine a removal percentage ranging from 20% to 30% is observed These behaviors are in accordance with the one show in Figure 3.29 a1), b1) and c1). It is a remarkable result if the final purpose of these MMMAs is taken into consideration: spent dialysate is a waste solution composed of hundreds of metabolites which need to be removed to regenerate water. Therefore, MMMAs can adsorb a variety of solutes without experiencing a decrease in adsorptive power.

## 3.5 MMMAs continuous adsorption experiments

Dynamic adsorption experiments were carried out according to the procedure described in paragraph 2.6.4 in the set up shown in Figure 2.6. To avoid data redundancy, the breakthrough curves of two MMMAs for each category, ZUF-based, ZSM5-based, AC-based, are reported. The dispersion curves necessary to calculate the dynamic adsorption capacities were obtained with NaCl as was found to be one of the few solutes not interacting with the membrane samples. Experiments were performed with layered stack of 5 membranes corresponding to 0.7 mL of column volume. In Figure 3.30 and 3.31 the dispersion curves of urea, creatinine and uric acid of MMMA_ZUF-5 and MMMA_ZUF_60 are reported:

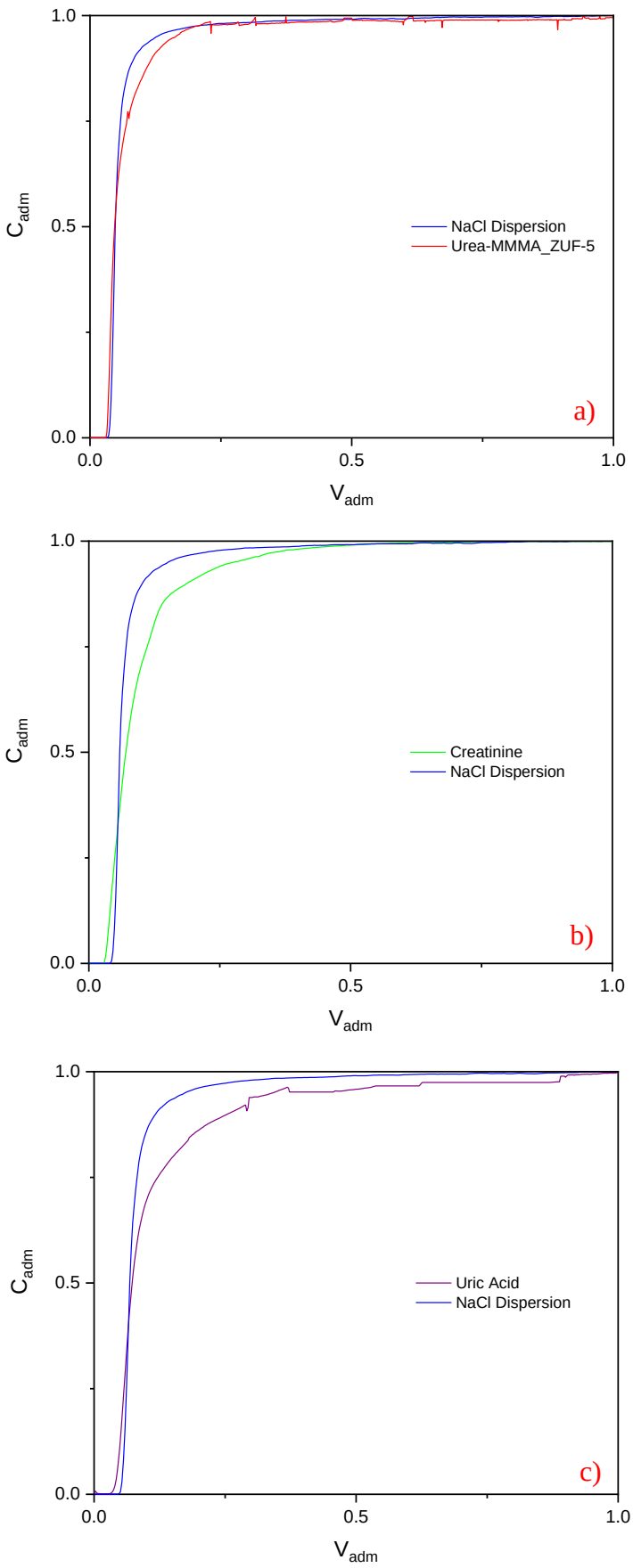


**Figure 3.30**: *Breakthrough curves of urea a), creatinine b) and uric acid c) for MMMA_ZUF-5 obtained at 0.5 mL/min feeding 40 mL of toxin solution.*

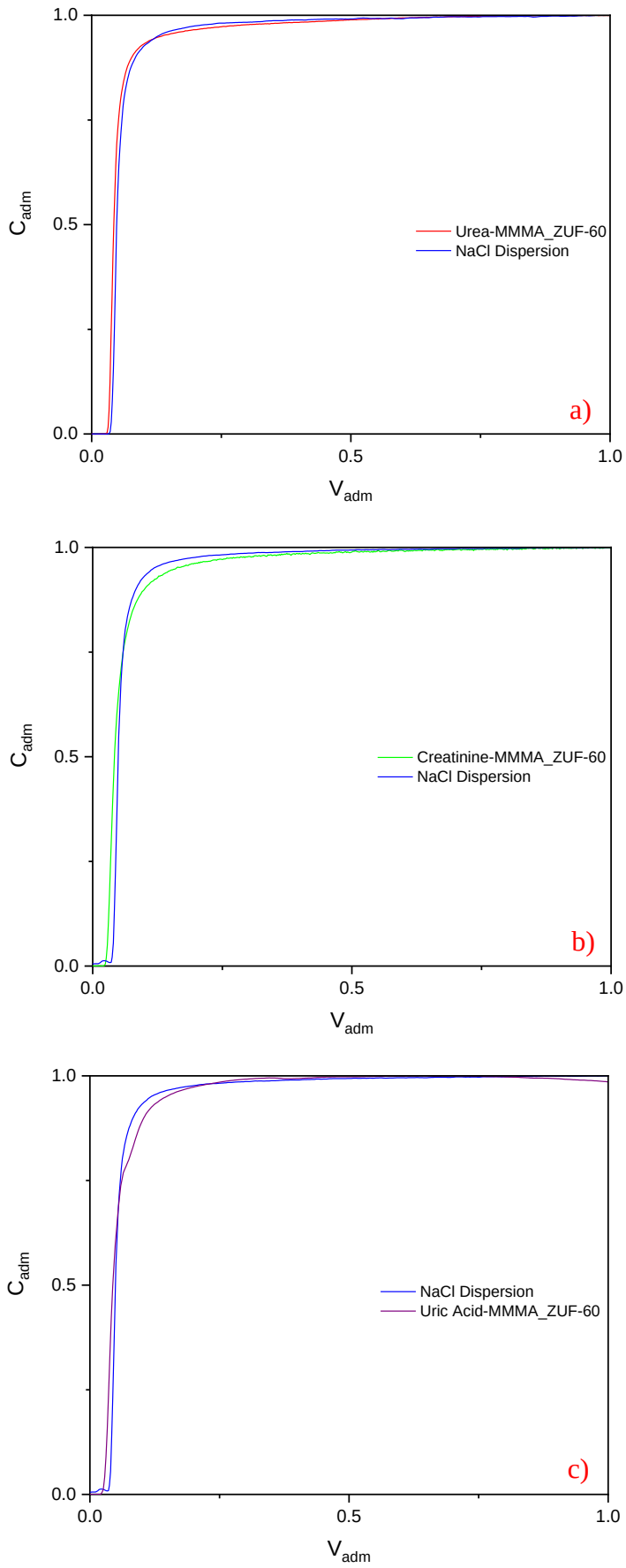


**Figure 3.31**: *Breakthrough curves of urea a), creatinine b) and uric acid c) for MMMA_ZUF-60 obtained at 0.5 mL/min feeding 40 mL of toxin solution.*

The mass of toxin adsorbed is given by the difference between the integrated area beneath the dispersion curve and the breakthrough. From Figure 3.30 and 3.31 is possible to see that the mass removed is not increased by the increased filler loading as it was obtained from the batch tests results. The experimental conditions are completely different from the one used for the batch adsorption experiments, thus the increment in the mass adsorbed with the filler content experienced in Figure 3.28 is not evident in Figure 3.30 and 3.31.

To have a better visualization of the results obtained, in Table 3.3 are reported the mass adsorbed of urea, creatinine and uric acid for all the ZUF-based MMMAs tested:

**Table 3.3**: *Mass of urea, creatinine and uric acid adsorbed by ZUF-based MMMAs in dynamic experiments conditions obtained at 0.5 mL/min feeding 40 mL of toxin solution.*

| **MMMAs** | **$Urea_{Feed}$ (mg)** | **$Urea_{Ads.}$ (mg)** | **$Creatinine_{Feed}$ (mg)** | **$Creatinine_{Ads}$ (mg)** | **U. $Acid_{Feed}$ (mg)** | **U. $Acid_{Ads.}$ (mg)** |
|---|---|---|---|---|---|---|
| *ZUF-5%* | 179.77 | 5.8 | 10.80 | 0.24 | 5.94 | 0.4 |
| *ZUF-30%* | 174.82 | 6.21 | 11.24 | 0.21 | 5.21 | 0.33 |
| *ZUF-60%* | 175.28 | 6.25 | 10.52 | 0.3 | 5.3 | 0.35 |

From Table 3.3 is evident that the mass adsorbed is not influenced by the increase of the filler content. These are non-equilibrium experiments, different from the batch adsorption tests in which the mass adsorbed is calculated after the equilibrium condition is reached.

The same behaviors can be seen for ZSM5-based MMMAs and AC-based one which are reported in Figure 3.32, Figure 3.33, Figure 3.34, Figure 3.35, Table 3.4 and Table 3.5 respectively.

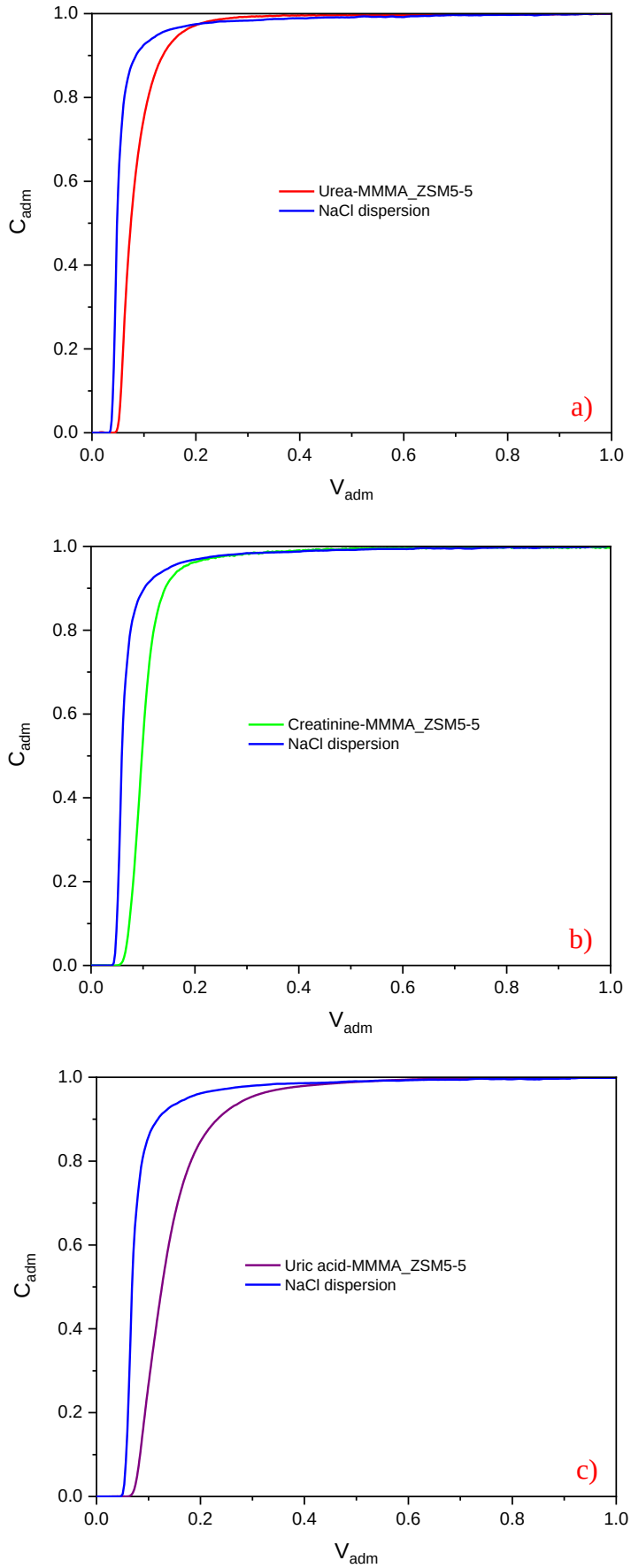


**Figure 3.32**: *Breakthrough curves of urea a), creatinine b) and uric acid c) for MMMA_ZSM5-5 obtained at 0.5 mL/min feeding 40 mL of toxin solution.*

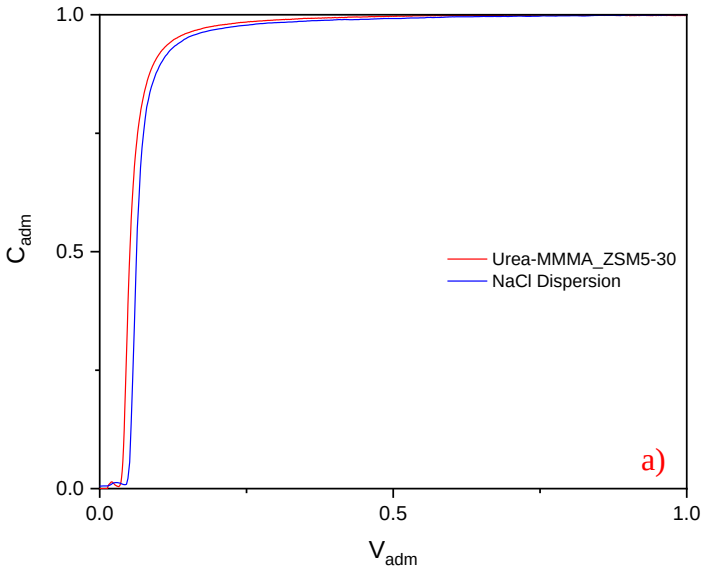
1.0
0.5
0.0
$C_{adm}$
0.0
0.5
1.0
$V_{adm}$
Urea-MMMA_ZSM5-30
NaCl Dispersion
a)

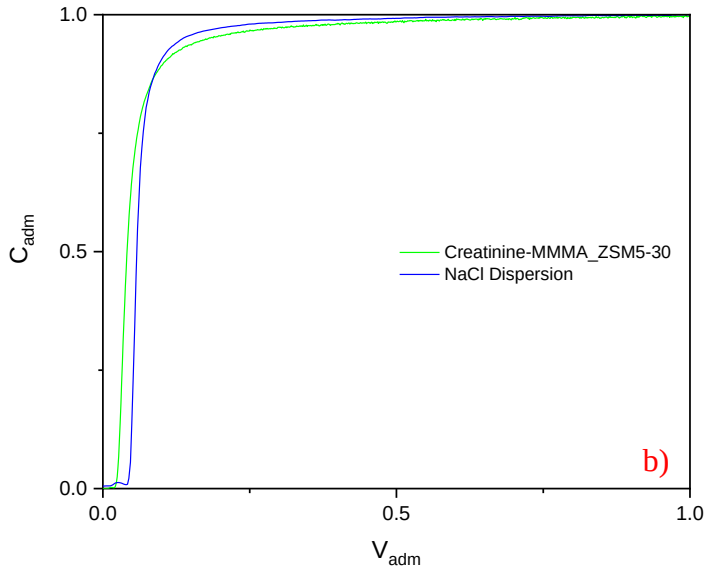
1.0
0.5
0.0
$C_{adm}$
0.0
0.5
1.0
$V_{adm}$
Creatinine-MMMA_ZSM5-30
NaCl Dispersion
b)

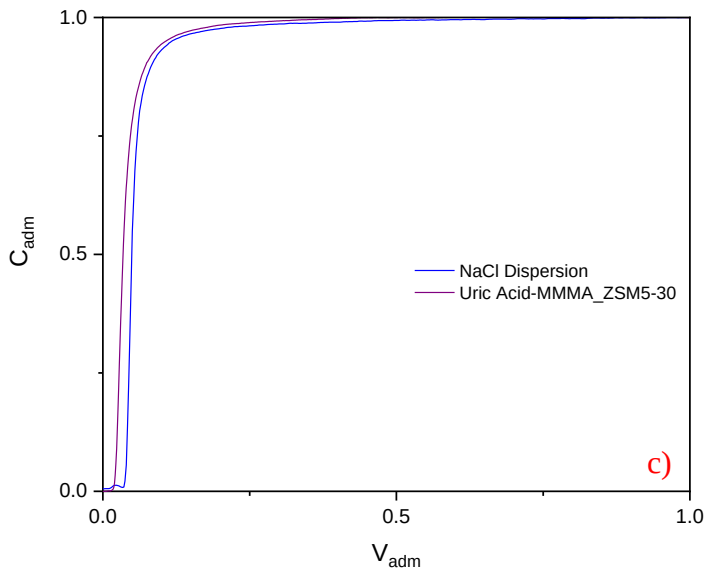


**Figure 3.33**: *Breakthrough curves of urea a), creatinine b) and uric acid c) for MMMA_ZSM5-30 obtained at 0.5 mL/min feeding 40 mL of toxin solution.*

**Table 3.4**: *Mass of urea, creatinine and uric acid adsorbed by ZSM5-based MMMAs in dynamic experiments conditions obtained at 0.5 mL/min feeding 40 mL of toxin solution.*

| MMMAs | $Urea_{Feed}$ (mg) | $Urea_{Ads.}$ (mg) | $Creatinine_{Feed}$ (mg) | $Creatinine_{Ads}$ (mg) | U. $Acid_{Feed}$ (mg) | U. $Acid_{Ads.}$ (mg) |
|---|---|---|---|---|---|---|
| *ZSM5-5%* | 170.58 | 5.31 | 10.40 | 0.08 | 5.1 | 0.26 |
| *ZSM5-10%* | 174.68 | 5.10 | 10.85 | 0.11 | 5.95 | 0.30 |
| *ZSM5-60%* | 173.65 | 6.24 | 10.42 | 0.15 | 5.60 | 0.24 |

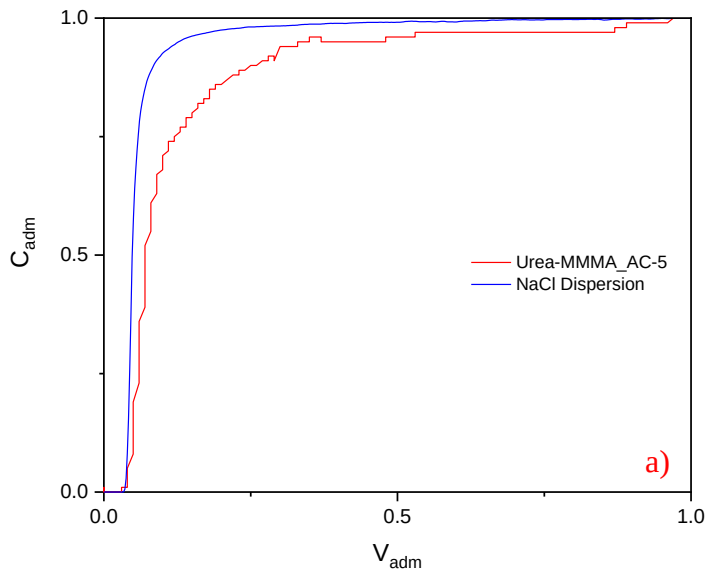

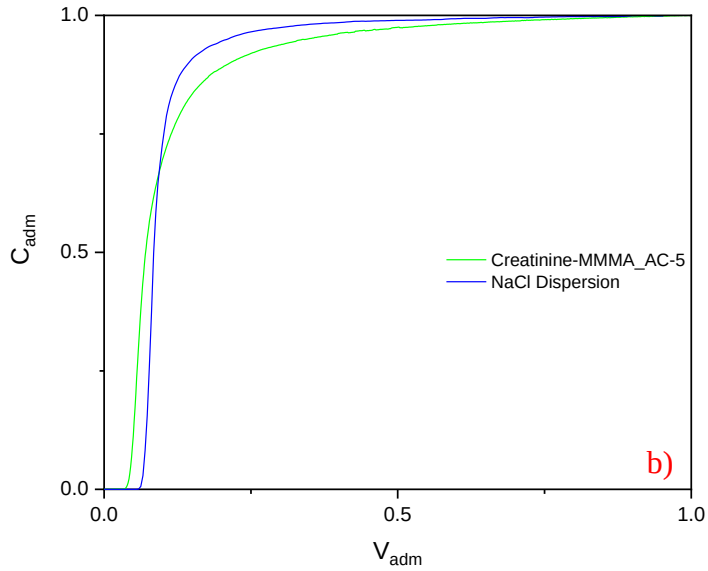


**Figure 3.34**: *Breakthrough curves of urea a) and creatinine b) for MMMA_AC-5 obtained at 0.5 mL/min feeding 40 mL of toxin solution.*

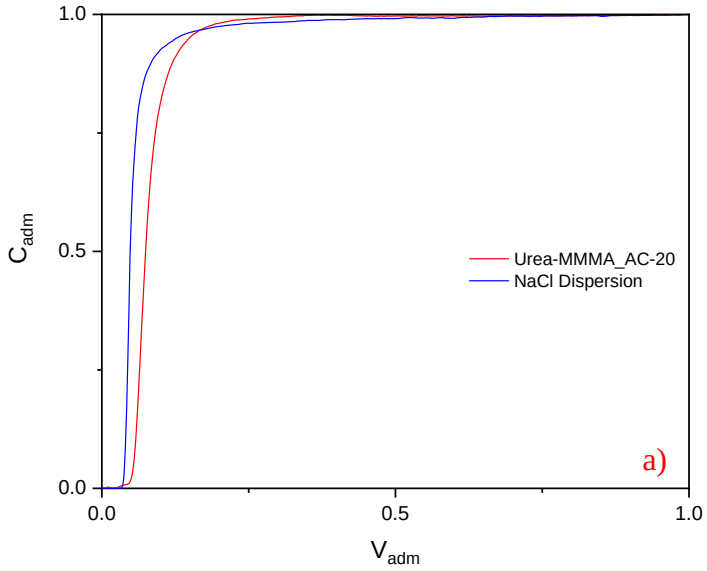

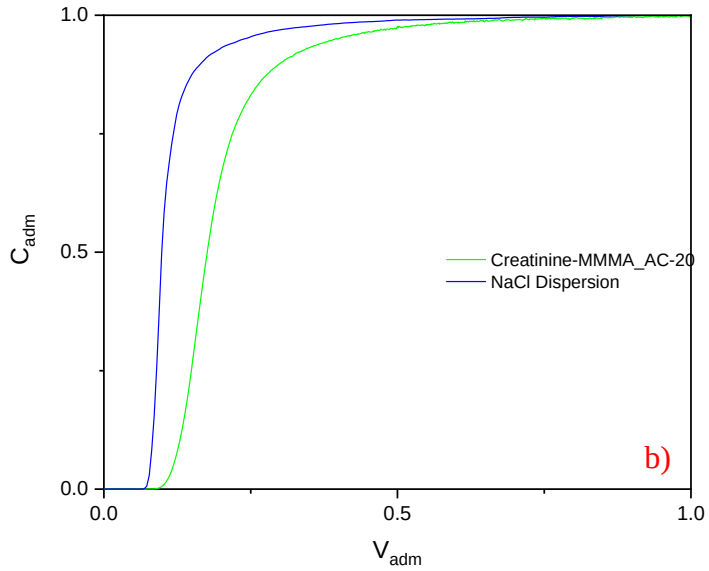


**Figure 3.35**: *Breakthrough curves of urea a) and creatinine b) for MMMA_AC-20.*

**Table 3.5**: *Mass of urea, creatinine and uric acid adsorbed by AC-based MMMAs in dynamic experiments conditions.*

| MMMAs | $Urea_{Feed}$ (mg) | $Urea_{Ads.}$ (mg) | $Creatinine_{Feed}$ (mg) | $Creatinine_{Ads}$ (mg) | $U.\ Acid_{Feed}$ (mg) | $U.\ Acid_{Ads.}$ (mg) |
|---|---|---|---|---|---|---|
| *AC-5%* | 180.58 | 3.89 | 10.35 | 0.19 | 4.98 | 0.08 |
| *AC-20%* | 168.4 | 6.24 | 9.86 | 0.31 | 4.85 | 0.36 |
| *AC-30%* | 170.52 | 5.90 | 10.05 | 0.20 | 5.01 | 0.2 |

### 3.5.1 Continuous adsorption experiments with a mixture of toxins using a MMMAs cartridge

The results obtained in the previous section with a stack of 5 membranes denote the necessity of a higher column volume to improve the MMMAs adsorption performances. 11 discs of MMMA_ZUF-60 and 11 of MMMA_AC-20 were packed in the membrane cell being these adsorbers the most promising from batch and continuous adsorption results. Tests were performed using a mixture of the three toxins at their $c_{MAX}$ to assess their removal in more realistic operative conditions, with 1.8 mL of column volume. The experiments were conducted according to the procedure described in paragraph 2.6.4.1. Data were analyzed with an HPLC following the procedure described in paragraph 2.6.3.1.

Tests were conducted at 3 different feed flow rates: 0.5 mL/min, 5 mL/min and 10 mL/min. The breakthrough curves were reproduced collecting the permeate volume at fixed time intervals for 40 mL of feed solution. Moreover, four different experiments were performed

collecting 2 mL, 5 mL, 10 mL and 15 mL in order to calculate the total mass adsorbed feeding fixed amounts of volume.

Figure 3.36 represents the three breakthrough curves for the 3 toxins for the two tests done at 0.5 mL/min. Figure 3.37 show the breakthrough curves for creatinine at the three different feed flow rates.

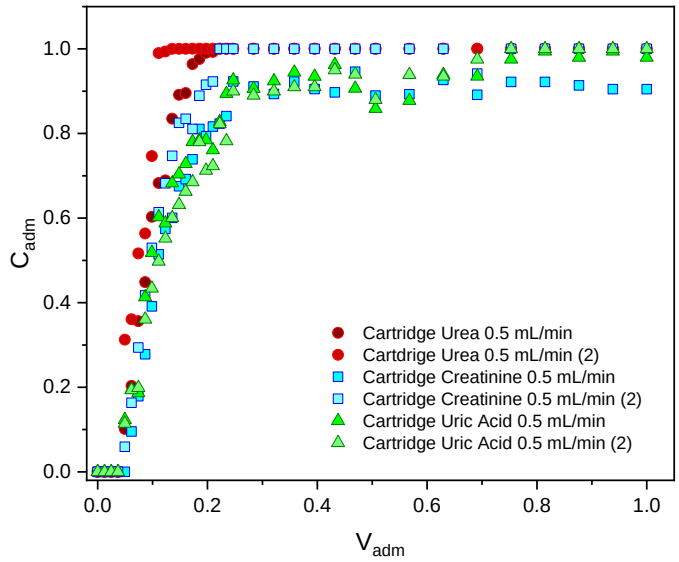


**Figure 3.36**: *Breakthrough curves of urea, creatinine and uric acid for the MMMAs cartridge in contact with a mixture of toxins at 0.5 mL/min.*

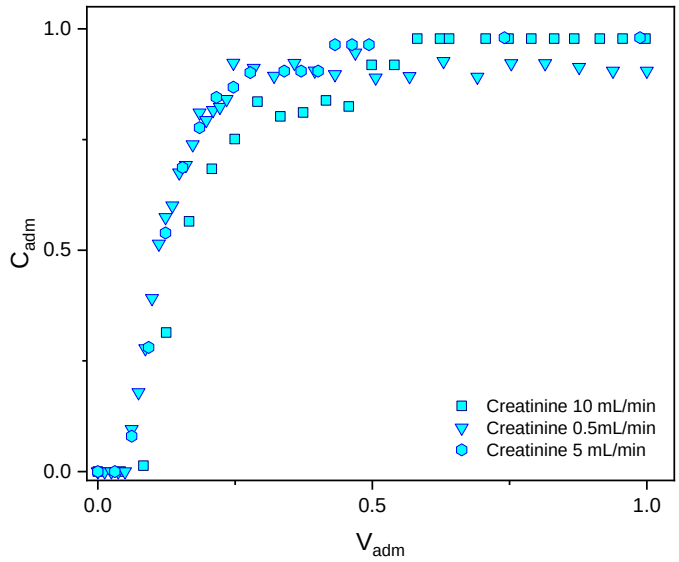


**Figure 3.37**: *Breakthrough curves of creatinine for the MMMAs cartridge in contact with a mixture of toxins at the three different feed flow rates.*

The data scattering is due to the unavoidable errors done during diluting the solutions, in the HPLC analysis itself and in the HPLC data elaboration since it requires a manual peaks integration. Figure 3.36 shows the breakthrough curves at 0.5 mL/min. Even if there is an uncertainty due to the errors in the measurements, data are reproducible.

From Figure 3.37, apart from the uncertainty affecting the data, it is possible to see that increasing the flow rate from 0.5 mL/min to 10 mL/min does not modify the steepness of the breakthrough curves.

In Table 3.6 the mass of toxins adsorbed by the MMMAs cartridge for fixed amount of feed solution volumes at 0.5 ml/min, 5 mL/min and 10 mL/min.

**Table 3.6**: *Mass of urea, creatinine and uric acid adsorbed by the MMMAs cartridge from a mixture of toxins in four different experiments for each flow rate.*

| | $V_{collect.}$ (mL) | $Urea_{Feed}$ (mg) | $Urea_{Ads.}$ (mg) | $Creat._{Feed}$ (mg) | $Creat._{Ads}$ (mg) | $U.\ Acid_{Feed}$ (mg) | $U.\ Acid_{Ads.}$ (mg) |
|---|---|---|---|---|---|---|---|
| **0.5 mL/min** | **2** | 8.30 | 8.30 ± 0.0 | 0.88 | 0.88 ± 0.00 | 0.32 | 0.32 ± 0.00 |
| | **5** | 20.75 | 18.24 ± 2.0 | 2.19 | 2.05 ± 0.07 | 0.80 | 0.72 ± 0.00 |
| | **10** | 41.46 | 34.50 ± 2.1 | 4.38 | 3.92 ± 0.22 | 1.60 | 1.36 ± 0.01 |
| | **15** | 62.24 | 19.25 ± 1.9 | 6.56 | 3.60 ± 0.25 | 2.41 | 1.26 ± 0.41 |
| **5 mL/min** | **2** | - | - | 1.09 | 1.07 ± 0.02 | 0.28 | 0.28 ± 0.00 |
| | **5** | - | - | 2.19 | 1.96 ± 0.01 | 0.55 | 0.52 ± 0.01 |
| | **10** | - | - | 4.38 | 3.07 ± 0.01 | 1.11 | 0.98 ± 0.01 |
| | **15** | - | - | 6.56 | 2.94 ± 0.06 | 1.66 | 0.78 ± 0.01 |
| **10 mL/min** | **2** | - | - | 0.96 | 0.96 ± 0.00 | 0.28 | 0.28 ± 0.00 |
| | **5** | - | - | 1.92 | 1.76 ± 0.02 | 0.56 | 0.54 ± 0.01 |
| | **10** | - | - | 3.84 | 2.88 ± 0.01 | 1.13 | 0.75 ± 0.01 |
| | **15** | - | - | 5.75 | 1.94 ± 0.04 | 1.69 | 0.45 ± 0.00 |

From Table 3.6 is possible to see that the mass adsorbed increases up to 10 mL of feed solution sent to the membrane column while at 15 mL the mass adsorbed start to decrease indicating a MMMAs beginning of saturation.

### 3.5.2 Sizing of a cartridge for purification of spent dialysate

The results obtained in Table 3.6 denote the possibility of a continuous removal of urea, creatinine and uric acid from multicomponent toxin solutions. Thus, they were used for

sizing of a cartridge able to remove uremic toxins from spent dialysate in real hemodialysis conditions. A maximum binding capacity, $DBC_{max}$, was calculated for each toxin at every flow rate considered, according to Equation (66):

$$DBC_{max} = \frac{m_{ads,max}}{V_{Column}} \quad (66)$$

where $m_{ads,max}$ is the maximum mass adsorbed (mg) among the four volumes fed in the different experiments and $V_{Column}$is the column volume (mL) corresponding to 1.8 mL.

Normally, a hemodialysis process last 3,5 hours, with a dialysate flow rate of 450 mL/min. In uremic patients the maximum concentration of urea, creatinine and uric acid is not fixed, but varies in a range. Therefore, to calculate the cartridge volume needed to remove the 90% of toxins from the spent dialysate, a mean maximum concentration was used.

Then, fixing the $DBC_{max}$, these cartridge volumes were obtained:

**Table 3.7***: Cartridge volumes obtained for the different flow rates.*

| Flow rate (mL/min) | Cartridge volume for Urea (L) | Cartridge volume for Creatinine (L) | Cartridge volume for Uric Acid (L) |
|---|---|---|---|
| ***0.5 mL/min*** | 12 | 6 | 8 |
| ***5 mL/min*** | - | 8 | 12 |
| ***10 mL/min*** | - | 12 | 27 |

Unfortunately, the data for urea were obtained only at 0.5 mL/min due to the impossibility of resolving the peaks in the HPLC analysis. The increase in cartridge volume with increasing flow rate is attributed to diffusion limitations. This is confirmed by Figure 3.38 where the $DBC_{max}$ is plotted as a function of the flow rate.

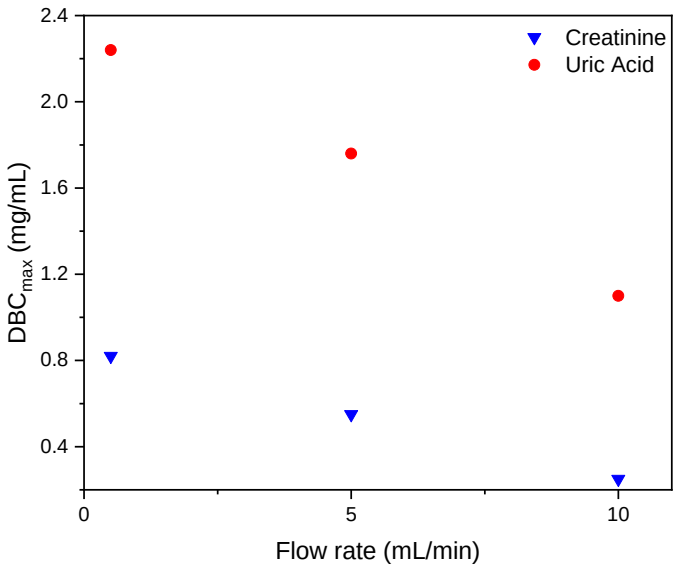


**Figure 3.38**: *Maximum adsorption capacities, $DBC_{max}$, as a function of the flow rates.*

Urea is the toxin that determines the final size of the cartridge. Indeed, this was expected since urea by far is the most abundant toxin in the spent dialysate and it is also the most difficult to remove from it. Thus, in designing the system, the volume chosen should be one obtained for urea results. Since this system is not projected to work in series with the hemodialyzer, is preferable to work at low flow rates to avoid an extremely large column.

#### *3.5.2.1 Cartridge washing procedure*

The MMMAs cartridge is easily cleanable with water. Even though it is meant to be disposable, for a single use only, the MMMAs can be washed with water for at least 40 minutes to remove the toxins physically adsorbed inside the membranes and filler pores. The water flux was monitored with the FPLC set-up as well as the pressure drop across the membranes pack. This procedure was done after every test to restore the MMMAs adsorption capacity. Since cellulose acetate is a substrate subjected to microbial growth, a 0.1 M NaOH solution was used to clean the cartridge properly when needed. This is crucial to prevent membrane degradation.

## 3.6 Hybrid CA/$SiO_2$ ultrafiltration membranes characterization

Hybrid CA/$SiO_2$ ultrafiltration membranes for artificial kidney applications were synthesized according to the procedure described in paragraph 2.4.2. CA_30 and CA_22 membranes were characterized for their MWCO and hydraulic permeabilities. The

membrane was mounted in the surrogate system of an artificial kidney, and were conditioned 2 hours at 0.1 bar to avoid variations in the membrane structure during the experiments. In Figure 3.39 and 3.40 the MWCO and hydraulic permeabilities of CA_30 and CA_22 are reported.

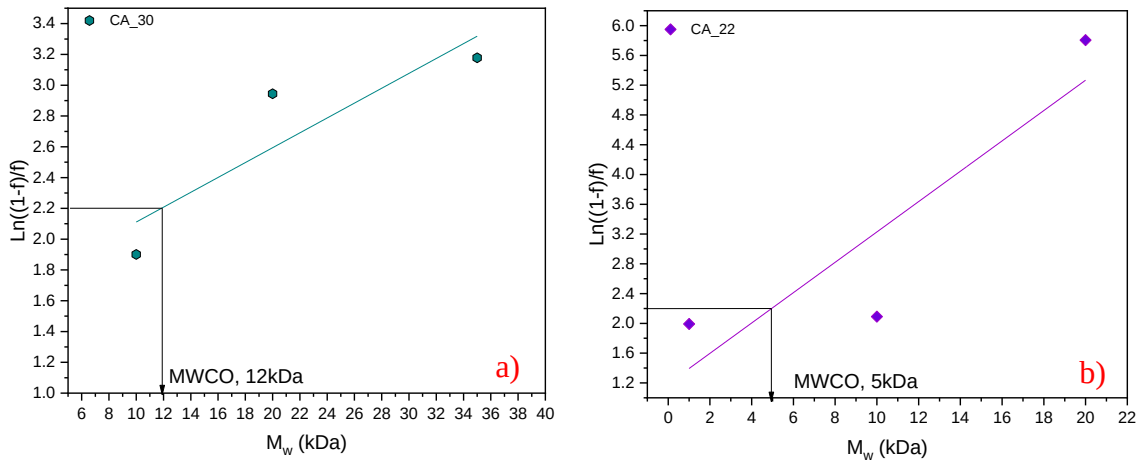


**Figure 3.39**: *MWCO of CA_30 a) and CA_22 b) obtained visually from the intersection between the Ln((1-f)/f) when f = 0.9 (which is 2.2) and the linear regression of the PEG rejection coefficients.*

The MWCO shown in Figure 3.39 are in accordance with the results previously obtained for the same membranes, tested in a different installation [9]. The difference in MWCO between CA_30 and CA_22 is in accordance with the different pore structure expected: CA_22 are prepared from a casting solution containing less formamide (the pore generator) so it has a tighter pore structure [10], resulting in a lower MWCO. On the other hand, the MWCO of CA_30 [11] is higher due to a higher amount of formamide in the casting solution leading to a looser pore configuration.

In Figure 3.40 the permeation fluxes as a function of the transmembrane pressure (TMP) for CA_30 CA_22 are reported. The results are obtained following the procedure described in paragraph 2.7.1:

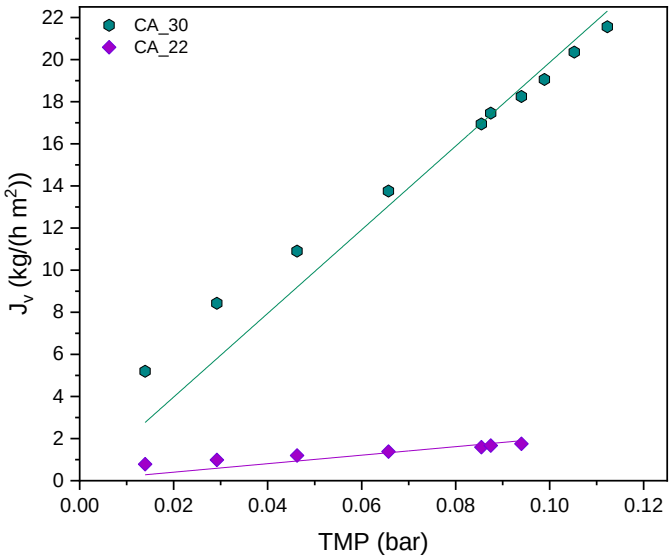


**Figure 3.40**: *Permeation fluxes as a function of the transmembrane pressure for CA_30 and CA_22.*

From Figure 3.40 it is possible to see that the membranes follow Darcy's law (Equation (2)) for which the fluxes increase linearly with increasing the TMP. The slope of the linear regression is the hydraulic permeability. The CA_22 membrane has a permeability of 20.7 kg/(h m$^2$ bar), while the CA_30 exhibits a permeability of 198.7 kg/(h m$^2$ bar). This tangible difference is connected to the different pore structure of the membranes.

## 3.7 Fluid mechanics characterization of a surrogate system of an artificial kidney (AK)

The two flat sheet ultrafiltration membranes, CA_22 and CA_30 are used to perform the fluid mechanics characterization of the surrogate system of an artificial kidney (AK) represented in Figure 2.8. The configuration of the feed channel of the AK is reported in Figure 2.11: it has a slit geometry with the height of the slit much smaller than the height and the width. Previous studies have pointed out that surface phenomena, such as pressure drop due to surface roughness gain huge importance in scaling down the system to mini and microchannels. They become even more important when suction is present. Therefore, theoretical pressure drops were calculated with the Hagen-Poiseuille equation (Equation (61)) for a slit and the results compared with the experimental data obtained in the AK surrogate system.

In Figure 3.41 are reported the theoretic pressure drop calculated with the Equation (61) with different slit heights (h): considering the thickness of an acetate film and the thickness of the membrane and the filter paper that is normally used to protect the membrane from

deformation during the experiments. Moreover, the experimental pressure drop with impermeable walls conditions are shown.

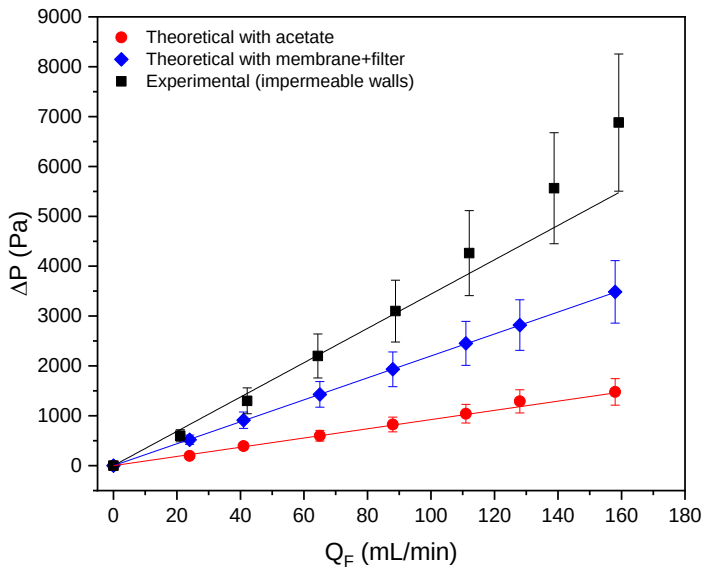


**Figure 3.41**: *Theoretical pressure drop calculated with different slit heights and experimental pressure drop with impermeable walls conditions.*

The linear dependence of pressure drop, ΔP, on the flow rate, Q, with the slope increasing with the channel height reduction (red and blue series) confirms the fully developed laminar regime of a Poiseuille-type flow [12]. Therefore, the velocity profile described by Equation (67) is display in Figure 3.41:

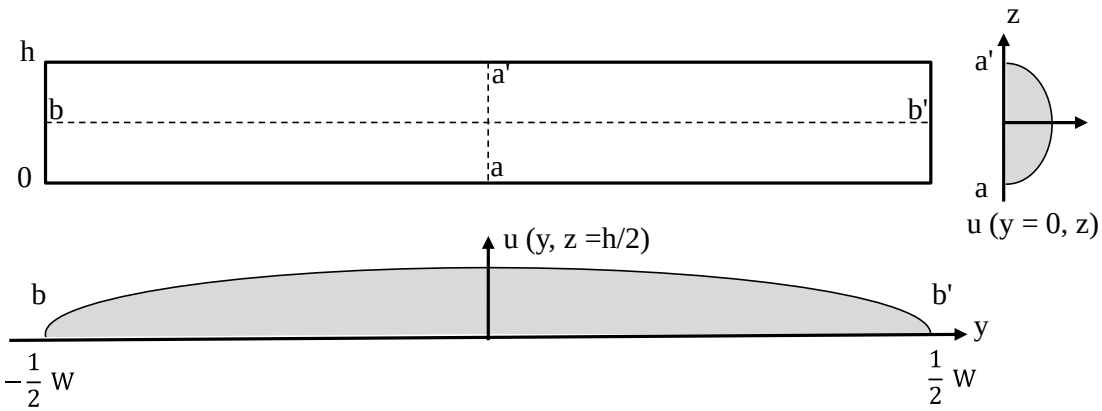


**Figure 3.42**: *Theoretical velocity profile u (y,z) at the slit middle planes, vertical and horizontal respectively (y=0; z=h/2).*

$$u(y,z) = \frac{4\,h^2 \Delta P}{\pi^3\,\mu\,L} \sum_{n,odd}^{\infty} \frac{1}{n^3} \left[1 - \frac{\cosh\left(n\pi \frac{y}{h}\right)}{\cosh\left(n\pi \frac{W}{2h}\right)}\right] \sin\left[n\pi \frac{z}{h}\right] \tag{67}$$

As the slit height increases (blue curve compared to the red one), the ΔP increases considerably. This is expected since, for a fixed flow rate a smaller height leads to a larger maximum velocity. Therefore, the shear stresses at the walls, both vertical and horizontal,

increase leading to higher pressure drops. This is in accordance with the results obtained in previous works [13][14].

The discrepancy between the experimental value of ΔP (black series) and the theoretical values, can be ascribed to the wall surface roughness, since the uncertainty exaggeration considered is not enough to cover the difference between the experimental and theoretical data. This can be modelled with a fictitious viscosity [15]. It is possible to define an apparent viscosity, $\mu_{app}$, expressed by Equation (68):

$$\mu_{app} = \mu + \mu_{rough} \tag{68}$$

where $\mu_{rough}$ is a fictitious viscosity introduced to take into account the local effects of the change in velocity profile due to wall roughness on pressure drop. It is possible to write the Hagen-Poiseuille equation for a slit (Equation (30)) both for $\mu$ and $\mu_{app}$:

$$\mu = \Delta P_{theor.} \frac{W\,h^3}{12\,L\,Q}\left[1 - 0.63\,\frac{h}{W}\right] \tag{69}$$

$$\mu_{app} = \Delta P_{exp} \frac{W\,h^3}{12\,L\,Q}\left[1 - 0.63\,\frac{h}{W}\right] \tag{70}$$

and therefore, the expression for $\mu_{rough}$ is obtained:

$$\mu_{rough} = (\Delta P_{exp.} - \Delta P_{theor.}) \frac{W\,h^3}{12\,L\,Q}\left[1 - 0.63\,\frac{h}{W}\right] \tag{71}$$

The results of $\mu_{rough}$ obtained range between 0.29 $\mu$ and 0.96 $\mu$, which are in accordance with [14] validating the hypothesis done.

In Figure 3.43 are show the results obtained with permeation using CA_30 and CA_22:

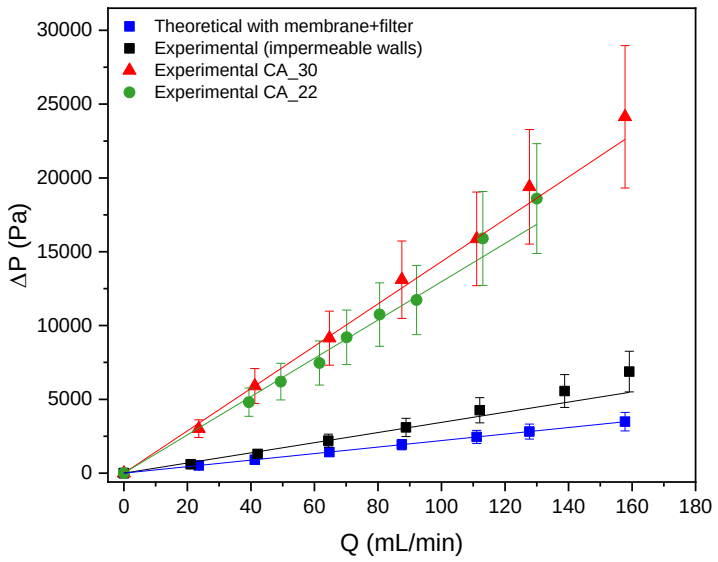


**Figure 3.43**: *Theoretical and experimental pressure drop (permeable and impermeable walls conditions).*

From Figure 3.43 is possible to see the fully developed laminar regime of a Poiseuille-type of flow as for Figure 3.40. The difference in pressure drop between the two series obtained with CA_30 (red) and CA_22 (green) is not particularly marked and the results fall in the uncertainty range. This means that the roughness of the membranes surface can be considered of the same order of magnitude. So, the effect on ΔP due to local velocity changes caused by the membrane surface roughness is similar in both cases.

Even if large uncertainties were considered for both experimental (± 20%) and theoretical values (± 18%) it is clear that the data obtained with permeation (red and green series) are much larger than the ones with impermeable walls conditions. Surface roughness cannot be the only reason for this big increase, therefore, the hypothesis of considerable global deformation of the velocity profile was made to explain this behavior. The presence of suction shifts the location of the maximum of the velocity in the vertical direction towards the membrane surface. This can be only confirmed by computational fluid dynamics (CFD) simulation, but this hypothesis is sustained by the lower ΔP showed by the CA_22 membrane: the tighter pore structure of CA_22 leads to lower permeation fluxes with respect to CA_30 and therefore, to lower global deformation of the velocity profile.

To assess the effect of viscosity changes on the ΔP, the pressure was monitored for all the rejections tests done with the five solutes listed in paragraph 2.7.2. In Figure 3.44 the results are shown:

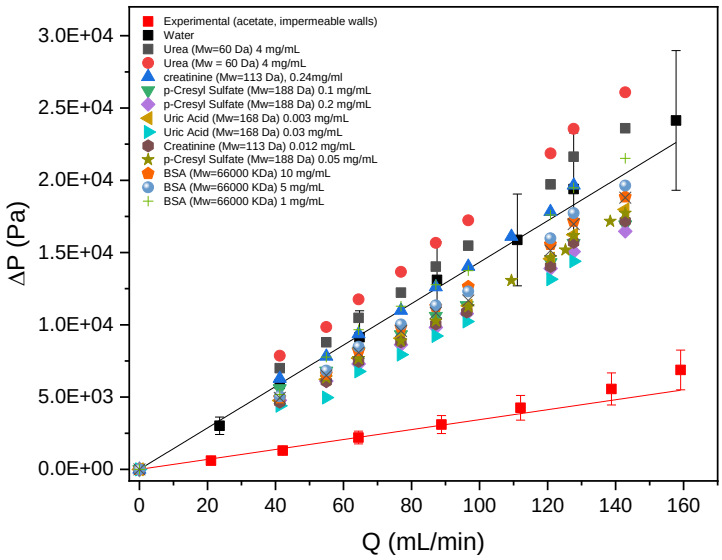


**Figure 3.44**: *Experimental pressure drops (permeable and impermeable walls conditions) with different solutes at different concentrations.*

From Figure 3.44 is possible to see how, even if the solutes results are mildly dispersed with respect to the one of water, the difference in ΔP falls within the experimental uncertainty. Therefore, the effect of change in viscosity solution is much smaller than the one of suction.

The working plan included also the testing of a third type of cellulose acetate/$SiO_2$ membrane, with a looser pore structure with respect to CA_30. This would have probably confirmed the hypothesis done, but unfortunately, due to the COVID-19 pandemic, it was not possible to conclude the experimental work planned.

## 3.8 Development of a new dimensionless mass transfer correlation

To develop the new dimensionless mass transfer correlation, rejections experiments were done with the five solutes presented in paragraph 2.7. The solutions were prepared at different concentrations and the tests done for several feed circulation velocities. Experiments were done with CA_30.

In Figures 3.45, 3.46, 3.47, 3.48 and 3.49 the permeation fluxes as a function of the transmembrane pressure are reported to verify the presence of concentration polarization:

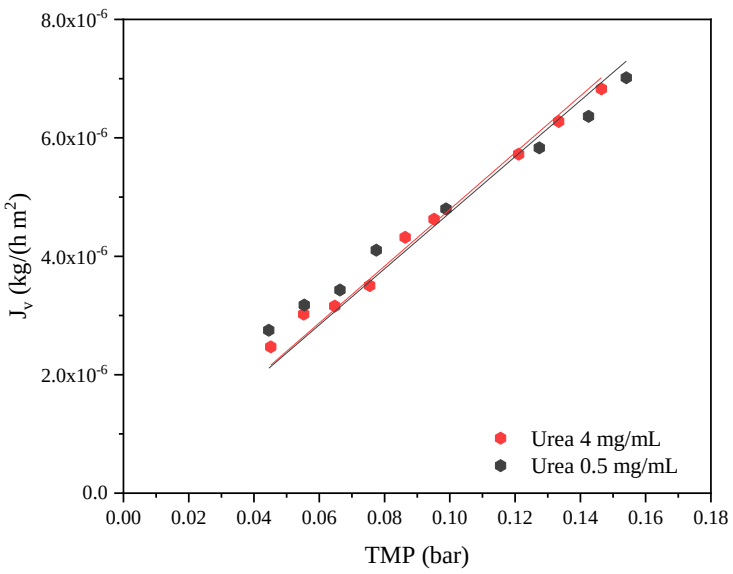


**Figure 3.45***: Urea permeation fluxes at 4 mg/mL and at 0.5 mg/mL.*

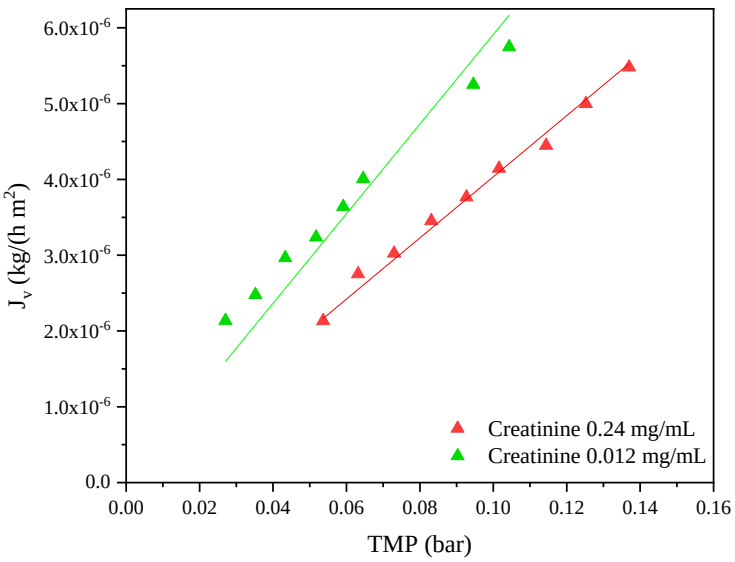


**Figure 3.46***: Creatinine permeation fluxes at 0.24 mg/mL and at 0.012 mg/mL.*

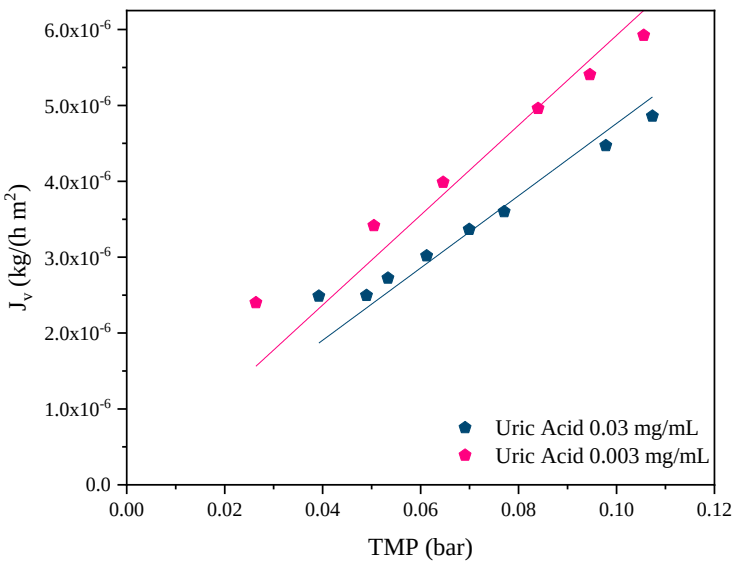


**Figure 3.47**: *Uric acid permeation fluxes at 0.03 mg/mL and at 0.003 mg/mL.*

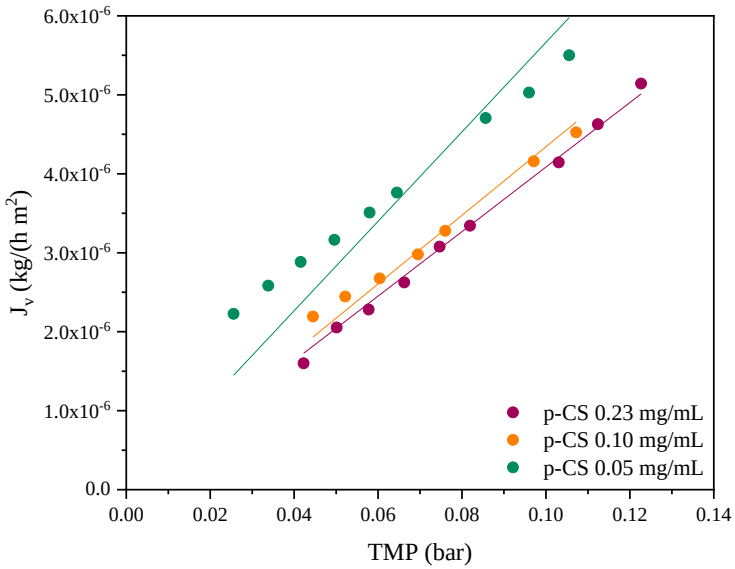


**Figure 3.48**: *para-Cresyl Sulphate (p-CS) permeation fluxes at 0.23 mg/mL, 0.10 mg/mL and at 0.05 mg/mL.*

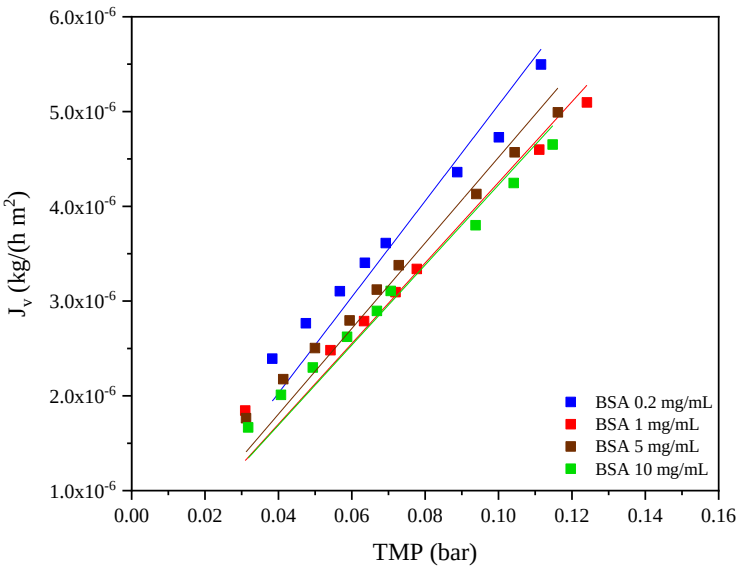


**Figure 3.49**: *Bovine Serum Albumin (BSA) permeation fluxes at 10 mg/mL, 5 mg/mL, 1 mg/mL and at 0.2 mg/mL.*

From the graphs reported above, is possible to notice the permeate flux decrease by increasing the feed concentration. This indicates the occurrence of the concentration polarization phenomenon. CA_30 is a hybrid ultrafiltration membrane for kidney applications and therefore, should retain BSA and remove low and middle molecular weight solutes. Urea, creatinine, uric acid and p-CS pass effectively through the membrane pores, but increasing their concentration in the feed solution a polarization gel starts to form on the membrane surface slowing down the transport across the membrane. This is visible also from Figure 3.50, 3.51, 3.52, 3.53 and 3.54 where the apparent rejections coefficients are reported as functions of the TMP:

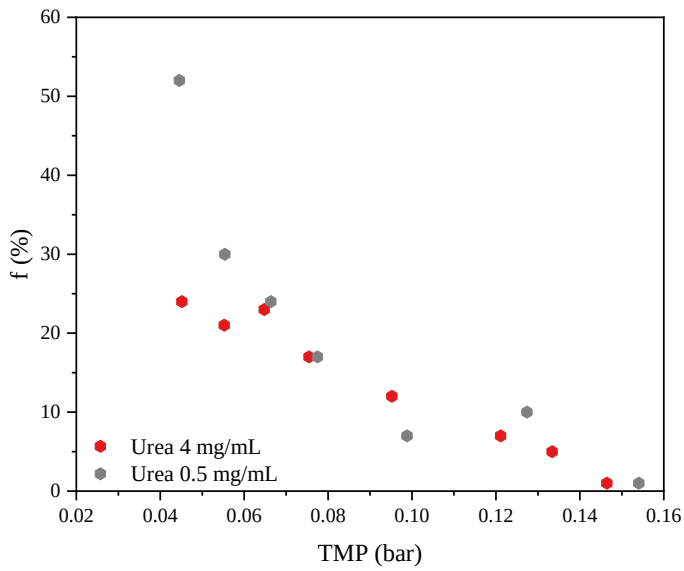


**Figure 3.50***: Urea apparent rejection coefficients at 4 mg/mL and at 0.5 mg/mL.*

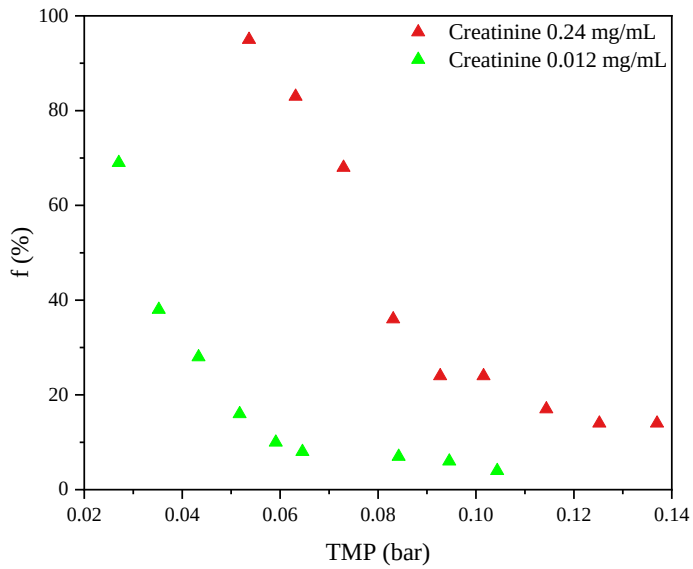


**Figure 3.51***: Creatinine apparent rejection coefficients at 0.24 mg/mL and at 0.012 mg/mL.*

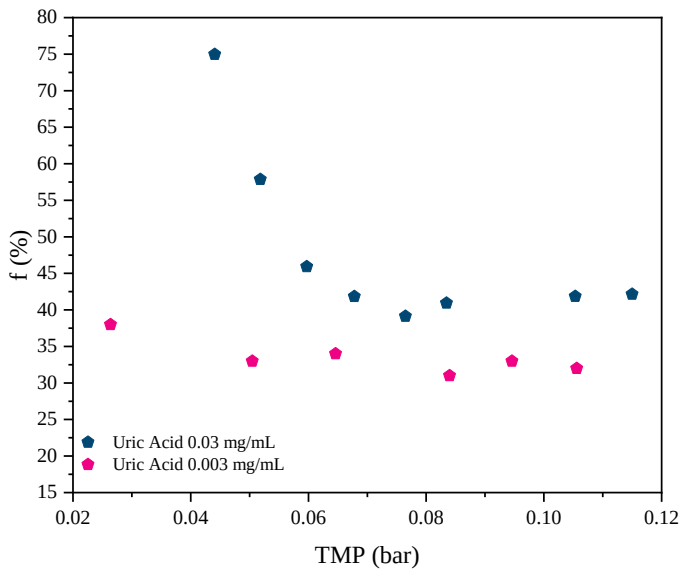


**Figure 3.52***: Uric acid apparent rejection coefficients at 0.03 mg/mL and at 0.003 mg/mL.*

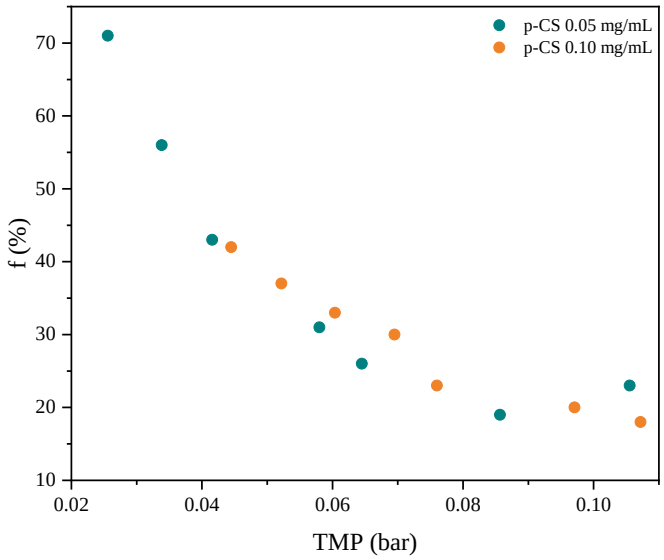


**Figure 3.53***: para-Cresyl Sulphate (p-CS) apparent rejection coefficients at 0.10 mg/mL and at 0.05 mg/mL.*

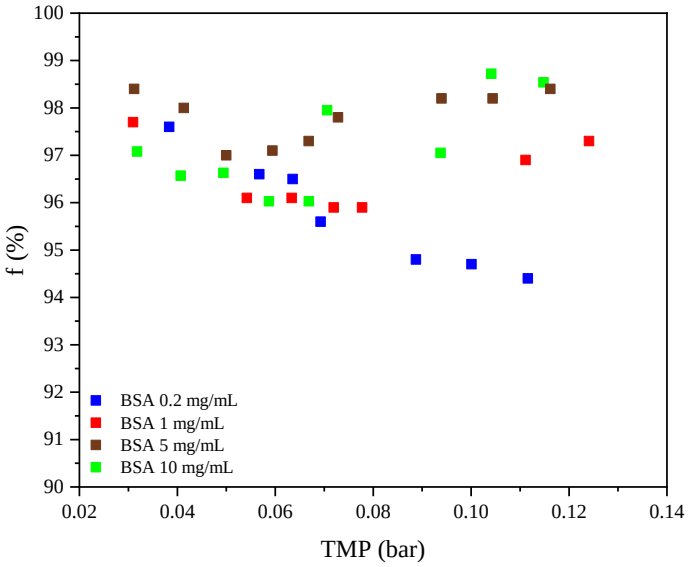


**Figure 3.54**: *Bovine Serum Albumin (BSA) apparent rejection coefficients at 0.2 mg/mL, 1 mg/mL, 5 mg/mL and at 10 mg/mL.*

The rejection coefficients decrease with the TMP as it is expected when the driving force is enhanced. Moreover, increasing the concentration of the feed solution the concentration polarization start acting as an additional resistance to mass transport, reducing the permeate fluxes and increasing the rejection coefficients.

To determine the new mass transfer correlation, the rejection and flux data were elaborated following the procedure described in paragraph 2.9.5.2.

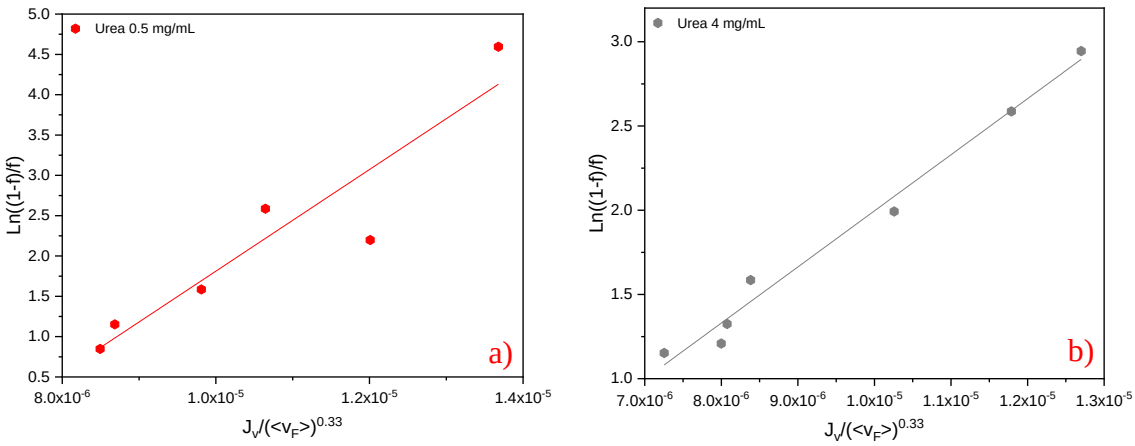


**Figure 3.55**: *Urea data elaboration for rejections experiments at 0.5 mg/mL a) and 4 mg/mL b).*

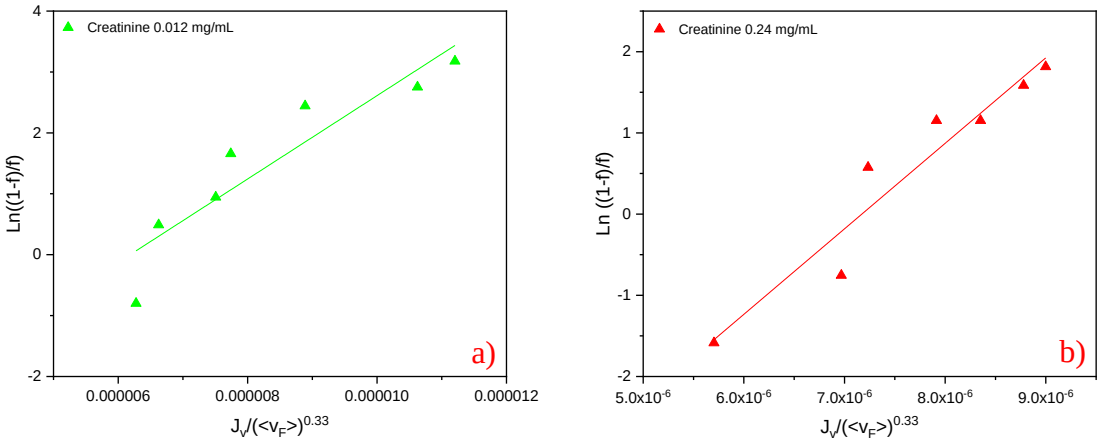


**Figure 3.56***: Creatinine data elaboration for rejections experiments at 0.012 mg/mL a) and 0.24 mg/mL b).*

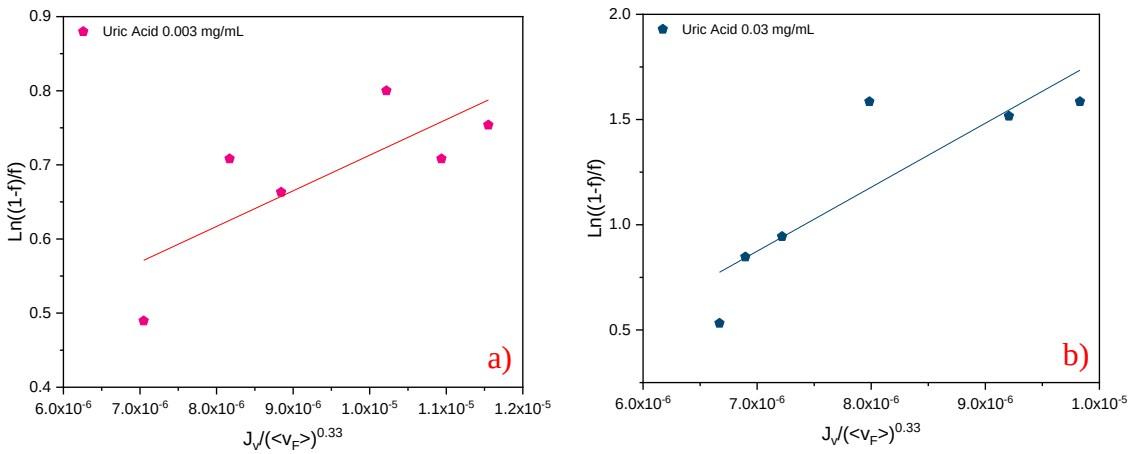


**Figure 3.57***: Uric acid data elaboration for rejections experiments at 0.03 mg/mL a) and 0.003 mg/mL b).*

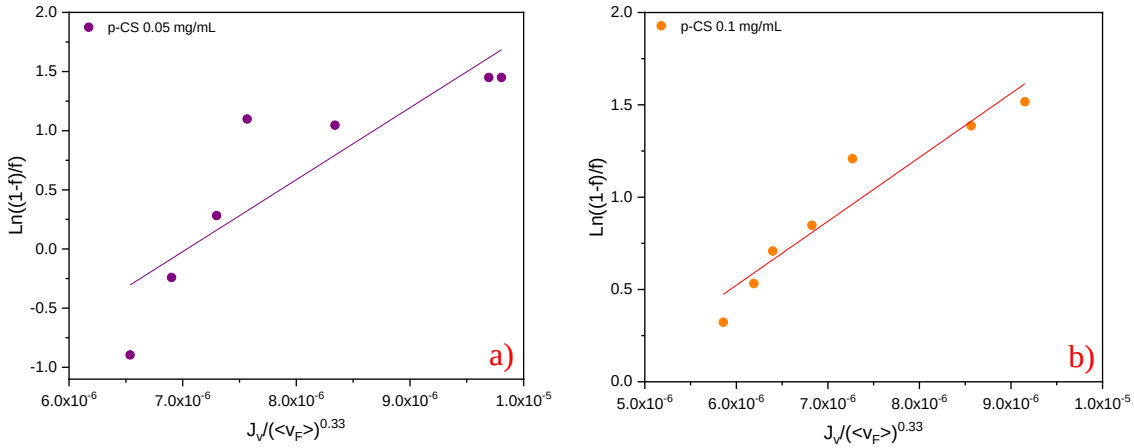

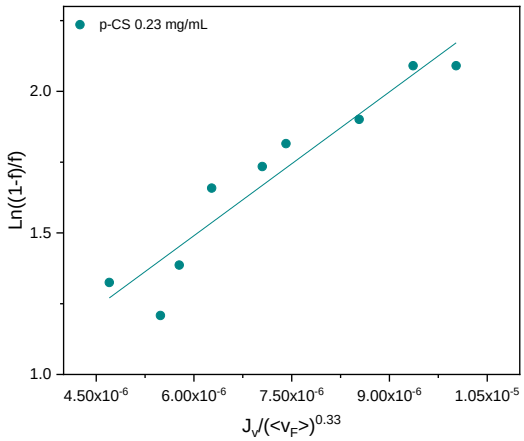


**Figure 3.58**: *para-Cresyl Sulphate (p-CS) data elaboration for rejections experiments at 0.05 mg/mL a), 0.1 mg/mL b) and 0.23 c).*

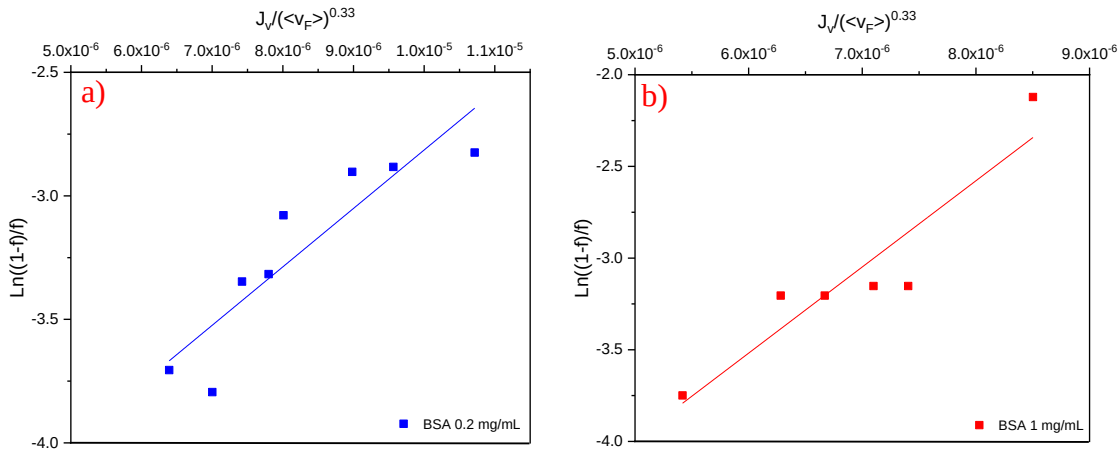


**Figure 3.59**: *Bovine Serum Albumin (BSA) data elaboration for rejections experiments at 0.2 mg/mL a) and 1 mg/mL b).*

From the slope of the linear regressions of all the data sets, experimental mass transfer coefficients, $k_{exp}$, were calculated for each feed circulation velocity. Then, the experimental Sherwood numbers were calculated and with the least square method, using a multilinear regression algorithm, the dimensionless mass transfer correlation was found.

From Table 3.8-3.11 are reported the experimental and calculated Sherwood numbers after running the algorithm:

**Table 3.8**: *Experimental and calculated Sherwood number for urea.*

| | $Sh_{exp}$ | $Sh_{corr}$ |
|---|---|---|
| *Urea 4 mg/mL* | 0.34 | 0.19 |
| | 0.37 | 0.22 |
| | 0.39 | 0.26 |
| | 0.42 | 0.29 |
| | 0.45 | 0.28 |
| | 0.48 | 0.30 |
| | 0.49 | 0.29 |
| *Urea 0.5 mg/mL* | 0.20 | 0.20 |
| | 0.21 | 0.23 |
| | 0.22 | 0.24 |
| | 0.24 | 0.27 |
| | 0.26 | 0.29 |
| | 0.27 | 0.29 |

**Table 3.9**: *Experimental and calculated Sherwood number for creatinine and uric acid.*

| | $Sh_{exp}$ | $Sh_{corr}$ |
|---|---|---|
| *Creatinine 0.24 mg/mL* | 0.17 | 0.47 |
| | 0.18 | 0.44 |
| | 0.19 | 0.49 |
| | 0.20 | 0.50 |
| | 0.21 | 0.52 |
| | 0.22 | 0.56 |
| | 0.23 | 0.62 |
| *Creatinine 0.012 mg/mL* | 0.23 | 0.32 |
| | 0.25 | 0.39 |
| | 0.27 | 0.40 |
| | 0.28 | 0.45 |
| | 0.31 | 0.48 |
| | 0.34 | 0.51 |
| | 0.35 | 0.54 |
| *Uric Acid 0.04 mg/mL* | 0.39 | 0.42 |
| | 0.37 | 0.47 |
| | 0.39 | 0.53 |
| | 0.42 | 0.63 |
| | 0.46 | 0.58 |
| | 0.57 | 0.62 |
| | 0.47 | 0.60 |

**Table 3.10**: *Experimental and calculated Sherwood number for para-Cresyl Sulphate (p-CS).*

| | $Sh_{exp}$ | $Sh_{corr}$ |
|---|---|---|
| *p-CS 0.2 mg/mL* | 0.97 | 0.46 |
| | 1.07 | 0.51 |
| | 1.13 | 0.56 |
| | 1.19 | 0.60 |
| | 1.24 | 0.60 |
| | 1.29 | 0.62 |
| | 1.38 | 0.65 |
| | 1.41 | 0.61 |
| | 1.46 | 0.63 |
| *p-CS 0.1 mg/mL* | 0.52 | 0.47 |
| | 0.55 | 0.52 |
| | 0.58 | 0.59 |
| | 0.60 | 0.62 |
| | 0.63 | 0.63 |
| | 0.67 | 0.65 |
| | 0.69 | 0.63 |
| *p-CS 0.05 mg/mL* | 0.27 | 0.31 |
| | 0.30 | 0.39 |
| | 0.31 | 0.43 |
| | 0.33 | 0.48 |
| | 0.36 | 0.54 |
| | 0.38 | 0.56 |
| | 0.39 | 0.57 |

**Table 3.11**: *Experimental and calculated Sherwood number for Bovine Serum Albumin (BSA).*

| | $Sh_{exp}$ | $Sh_{corr}$ |
|---|---|---|
| *BSA 1 mg/mL* | 4.92 | 6.65 |
| | 5.71 | 8.64 |
| | 6.05 | 9.53 |
| | 6.30 | 9.99 |
| | 6.52 | 10.51 |
| | 7.02 | 11.08 |
| *BSA 0.2 mg/mL* | 10.75 | 7.22 |
| | 11.34 | 7.60 |
| | 12.01 | 8.38 |
| | 12.53 | 8.97 |
| | 12.95 | 9.57 |
| | 13.94 | 10.38 |
| | 14.20 | 10.16 |
| | 14.73 | 9.90 |

In Figure 3.60 data are reported in a comparison graph between the Sherwood experimental, $Sh_{exp}$ and the Sherwood calculated, $Sh_{corr}$.

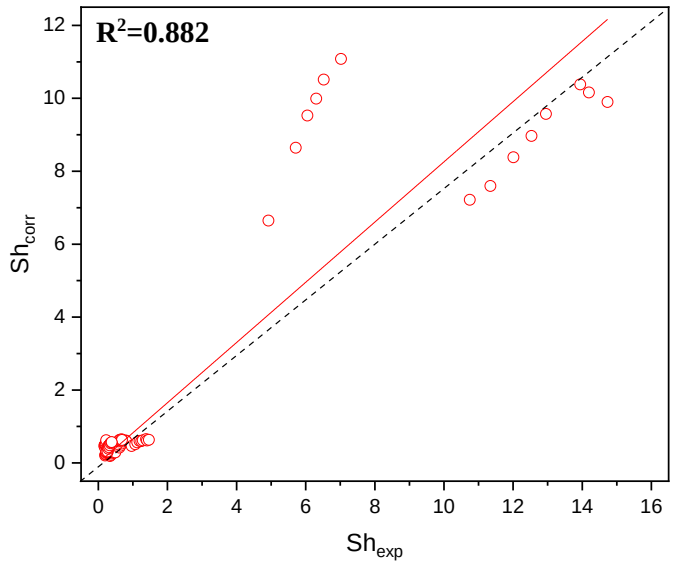


**Figure 3.60**: *Comparison graph between $Sh_{exp}$ and $Sh_{corr}$.*

The multilinear regression algorithm lead to this mass transfer correlation:

$$Sh = 1.69E^{-15} Re^{1.37}\, Sc^{1.07}\, {Re_p}^{-1.19}$$

The value of A is very small, indicating that the Reynolds number does not play an important role in the final compute, while what is governing the correlation is the Reynolds of permeability, since it is very low, in the order of $10^{-8}$. Therefore, due to this low value of the constant A and the negativity of the exponent d, a different form for the correlation was designed so that the values of $Re_p$ were made with an order of magnitude comparable to that of the other parameters and to avoid an infinite Sherwood number for impermeable situations:

$$Sh = ARe^{b}\, Sc^{c}\, \frac{1}{(1+Re_p)^{d}} \qquad (72)$$

Removing the data of BSA at 1 mg/mL that were decreasing the $R^2$ of the correlation, a new set of parameters was obtained with an $R^2$=0.992, indicating an excel data fitting:

$$Sh = 1.919 \times 10^{-5} Re^{1.261}\, Sc^{1.072}\, \frac{1}{(1 + Re_p)^{1.471}}$$

This last version of the correlation is the one proposed in this work of thesis to quantify the effect of permeation rates on the global mass transfer rates which is a key point of the present Renal Replacement Therapies (RRTs) that are characterized by high convective removal rates.

## References

[1] U.S. Embassy, Crystal Structure and Structure-Related Properties of ZSM-5, (1981) 2238–2243.

[2] Activated Carbon Consortium. http://www.reachactivatedcarbon.eu/achigh.html.

[3] A. Woszuk, L. Bandura, Application of zeolites as fillers in mix asphalt, 14 (2015) 127–134.

[4] J. Seewny. 29th Annual NANT Symposium, 2012.

[5] National Library of Medicine. https://pubchem.ncbi.nlm.nih.gov/compound/urea

[6] National Library of Medicine. https://pubchem.ncbi.nlm.nih.gov/compound/creatinine

[7] National Library of Medicine. https://pubchem.ncbi.nlm.nih.gov/compound/uricacid

[8] National Library of Medicine. https://pubchem.ncbi.nlm.nih.gov/compound/139600838

[9] G. Mendes, M. Faria, A. Carvalho, M.C. Gonçalves, M.N. de Pinho, Structure of water in hybrid cellulose acetate-silica ultrafiltration membranes and permeation properties, Carbohydr. Polym. 189 (2018) 342–351. doi:10.1016/j.carbpol.2018.02.030.

[10] M.J. Beira, M.P. Silva, M. Condesso, P. Cosme, P.L. Almeida, M.C. Corvo, P.J. Sebastião, J.L. Figueirinhas, M.N. de Pinho, Molecular order and dynamics of water in hybrid cellulose acetate–silica asymmetric membranes, Mol. Phys. 117 (2019) 975–982. doi:10.1080/00268976.2018.1537526.

[11] M. Faria, C. Moreira, T. Eusébio, P. Brogueira, M. N. de Pinho, Hybrid flat sheet cellulose acetate/silicon dioxide ultrafiltration membranes for uremic blood purification, Cellulose 27 (2020) 3847-3869. doi:10.1007/s10570-020-02985-2.

[12] G. Silva, N. Leal, V. Semiao, Micro-PIV and CFD characterization of flows in a microchannel: Velocity profiles, surface roughness and Poiseuille number, Int. J. Heat Fluid Flow 29 (2008) 1211-1220. doi:10.1016/j.ijheatfluidflow.2008.03.013.

[13] H. Bruus, Theoretical microfluidics, 2008, Oxford University Press Inc.

[14] V. Magueijo, V. Semiao, M. Norberta de Pinho, Effects of ultrafiltration permeation rates on the hydrodynamics of a minichannel/slit laminar flow, Chem. Eng. Sci. 61 (2006) 7139–7150. doi:10.1016/j.ces.2006.07.041.

[15] G- Hetsroni, A. Mosyak, E. Pogrebnyak, L. P. Yarin, Fluid flow in micro-channels, Int. J. Heat Fluid Flow 48 (2005) 1982-1998. doi:10.1016/j.ijheatmasstransfer.2004.12.019

# 4 CONCLUSIONS

Hemodialysis is the primary extracorporeal treatment for patients with severe kidneys damage. Several drawbacks are associated to this renal replacement therapy: large water, energy and materials consumptions burden on both the environment and the health care system. Moreover, it cannot substitute the native kidney functions efficiently leading to the insurgence of several pathologies connected to the accumulation of uremic waste products in patient's blood. This thesis was aimed to assess primarily the massive usage of water that every year worldwide is estimated to be 156 billion of liters. Following the new technology proposed in literature that combines both filtration and adsorption, new porous Mixed Matrix Membrane Adsorbers (MMMAs) were successfully synthesized and characterized for the removal of uremic toxins from aqueous solutions. This should allow the spent dialysate regeneration and a consequent savings of a great amount of water. The other part of the work was focused on the characterization in terms of fluid mechanics and mass transfer of a surrogate system of an artificial kidney (AK). A particular focus was given on the effect of surface phenomena on the velocity profile when permeation is concerned and on the development of a new dimensionless mass transfer correlation for laminar flow regime accounting for the permeation phenomenon valid for a range of Schmidt number typically involved in hemodialysis processes. The permeation effect is important in assessing the overall mass transport rates.

MMMAs were successfully casted by dispersing ZUF, ZSM-5 and AC in cellulose acetate. They were tested to evaluate their uremic toxin adsorption capacity. SEM images highlight the asymmetric morphology of the membranes and the change of pore conformation due to the presence of the adsorbent that was qualitatively confirmed by EDS analysis. The removal capability of the plain adsorbents and of the MMMAs towards small molecular weight uremic toxins has been investigated. From batch experiments on the plain adsorbents, it can be concluded that ZSM-5, ZUF and activated carbon are suitable for uremic toxin adsorption. ZSM-5 is the adsorbent with the lowest removal capacity, while activated carbon and ZUF are capable to remove a large amount of toxins from aqueous solutions. The removal ability of cellulose acetate towards urea and creatinine is enhanced by the addition of the fillers, while that of uric acid is almost not affected. The enhancement is lower than expected in some cases, due to probable partial masking of the adsorbent by the

polymer. MMMAs were also tested for water permeability, and it was found that the presence of ZUF enhances the water permeability of the polymeric membrane up to 20% in weight. The obtained results indicate the potentiality of porous materials and MMMAs in toxin removal for the hemodialysis process. Urea and creatinine in batch adsorption tests were removed up to a 30% while uric acid is completely adsorbed by the MMMAs. Therefore, the most promising MMMAs according to batch adsorption results were used in dynamic adsorption experiments. Despite continuous removal experiments with a lab-scale chromatographic cartridge packed with 22 MMMAs show promising adsorption capability, the need of a larger membrane volume to achieve higher stream purification is denoted. The results allowed the sizing of a cartridge for the dialysate purification applicable to hemodialysis processes. The toxin governing the design of the cartridge is urea, being the most abundant molecule in the spent dialysate and the most difficult to remove. To not oversize the column, low flow rates are preferable even if the time needed for the process will be higher.

Porous MMMAs can revolutionize the way in which filtration and adsorption are conceived not only for the biomedical field. They can potentially combine the two processes in a unique step eliminating the drawbacks connected to chromatography (high pressure drops, difficulties in packing a stable bed). They can also be revolutionary in term of cost related to the process since the presence on water on earth is going to diminish year after year and its cost is going to increase consequently. They can represent an opportunity to recycle water and make it available for other processes, with a consequent save of money, also preserving the environment. MMMAs could represent a novelty among the membrane separation technology, combining filtration and adsorption in a unique step. Nevertheless, research needs to be done focusing on tailoring the materials to improve molecules targeting and to increase their mechanical resistance to processes conditions.

Hybrid cellulose acetate/$SiO_2$ ultrafiltration membranes (CA_30 and CA_22) for artificial kidney applications were successfully prepared through the coupling of the sol-gel process and the solution casting technique. Their hydraulic permeabilities and MWCOs were calculated as prerequisites for the fluid mechanics and mass transfer characterization of the surrogate system of an artificial kidney (AK). Surface phenomena, such as pressure drop due to surface roughness, gain a huge importance in scaling down the systems to micro or

mini channels. They become even more significant when permeation is concerned. From the fluid mechanics characterization of the AK surrogate system was confirmed, thanks to the linear increase of pressure drop with the feed flowrate, the laminar regime of a fully developed Poiseuille-type flow. It is also underlined that, as the slight height decreases, an increment of pressure drop for a fixed flowrate is experienced. The conspicuous difference between the theoretical pressure drop calculated and the one experimentally obtained in impermeable walls conditions lead to conclude that the wall surface roughness induces unneglectable changes in the velocity profile. This was successfully modelled with the introduction of a fictitious viscosity to take into account the effect that the local changes in velocity profile due to surface roughness have on pressure drop. The values of fictitious viscosity obtained range from 0.29μ to 0.96μ which are congruent with previous results obtained in similar conditions, but in a different apparatus. Comparing the values of pressure drop obtained with CA_30 and CA_22 with the ones determined with the impermeable wall conditions it is possible to hypothesize that suction strongly deforms the global velocity profile, moving the maximum velocity position towards the membrane. This effect is more pronounced for higher permeate fluxes (CA_30). The hypothesis done, even if is sustained by the experimental results, can only be validated with CFD.

The main objective of the characterization of the surrogate system of an artificial kidney (AK) was the development of a new dimensionless mass transfer correlation valid for Reynolds numbers ranging from 33<Re<114 and for Schmidt numbers varying from 384<Sc<7881. The novelty associated to this correlation is the quantification of the effects of permeation rates on the global mass transfer rates. This is done inserting in the correlation a Reynolds number accounting for the permeation, $Re_p$. Exploiting the integrated model, a new correlation was found elaborating the rejections experiments results with the velocity variation method. Experimental and calculated Sherwood were then modelled with a multilinear regression using the least square method and this correlation was obtained:

$$Sh = 1.919 \times 10^{-5} Re^{1.261}\, Sc^{1.072}\, \frac{1}{\left(1 + Re_p\right)^{1.471}}$$